1   **Advanced applications of cellulose nanocrystals: a mini review**

2   Aref Abbasi Moud *

3   Department of Chemical and Biological Engineering, University of British Columbia Vancouver
4   Campus Vancouver, BC Canada V6T 1Z3

5   *Corresponding Authors:

6   E-mails: Aabbasim@ucalgary.ca (Aref Abbasi Moud)

7   **Abstract:** Cellulose that has been acid hydrolyzed is what makes up cellulose nanocrystals (CNC).
8   Due to CNCs biodegradability, renewability, sustainability, and mechanical properties, they have
9   a wide range of applications in the biomedical, photonics, and material engineering fields.
10   Rheology, or the flow behaviour of CNC dispersion, is integrally tied to the processing and design
11   of CNC-based products, thus it is important and warrants inquiry to carefully examine the
12   relationship between rheology's flow behaviour and their attributes. In this paper, we report the
13   most recent findings on the advanced application of CNC suspension, aerogel, and hydrogels.
14   Applications to technology and material science for developing advanced materials such as
15   photonic tunable crystals, responsive materials, and thermal insulation packing materials were
16   also covered.

17   *Keywords: Cellulose •Microscopy • Nanocrystals • Rheology*

18   **1.   Introduction**

19

20   The linear polymer known as cellulose provides structural support for the primary cell walls of
21   plants, algae, and oomycetes [1]. It is a chemical compound having the molecular formula
22   polysaccharides, which are composed of hundreds or thousands of linked D-glucose units [2-4].
23   CNCs, which are needle-shaped, stiff, negatively charged particles with a crystallinity of around
24   70%, may be created from acid hydrolysis of cellulose [5]. While hydrochloric acid procedure results
25   in development of less negative charge and makes CNC susceptible to agglomeration, acid
26   hydrolysis with sulfuric acid produces less thermally stable sulphate groups [6]. Studies have been
27   conducted with the goal of enhancing the surface charges of CNC colloids to improve their
28   dispersion stability. For instance, Yu et al. found that employing $NH_3 \bullet H_2O$ as the neutralising
29   agent allowed CNC colloids produced by hydrochloric acid hydrolysis to stay stable for more
30   than 24 hours[7]. Due to their nanometric size and agitation by the thermal motion of the medium
31   molecules, these particles are Brownian colloids when they are suspended in a liquid.
32   Mercerization is the process of swelling natural cellulose fibres by immersing them in a highly
33   concentrated aqueous NaOH solution, then washing and drying them. The crystal structure is
34   converted from cellulose I to cellulose II while remaining solid during this process.

CNC suspensions' ultimate physical traits and structural features are determined by the colloidal transition, which includes liquid-solid (alternatively sol-gel) and isotropic-anisotropic transitions (liquid crystal formation). Gel formation occurs when Brownian colloids are held together by sufficiently strong attractive forces and convert into a viscoelastic substance. This transition is linked to slowed diffusion of particles, solid-like viscoelasticity and other nonlinearities (e.g., yielding, shear thinning, deviation from Cox-Merz rule)[8-9]. Gel made from nanoparticles has found a foothold in a variety of industries, including foods, 3-D printed products[10-12]. More advanced applications include a novel three-dimensional direct-write construction process for porous scaffolds, photonic crystals, and microfluidic devices[13]. Viscoelastic traits of gel such as the low-frequency peak of the storage modulus and the yield stress have received a lot of attention in the litearture[14-17]. These traits are connected to particle geometry, interaction and synergistic characteristics [17]. Moreover, there has also been some research focused on the relationship between linear and non-linear viscoelastic traits of these complex fluids[18] under new mathematical frameworks. Formation of liquid crystals affect rheology emergence of viscosity maximum in plot of viscosity versus concentration curve due to ease of orientation of liquid crystalline domains [19]. Therefore, a unifying account such as current manuscript is needed to provide a mini overview on recent studies in the literature.

Per a literature survey [20-22] [23], the overall flow pattern of cellulose nanocrystal solutions during shearing, and also the effects of dosage, charge density, sonication, and temperature levels, liquid crystal formation[20, 22, 24] on its viscosity, have all been investigated for isotropic CNC solutions. As the CNC concentration further increases, the suspensions undergo another LC to gel transition[21, 25]. State of CNC suspension i.e. isotropic, biphasic, liquid crystalline and liquid crystalline gel are distinctly different in terms of topology[26-27] therefore they have an immediate impact on the rheological properties of CNC solutions. Topology of CNC recently using chemical alteration has been found to be also adjustable [28-29].

Nanocellulose is also gaining popularity because to its renewable and carbon-neutral nature, remarkable biocompatibility, tailorable surface chemistry, and unmatched optical and mechanical properties[5]. The purpose of this study is to provide an up-to-date appraisal of recent nanomaterial advances and their potential applications in soft robotics, energy storage, and medicinal science that benefit from CNC LC formation. Over the last few decades, technological improvements have frequently coincided with the creation of novel materials. Material scientists and engineers put forth a lot of effort to learn from nature's complex design principles while looking for inspiration [30]. For example, stimuli-responsive "smart" materials that alter form reversibly in reaction to external triggers open the way for soft robotics[31] and self-regulating device[32], and bioinspired hierarchical surfaces in wettability control and adhesion[33]. The CNC chiral nematic LC has unique optical capabilities that are unmatched by other rod particles due

71 to its intrinsic periodic spirally organized LC structure. Some account of research on CNC LC
72 formation and its properties are reviewed here.

73 Concerning the rheological behaviour of nanocellulose, reports[5, 34-35] have given much-needed
74 information both for the rheological features of CNC and CNF[5, 34], including such shear thinning
75 behaviour, high and small amplitude oscillatory shear and slide behaviour[36]. However, there is
76 an absence of a study that provides a comprehensive overview of the advancement of rheology
77 application on CNC suspension\gels\glass augmented with a chronology, which is why the
78 current review publication is being disseminated. The work of this publication, in conjunction
79 with current reviews on cholesteric rheology[9, 37], is anticipated to help interpret the results of the
80 experiment on cholesteric liquid crystals, which will advance the creation of innovative materials
81 and structures including the use of films such as this for gas sensors or optoelectronic materials.
82 Moreover, products using LC formation of CNCs are covered. Some of the discussion and topics
83 used here can be also found in our previous publications[38-39].

84 **2. Background**

85

86 CNC suspension viscoelastic research has contributed dramatically ever since its inception in the
87 1900s. CNC rheological properties gained historical relevance with the first published rheological
88 research on CNC suspension in 1961[40]. Since then, there has been a sustained interest in CNC
89 viscoelastic and shear flow behaviour, with research work focusing on topics such as defining the
90 aspect ratio of CNCs, assessing direction using rheology, and others.

91 Marchessault et al. [40] conducted the first study on CNC rheology between 1961 and 1992,
92 demonstrating that the width and length profiles of cellulose particles in suspensions had a
93 significant influence on the hydrodynamic properties of whiskers. Whisker had a distinct flow
94 curve in an isotropic state; matter of fact, plots of steady shear viscosity vs. shear rate acquired
95 for regular isotropic suspensions typically show two major areas: a continual viscosity plateau at
96 low shear rates and a quick drop at high shear rates (shear thinning behaviour) [41].

97 Subsequently, Onogi and Asada [19] demonstrated typical rheological behaviour for LC polymer
98 in fluids, with three unique shear dependences of the viscosity profile. At decreasing shear rates,
99 the first area (yielding region) is observed and shows a steady drop in viscosity. The second zone
100 is distinguished by the appearance of a plateau at moderate shear rates (central region). The third
101 zone (power-law region) is indicated by a steady reduction in viscosity at higher shear rates. This
102 is typical of LC and has seldom been seen in a single system, most likely due to the small
103 empirically available shear rate window.

104 Orts et al. [24] illustrated the fluctuation of viscosity as a result of shear rate revealing three separate
105 areas for the cellulose whiskers in mixed forms of LC and isotropic conditions (aspect ratio 30-

45). The first region was discovered at very low shear rates and correlates to shear thinning when the LC macro-domains begin to detect the shear field and flow. The subdomains are split apart when the shear rate increases, resulting in the presence of a plateau in the curve.

Shear thinning occurs with the orientation of single rods at increasing shear rates. A fast-organizing behaviour of the cellulose whiskers occurred in our SANS research at regime II, showing that the order achieved a plateau in the shear-thinning regime. The origin of region I, the earliest shear thinning region, is still debated [42], although it is typically related to changes in the polydomain texture's disclination lines. At the intermediate region II, director wagging[43] and vorticity alignment[44] have been observed. The alignment of particles along the flow direction relates to region III, which has a lower gradient than Region I. This tendency has also been seen in appealing emulsions [44] and lyotropic SWNT colloids in super-acids[45].

In 1988, [46] the growing interest in CNC got ignited by their ability to spontaneously organize into a left-handed chiral nematic LC order that could be retained in a solid state; 4 years later, [47] writers claimed at low CNC concentration tactoids are formed, that later settle due to gravity then solidify form LC domains at the bottom of the container.

The viscoelastic characteristics of sea squirt (tunicate) cellulose whiskers (high aspect ratio~140) were examined in 2 distinct regions: in the isotropic-at-rest regime (concentration < 0.8 wt%) and even in the anisotropic-at-rest regime (concentration > 0.8 wt%). A few years later, the very first try at trying to distinguish between the rheological characteristics of isotropic CNC suspension and CNC LC was made. [20]. For the first regime (c < 0.85 wt%), the curves at the concentrations at low shear rates corresponds to the randomly oriented whiskers, and a second behaviour at higher shear rates indicates that the rods are well oriented, and the increase of the shear rate did not alter the rod orientation and consequently no change in the viscosity is observed. The rheological behaviour under an anisotropic regime was similar to Orts et al [24] reminiscing shear rheology of LC polymers.

The subsequent years' effort was focused on improving understanding, and further tests were conducted to look at how CNC charges affect rheological behaviour. In actuality, rheological responses to whisker suspensions treated with HCl and H_2SO_4 were different [48]. One distinction, in addition to revealing shear thinning behaviour, was that H_2SO_4-treated mixtures with bigger charges did not display any temporal reliance in their viscose behaviour[49]. In contrast, HCl-treated suspensions were thixotropic at concentrations above 0.5 wt % and anti-thixotropic at concentrations below 0.3 wt %. The reaggregation of particles at low concentrations caused by their alignment with the shear field was the cause of the anti-thixotropic effect.

In 2000, [50] investigations were enlarged to include a highly viscous but steady suspension of cellulose microcrystals. This time, samples under flow had shown flow birefringence at low solid

content (circa <1%); at higher solid content (circa 2-3%), the suspension still was starting to flow but displayed intricate birefringent patterns, which persisted after the flow had stopped. When the solid content was high (7.1%), the suspension lost its ability to move and developed a tiny crosshatch texture along with a frozen-in birefringent pattern. These features showed that the post-sulfated solution behaves markedly differently from the suspension produced by direct cellulose hydrolysis with concentrated sulfuric acid in that it produces a "birefringent glassy phase," like that observed in a suspension of boehmite rods.

Yet another report[51] noted unplanned nematic phase separation of particles upon complete desalinated water; after the addition of a detectable electrolyte (<1mM NaCl), the anisotropic phase became chiral nematic, also known as "Cholesteric." Between 2001 and 2010, efforts were concentrated on recognising the LC behaviour of microcrystal suspension in much more specific. The screening of surface charges, which exposes CNCs that convert cylindrical nanoparticles into twisting rods, so altering particle shape, may help to explain this astonishing shift in LC behaviour. Later in 2005, it was shown that the volume ratio of the anisotropic to the isotropic phase was in direct proportion to the CNC concentration, and only the anisotropic phase existed at higher concentrations[52]. Epoxypropyl trimethylammonium chloride produces CNCs with a positive charge, in contrast to all other attempts, which were focused on a negative charge[53]. Shear flow birefringence was once more detected in suspensions. The results showed that suspension was able to generate chiral nematic structures when these surface treatments were afterwards enlarged to a particle with grafts [54] [55].

Under 35 °C, the temperature had no impact on rheology and phase behaviour, according to an investigation of its effects on sulfonated CNC suspensions in 2011[21]. Nevertheless, there was a noticeable shift in both the rheological characteristics and the proportion of the isotropic phase between 35 and 40 °C. The constant shear viscosity did not reach a peak with an increase in concentration, in contrast to many *lyotropic* suspensions. Predominantly isotropic samples showed a broad Newtonian plateau at all tested temperatures and had a shear thinning zone starting at 30 s^{-1} that was visible at 10 and 25 °C, as expected for predominantly isotropic dispersion viscosity to rise when temperature is reduced. At all three of the tested temperatures, the CNC dispersions displayed three-region behaviour; however, while the viscosity typically decreased with increasing temperature, no change was seen in the region I. It's interesting to note that region II was visible, compared to lyotropic SWNT-superacid dispersions[45]. Larger rods shear thin at lower shear rates because they have longer rotating relaxation durations. [56] SWNTs are longer and more polydisperse than CNCs, which may result in a smaller range of shear rates at which region II is visible. The structure wasn't stable at 40 °C, which led to significant changes in the measurements made, that are not unusual for samples towards the centre of the biphasic zone. The temperature had no impact on the viscosity of the 12.1% (predominantly LC material) samples between 10 and 35 °C. Despite the CNC's extremely low aspect ratio, this result suggests

178 that temperature did not affect *mesogen* rearrangement between 10 and 35 °C. It's interesting to
179 see that viscosity rose dramatically around 40 °C, especially at low shear rates.

180 The loss modulus could be successfully superimposed over time, but not the storage modulus.
181 This shows that the elastic relaxation but not the viscous response is both influenced by the
182 interface in biphasic samples. Higher concentrations resulted in the dispersions behaving like
183 rheological gels and losing the fingerprint texture of the LC phase. There is an inverse link
184 between chiral nematic pitch and concentration in CNC suspensions, according to authors who
185 later in 2014 concentrated on the pitch length of CNCs suspensions. This is explained by increased
186 CNC interactions, which increase the intrinsic twist and reduce pitch[57]. The two essential
187 concentrations of CNC were dependent on the aspect ratio, according to Wu et al. [58]. Because the
188 switchgrass CNC suspension had a larger aspect ratio than the cotton CNC suspension, it
189 changed into a biphasic condition and produced a gel at lower doses.

190 Later in 2017[59], the flow properties of two CNCs with different aspect ratios but similar surface
191 charges were examined. The solution vitrifies from a dilute soliton to colloidal glass with
192 increasing CNC concentration. The viscosity profile displays a single shear thinning feature over
193 the full range of shear rates examined, and this feature gets stronger as CNC concentrations
194 increase. The viscosity of un-sonicated samples is much higher than that of sonicated samples.
195 Xu et al. [60] examined the impact of salinity level on the yield stress of an aqueous CNC solution
196 one year later; they found that increasing salinity level decreased the yield point (repulsive glass).
197 The applied stress subsequently climbed over a threshold NaCl concentration (attractive glass).
198 For CNF particles, higher homogenization pressure or number of homogenizations passes, as
199 well as higher surface charges, was found to be reducing the viscosity of TEMPO-CNF
200 suspensions[61]. One of the most used chemical pretreatments is TEMPO ((2,2,6,6-
201 tetramethylpiperidine-1-yl)oxyl) mediated oxidation, which converts C6 hydroxyl groups to
202 carboxylate groups[62]. As a result, when fibrils are separated from the fibril bundles by further
203 mechanical refinement, such as mixing or highly pressurized homogenization, negative charges
204 are produced on the surface of the fibrils, helping to resist and stabilise fibrils in suspension[63-64].
205 TEMPO-mediated oxidation produces fibrils with smaller diameters and narrower size
206 distributions when combined with mechanical treatment: widths between 3 and 5 nm, lengths
207 between 0.5 and 10 nm, A similar goal of carboxymethylation [65], a typical chemical preparation,
208 is to introduce charges on the fibril surface by oxidation to speed up the disintegration process.
209 Chemically processed CNFs of diverse qualities have been applied in areas as rheological
210 modifiers by using the variable surface charge and shape.

211 Prior rheological research largely focused on the gel or diluted regimes to examine the impact of
212 CNF shape and surface charge. Here, samples that exhibit solid-like behaviour are categorised as
213 belonging to the gel regime because G′ > G″ throughout a broad frequency range[35, 66]. Prior

214 research that employed pressure homogenization to alter the nanofibril shape found that the
215 number of passes through to the homogenizer or the homogenization pressure enhanced the
216 viscosity of the flow curves. According to Shogren et al.[67], G′ initially rose until it peaked after the
217 second homogenization pass, then began to fall as the number of passes was increased. The
218 rheology of CNF suspensions that have undergone chemical pretreatment is also impacted by
219 changes in surface charge. The carboxylate concentration on the fibril surface, which can be
220 controlled by the concentration of the oxidising agent and the reaction duration, has been
221 demonstrated to be linked with surface charge for TEMPO-mediated oxidised CNF (TEMPO-
222 CNF) samples. Higher carboxylate concentration often results in a reduction in viscosity (or
223 modulus G′)[68]. Although some researchers have noted an initial rise followed by a reduction in
224 viscosity as the carboxylate concentration increases, the opposite tendency has also been noted[69].
225 G′ values for CNF suspensions in the diluted regime are significantly lower than G″ values, and
226 their steady shear viscosity scales linearly with concentration [70]. The inherent viscosity and the
227 aspect ratio of the nanocellulose have been shown to be correlated [71].

228 The effect of CNC concentrations on the static, dynamic, and real yield points of supersaturated
229 CNC aqueous suspensions was recently discussed by authors [72]. The author stated a linear
230 relationship between concentration and yield stress. The microstructure of CNC gelified with
231 non-ionic hydroxyethyl cellulose (HEC) solutions was examined using large amplitude
232 oscillatory shear (LAOS), a technique that is gaining popularity [73-74] among researchers and can
233 identify the beginning of nonlinearities in complicated materials[75]. Above C* (overlapped
234 content) of HEC, gel exhibited a shear thinning tendency. Using state-of-the-art, LAOS analysis,
235 CNCs/HEC mixtures showed type III behaviour with inter-cycle stress softening, while the
236 samples showed stress stiffening in single cycles. In 2021[76], shear-induced birefringence of CNC
237 suspension was reported as $\Delta n \approx 3 \cdot 10^-$ ($\dot{\gamma} \approx 100$ 1/s) and $\Delta n \approx 9 \cdot 10^{-6}$ ($\dot{\gamma} \approx 400$ 1/s). The fluid was
238 regarded as isotropic with 0% flow birefringence for shear rates under 40 1/s. According to ref [76],
239 extensional forces are four significantly more efficient than shear forces for aligning CNCs. The
240 modelling results showed that particle aspect ratio is closely associated to particle alignments and
241 direction at the continuous shear rate and ref. [77]. later confirmed the findings of this work. For
242 shear force alignments of larger CNCs vs shorter CNCs generated from wood, similar results
243 were attained[78]. Researchers have just lately developed an interest in utilising capillaries to
244 explore the confinement impact on LC. [79-80] Mesogens are nematically aligned during the filling
245 of the capillary tube because of the shear force. The mesogens eventually rearrange themselves
246 into their preferred LC phase. A concentric cylindrical chiral nematic structure with a radial
247 cholesteric axis is formed when CNCs reorganise into the cholesteric phase.

248 The influence of aspect ratio and size distribution on CNCs with equivalent charges were
249 correlated by [81] authors using small amplitude oscillatory shear (SAOS); the results show that
250 longer CNCs have a lower gel point than shorter ones and produce more orderly structures at

comparable levels. Going back to shear rheology, researchers [82] looked at the impact of sonication on yield stress. They found that yield stress reduced as sonication energy increased. The impact of ultrasonic treatment on yield stress and physiochemical characteristics of condensed CNC gel within sonication levels of 0-5000 J/g CNC could be explained by four separate unique zones. The sonication energy minimally affected the particle size in Region I between the energy levels of 0-100. While the power law index somewhat reduced, the yield did not. The agglomeration loosening in Region II at an energy level of 100–500 led to a reduction in the z-average and the separations between the particles. While the power law index somewhat rose, the yield stress underneath this sonication regime reduced much further. The cholesteric region controlled the structure of the CNC suspension in Region III at an energy level of 500–1000 j/g, therefore yield stress persisted with three regime LC flow curves. Sector IV. Nearly all CNCs are free of their original agglomerates at an energy level of 1000–5000 J/g, and POM images revealed a completely LC microstructure.

Utilizing a CNC grafted with an ionic liquid to induce LC organisation from 3.0wt % to 1.0wt % was an attempt to push the point of phase separation to a lower concentration[83]. Additionally, the tactoids (which have a texture like a fingerprint and exhibit ionic liquid grafted CNC varying concentrations from 1.0 to 4.0 wt %) coexist with the disorderly CNC phase rather than splitting into two phases. Contrary to original CNCs, when utilising ionic liquid grafted CNC, the pitch of chiral nematic tactoids rises with increasing concentrations.

Rheological properties, a flexible tool, were also able to accurately identify the microstructure of the CNC solution with polyethylene glycol (PEG) added in ref[84]. PEG was added to the CNC suspension, which resulted in the appearance of liquid-like behaviour as the loss modulus (G'') exceeded the storage modulus (G') over the entire observed frequency range. As Beuguel et al. [85] found, the PEG molecules will therefore help to lessen the repulsive forces brought on by the depletion forces. A larger local concentration of each ingredient causes the microphase difference among PEG and CNC. This greater local population of high aspect ratio CNC particles in these CNC-rich microspheres causes the particles to self-assemble and organise into LC structures.

3. Gelation

 Colloidal gel networks are defined as systems with solid-like properties that must meet two requirements: the development of 3-D spanning networks and local kinetic arresting of particles [86]. Increasing loading concentration[22, 87], mixing with macromolecules[88-90] like hydroxyethyl cellulose (HEC) and PEG   [85, 91], mixing with organic coagulants[88, 91-92], or surfactants[93-94], hydrothermal methods[95], or using routine freeze-thaw cycling [96] are just a few of the ways that CNC suspension can be made to gel.

286 The authors[95] used hydrothermal techniques at high temperatures to gelify CNC water.
287 Desulfation of the CNC surface happened during treatment, which then caused the CNCs in
288 suspension to become less stable. The loss of negatively charged groups also decreased the
289 electrostatic repulsion between the CNCs, which resulted in gelation. To offer an example, the
290 sulphur content declined from 0.6 weight percent to less than 0.4, 0.4, 0.4, and 0.1 weight percent
291 after 20 hours of annealing at 60, 80, 100, and 120 degrees Celsius. If writers had compared the
292 zeta potential as well, that would have been fascinating for comparison's purposes.

293 For wearable sensors that track physiological signals, soft ionotronics with self-healing
294 capabilities and durable mechanical qualities are very desirable. Rapid prototyping using 3D
295 printing broadens design possibilities to improve the functionality of wearable sensors. But
296 concurrently achieving printability, mechanical toughness, and self-healing capabilities is still
297 difficult. Authors in ref [97], denoted that thermally induced gelation of CNCs in a deep eutectic
298 solvent is a straightforward method for creating 3D printed ionogels (DES). DES has been
299 employed as a non-volatile and ionic conductive medium for ionogels, however a significant
300 amount of CNCs must be disseminated in DES to obtain the optimal rheological behaviour
301 needed for the direct ink writing process. Their method greatly decreased the quantity of CNCs
302 required to make printable inks with strong physical networks in DES by triggering the
303 desulfation of CNCs at high temperatures. Therefore, in situations when standard procedures
304 are impractical or unavailable, the hydrothermal gelation process might offer special gelation
305 options.

306 In addition to the chemical characteristics of CNC particles, these systems' rheological
307 characteristics may be modified by varying their physical characteristics of individual CNCs,
308 such as changing crystallinity and length [98-99]. Recently, researchers [98] demonstrated that CNC
309 particles' aspect ratio significantly affects their rheological reactivity. For instance, it has been
310 demonstrated that shorter CNC particles exhibit gel-like rheological behaviour at greater
311 concentrations [99]. There exist other methods of gelation currently not being exercised for CNC
312 suspension such as high shear gelation[100] or gelation under confinement[101] that has applied to
313 other system. The origin of these methods is to put CNCs close enough like freeze thaw cycles so
314 thermal motions became ineffective in their separation.

315 Gel strength or storage modulus values reported in the literature signifies that depending on way
316 of gelation, aspect ratio and other not reported data such as crystallinity or source of CNCs
317 various gel strength can be obtained; attempting to generalize connection between storage
318 modulus and aspect ratio or zeta potential is crude[102] as parameters responsible for changing
319 storage modulus are many. The only trend observable on the literature for salt induced gelation
320 of CNCs is that higher valence ions can gelify CNCs at lower concentrations and storage modulus
321 tend to plateau after certain quantity of salt is added into the system[103].

A corpus of collective literature was used to illustrate the viscoelasticity of CNC suspension. Changes to the loading, temperature, salt content, or addition of more synthetic or biological macromolecules with long (polymer) and short (surfactant) chained molecules were all included in this. By considering these variables, the storage modulus reported in the literature ranged from 10^{-3} to 10^3 Pa. [21, 58, 88, 95, 104-115], These materials may be produced in a variety of ways, allowing for process flexibility and the development of goods that can meet different mechanical criteria. Rheology provides processing information prior to processing, which printable materials for 3-D printing applications require. The hydrogel might block the nozzles during 3-D printing processes; hence it is not recommended. High yield stress levels can result in gel-like structures that are challenging to print (typically accessible by a stress sweep test, SAOS research, or model fitting on flow corrected curves). However, low yield stress levels might result in extrudates drooping because of a delayed rate of healing or a failure to retain the mechanical tenacity needed for the products. According to the Through experiment, the optical yield stress for 3-D printing an ink is 100 Pa [116].

4. Rheological behavior of CNCs

The forces encountered during shear flow, or processing, are known to cause structural rearrangements in flocculated colloidal suspensions, which then change the suspension's rheological characteristics [117-118]. These architectural reorganisations involve modifications to the floc size[119-121], internal floc structure[119, 122], and degree of floc anisotropy[123-124] and occur more than a system-dependent [125 126]. Shear thinning, shear thickening, and finite normal stress differences are only a few of the rheological phenomena that are displayed by suspensions (solid particles submerged in a fluid). Shear thinning is a non-Newtonian behaviour in rheology that happens when a fluid's viscosity decreases under shear strain. There are times when it is perceived as the absence of time-dependent effects like thixotropy and is usually described as a synonym for pseudo-plastic behaviour.

A Newtonian fluid exhibits a plateau-like behaviour, such as very low concentration CNC suspensions (i.e., viscosity is independent of shear rate). Non-Newtonian fluids, on the other hand, exhibit rheological responses that differ from plateau-like behaviour in the wake of shear-thinning or shear-thickening behaviours. According to observations, CNC colloid gels have a shear-thinning characteristic when exposed to rotating shearing flow, high particle concentrations, or the addition of a polymer or surfactant [2, 127-131]Additionally, the degree of thinning behaviour rises as the network structure is strengthened, which is advantageous for most processing procedures like 3D printing. Similar to CNCs, longer cellulose nanofibrils also exhibit universally shear thinning properties[34].

357   Once the flow curves of the CNC suspension have been discovered in the lab, modelling of the
358   behaviour is next on the agenda; modelling allows for the acquisition of a clearer trend;
359   quantitative data such as yield point and shear thinning index. The model including Casson[132],
360   Herschel-Bulkley[133], power-law[134-135] and Bigham models are rather simple yet effective in
361   capturing the shear flow behaviour of cellulose particle suspension [136] [127]. There are also reports
362   on the description of CNC's rheological properties as Bingham fluids[137] as well; other similarly
363   complicated methods such as the application of the Folgar-tucker equation can be found in ref [127].
364   The results of these models are predicted to create a yield point of CNC gel solution, which is
365   critical for the processing of these gels.

366   One of the first rheological phenomena in colloid science is thixotropy. It is a topic of current
367   research since it is one of the trickiest issues in colloid rheology [125]. Herbert Freundlich's team at
368   the Kaiser Wilhelm Institute in Berlin persisted in their investigation of the phenomena. They
369   produced significant contributions that culminated in one of the very first works on rheology, a
370   monograph titled "Thixotropy" [138].

371   The definition of thixotropy that is often used today has the following key components [125]:

372   i)   it is based on viscosity.
373   ii)   it implies a time-dependent decrease of the viscosity induced by the flow.
374   iii)   the effect is reversible when the flow is decreased or arrested.

375

376   CNC suspensions are found to be thixotropic [2] similar to other nanoparticles [36, 139], which indicates
377   that their viscosity increases to the same level as before shearing. As seen previously, CNC-CTAB
378   gels showed diminishing thixotropic behaviour as a function of CTAB [2]. Faster recovery of gels
379   with CTAB can help with shape fidelity and sagging in 3-D printed extrudate or bio-inks [140]. Xu
380   et al. [60] also observed rapid structural recovery at low salinity (<10 mM) and high salinity (>50
381   nm); later sample with 11.9wt% CNC and low salinity showed significant thixotropic behaviour
382   with the yielding point completely disappearing during the backward shear stress ramp.
383   Interestingly, the samples with zero-added salt and high salt loading showed an immediate
384   structural recovery. The rate of structural recovery in this reference exceeded the structural
385   recovery of CNC suspension in refs[2] [141]. This may be due to mismatch of CNC concentrations [60];
386   additionally, it is noteworthy that hysteresis loop tests are time dependent; therefore results have
387   to be reported with time of shearing at each point. **Table 1** displays thixotropic behaviour
388   evaluation across literature; addition of other macromolecules can make CNC gel more\less
389   thixotropic as a result, significant experimental knowledge regarding "thixotropy" of CNC
390   suspensions\gels exists.

391   It is noteworthy that another strategy aimed at creating steric barriers around CNC particles has
392   been advocated in literature as a way to improve the stability of CNC dispersion [142]. However,

these methods might be most effective in situations where the addition of CTAB causes a charge inversion, which then induces an electrostatic attraction between particles; also mentioned as a potential mechanism for improved colloidal stabilisation is steric repulsion. In fact, the tetra-substituted ammonium cationic surfactant hexadecyl trimethyl ammonium bromide (CTAB) has a lengthy (C16) alkyl chain and positively charged quaternary nitrogen. For instance, CTAB has been employed to stabilise inorganic nanoparticles. Silver (Ag), gold (Au), copper (Cu), and platinum (Pt) nanoparticles has been historically stabilised using CTAB, according to Padalkar et al. [143]. An et al [144] preparation's of Ag nanoparticles using CNC as carriers/supports and CTAB as anchors revealed that CTAB's steric effects play a crucial role in stabilising Ag nanoparticles. Another advantage of CTAB over other stabilisers is its affordability given the surfactant's cheap cost and ease of acquisition, which has led to increased interest in CTAB across a variety of applications[145].

Table 1. Thixotropic behaviour evaluation across the literature.

Reference	Findings
[60]	At a CNC concentration of 11.9wt %, the samples with negligible salt addition and heavy salt loading showed a fast structural recovery.
[146]	Samples with more CTAB becomes recover quicker.
[141]	As concentration rose from 5-8wt %, there was more divergence from low to high and high to low shear ramps.
[53]	When the concentration reached 5wt %, the modified CNC with hydroxypropyl trimethylammonium chloride showed divergence from the low to high and high to low shear ramps.
[147]	De-sulfated CNC gel showed thixotropic behaviour.
[148]	CNC flocculated with carboxymethylcellulose (CMC) showed increasing thixotropic behaviour with increasing concentration of CMC and CNC.
[149]	The mixture of kappa-carrageenan/methylcellulose/cellulose nanocrystal was found thixotropic.

One can understand whether surfactant-salt molecule units contribute to the system's enhanced elasticity[150] by contrasting the structural variations among homogeneous and heterogeneous rod fractal clusters. The scheme goes into a state where particle interaction predominates over thermal forces, beginning to decrease local particle mobility. This state is brought on by the interaction of surfactant—salt molecule—units with the CNC surface, fine-tuning of a medium's ion concentration, and hydrophobic effects brought on by, for instance, attractive van der Waal or depletion forces [151] or effect of excluded volume [152]. Furthermore, particle mobility downscales to the order of rod width because of crowding or attraction interactions.

The is forced into kinematic arrest whenever it crosses this barrier, which macroscopically manifests as higher elasticity and non-ergodicity. Dynamics can be entirely stopped by cohesive and adhesive contacts amongst the densely packed network of rod gel particles; this type of dynamic arrest is comparable to a "traffic jam" situation. Despite having the capacity to move quicker than that of the traffic flow, individual cars in a jam discover that their motions are significantly constrained by other cars, much like the glassy nature of colloids. Due to the bulkiness of their fundamental forms, cars in such traffic situations find that their movement is significantly more restricted than in a glassy state, which may cause the CNC to be non-ergodic.

Examples that clearly illustrate how small angle oscillatory shear (SAOS) is applied are provided here[127, 131]. This significant difference in the concentration range could be explained by differences in the corresponding attachment among CNC particles and each of such ingredients, which also ultimately resulted in CTAB producing the very same screening-off effect as NaCl[94], though at a much lower percentage. It is necessary to add 1/10 of the Concentration of NaCl to accurate representation gel strength values. At low surfactant concentrations, those attractive forces are hydrophobic, but at high surfactant concentrations, they are electrostatic. In contrast to CTAB, SDS complexation displayed three-region behaviour, showing the presence of both attractive and repulsive forces at various surfactant levels, the supremacy of which regulates the viscoelastic characteristics of CNC suspensions. The quantity of NaCl needed to cause the same viscoelastic alteration was discovered to be around ten times more than that of CTAB. Additionally, the authors note that the gel strength of CTAB is greater than that of SDS[94]; the gel strength at equal mM follows the sequence of CTAB>SDS>NaCl[94], and the results are comparable to those of ref[2].

Nonlinear tests are highly sensitive to even minute changes in the interior microstructures of CNC-Salt-PVA system[127, 131], and they provide useful information on the topology of the nanofiller network. Likely, the rheological parameters determined inside the linear framework may not always provide this information. Confocal images and Lissajous-Bowditch plots were used to display CNC suspensions with varied salt applied loads and fixed particle contents to augment inferences about structure.

Confocal microscopy demonstrated that as the solution gelled due to increasing the salt level, Lissajous-Bowditch plots displayed dramatically different geometries. To provide both quantitative (such as inter- and intra-cycle variables) and qualitative nonlinear analyses, the authors also used additional methodologies, such as stress decomposition and sequence of physical events. All the suspensions and gels made of CNC/salt and CNC/salt/PVA exhibited Type III inter-cycle nonlinear behavior (significant overshoot as G' declines as G" increases and then decreases). It was discovered that the shear-thinning and strain stiffening properties of the viscous and elastic intra-cycle nonlinearity of CNC-based devices, respectively, could be used.

450 Furthermore, while the intra-cycle response of suspensions and gels was strongly frequency
451 dependent, the inter-cycle nonlinearity was frequency invariant.

452 Type I stream behaviour, a feature distinctive of polymer melts and suspensions in which
453 network constituents align themselves with the flow field, is initially seen in samples up to 1 mM
454 of CTAB concentration[73]. When the concentration threshold of 1 mM is crossed, the behaviour of
455 the storage and loss modulus shows an initial reduction in the storage modulus of the CNC-CTAB
456 material as a function of strain amplitude, accompanied by an initial increase, demonstrating type
457 III nonlinear viscoelastic behaviour in the CNC sample. The rate of drop in storage modulus
458 happens more commonly after overshoot than it does in loss modulus.

459 In actuality, the process is initiated when the loss modulus begins to climb (increase in
460 attenuation after flow initiation), and it's also the spot at which the stress-strain connection moves
461 away from linearity[153-156]. The maximum, also known as the "Payne effect," is a sign that yield
462 stress is present. The overshoot in storage modulus against frequency may also be described
463 using the Saramito Model, according to [157]. To predict the prevalence and association of storage
464 and loss modulus, the method is helpful.

465 It is possible to reap insight from microstructure of CNC gel based on nonlinearity index (T & S)
466 such as compaction of clusters at medium strain amplitude or sample strain hardening between
467 network rupture and viscose flow [127, 131, 158]. Frequency dependency another interesting area shows
468 that for CNC-salt coagulated system storage modulus and loss modulus in linear regime are
469 frequency independent however at higher frequencies nonlinear rheological response become
470 frequency dependent due to network rupture making the sample more viscose than solid.
471 Although the intra-cycle parameters S and T indices (defined based on mathematical framework
472 of Ewoldt et al.[159]) exhibited significant frequency dependence, the behavior that changed from
473 intra-cycle shear thickening to intra-cycle shear thinning behavior transitioned to larger strain
474 amplitude when the frequency was raised. Another striking feature of CNC salt gel behavior is
475 observance of a weak overshoot in loss modulus versus strain amplitude that is dubbed as a
476 measure visco-plastic fragility [157] or "Payne effect" as well. Overall LAOS is powerful to decipher
477 insight about gel microstructure; a detailed table showcasing LAOS findings on cellulose
478 products is provided in **Table 2.**

479 **Table 2.** Descriptive LAOS finding in the literature on CNC products are mainly in
480 hydrogel\suspension form.

Reference	LAOS findings
[131]	The intra-cycle viscoelasticity shows a substantial dependency of the samples' dynamic behaviour on salt content, CNC concentration, and rate of

	deformation, which is described using qualitative Lissajous-Bowditch plots and quantitative nonlinear parameters.
[160]	Weak strain overshoot during LAOS flow heralded improved phase affinity between CNC and poly(ε-caprolactone) (PCL)
[146]	Hybrid behaviour pass point of linearity (Type I and type III behaviour depending on concentrations of CTAB)
[127]	PVA-CNC hydrogels show type III behaviour at all CNC concentrations (1-3wt%)
[161]	The authors claim that a greater load of CNC particles in only *biphasic and liquid crystalline states* would result in stronger connections that would resist reformation during elastic deformation, which would cause the loss modulus to overshoot at the yielding point. Suspension showed no overshoot in dilute CNC suspensions. The state of suspension was 2wt% (isotropic), 3-5wt%(biphasic) and 6-9wt% (liquid crystalline).
[162]	According to the Authors, the observed type III response of hydrogels, which has been extensively documented in the literature, results from the wall-slip situation rather than the viscoelasticity that hydrogels naturally possess.

481

5. LC state rheology

483

A liquid is *isotropic*, meaning that its properties are constant in all directions since its molecules\particles are always moving at random. On the other hand, crystalline materials are *anisotropic*; this means that their optical properties as well as other traits like thermal and electrical conductivity are direction dependent. An LC phase contains many of the physical properties of a liquid, but the molecule\particle units are sufficiently organised to allow substantial anisotropy, particularly in the optical properties. The properties that are included in the sections are shear thinning, thixotropy, gelation (gel point), LAOS, SAOS, yielding and liquid crystalline CNC's rheology.

The finding by Gray and colleagues[47] that suspensions of rigid and rod-like CNCs, generated from natural cellulose sources by acid hydrolysis, may form a stable chiral nematic LC phase, was a turning point in the advancement of nanocellulose research and technology. The long-range orientational order of the nanorods paired with a helical variation of their alignment direction[163-164] defines the chiral nematic phase, also known as the "cholesteric" phase; as previously also called chiral or twisted nematic ordering of CNCs. The pitch of this helical modulation (in the chiral structure) is usually in the range of tens of micrometres in the fluid state, but during drying,

499   it frequently decreases to sub-micrometre values[165], causing dried films to Bragg to reflect visible
500   light, which means the substance obtains a photonic band gap with a consequent striking
501   iridescent colour [164]. Numerous attempts to use CNC films in innovative applications, such as
502   optical encryption[166] or chiral templates[167], have been motivated by the appealing optical
503   characteristics of this self-assembled bio-derived photonic crystal.

504   Since viscosity is one of the most important characteristics to characterise and process the LC
505   state, research on it began around 1900. These include emission and viscoelastic spectra [168]. Porter
506   and Johnson [169-170] published an excellent overview study on the rheology of LC, including
507   polymer LC, in 1967. Similar to polymer LC viscosity behaviour, well-sonicated specimens of
508   CNC reveal three distinct rheological zones as a result of the progression of LC formation and
509   ordering, including two shear thinning tendencies at low and high shear rates and a plateau at
510   medium shear rates[171] as described earlier. In **Figure 1b**, a typical flow curve related to LC entities
511   is depicted and is compared qualitatively against dilute, semi-dilute, and glassy state of
512   suspension also applicable to CNC suspensions. To achieve LC state in CNCs, upon increasing
513   the CNC concentration, one can observe the nanoparticles self-assemble into chiral nematic
514   organised structures that have textures resembling fingerprints [47, 171-173]. It's also important to note
515   that the previously stated effects of slip[174] and surface tension[175] can result in apparent shear
516   thinning behaviour that is readily misattributed to region I.

517   The growth in viscosity is not monotonous in an LC system, it might exhibit a maximum in the
518   concentration range where the two phases coexist. Viscosity typically increases in the isotropic
519   zone, but when it reaches the biphasic region, growth in viscosity is stopped, after which it
520   declines until it eventually rises again at greater concentrations. Other nanomaterials, such as
521   carbon nanotubes that have been treated with super acids, exhibit similar behaviour in a clear
522   manner[176]. At low concentration the preferred tumbling of rod-like particles during their
523   alignment in the flow direction, which necessitates a large, excluded volume, is what causes the
524   rise in viscosity, nevertheless, anisotropic phase forms when a certain concentration is attained.
525   The viscosity (stiffness) does not maintain the very same rates of rise with concentration as was
526   first reported because the flow gradually transforms to domains that slip one over the other and
527   need less free volume. Additionally, it is conceivable that the development of liquid crystals
528   reduces the amount of energy-dissipating CNCs suspended in the solution, causing viscosity to
529   decrease [177].

530   Rheological, optical, and scattering data support the idea that region I shear thinning results from
531   steady state molecular orientation; for systems with this region, molecular orientation in the low
532   shear regime is almost isotropic, whereas for samples lacking region I shear thinning behaviour,
533   shear structure is very ordered [43]. This discovery is consistent with the hypotheses advanced by
534   Larson and Doi[178] that the domain averaging when is sufficiently large to hold several liquid

crystalline domains, but that the domain size is tiny relative to the size of the averaging as a whole is a valid assumption for modeling suspensions of CNCs. CNCs within a single domain have ordering of liquid crystalline materials with a coherent orientational order however director associated with each domain can differ. If now one look at the whole system due to incoherent orientation of domains can perceive the overall macroscopic behaviour of the system to be isotropic despite at smaller scale, there exist local zones with anisotropic behaviour (See **Figure 1a**). Within the low shear regime, these domains can deform slightly and rotate. The model proposed by Larson and Doi[178] assume fluid within domains are not free flowing.

5.1 Flow behaviour

Steady shear viscosity flow curves may generally be affected by changes in the ratio of isotropic to anisotropic (entering biphasic region) state in suspension or changes in liquid crystalline domain size; therefore, formation of liquid crystalline domain can impact flow curves of CNC suspension. Sonication, as it impact not only charge but also average aspect ratio of particles for instance, can impose a direct impact on the structure and rheology of CNCs[22]. Sonication reduces viscosity by (i) increasing the aspect ratio of the CNC colloidal system in general, (ii) expanding the localized dense LC zones, and (iii) decreasing the effective volume fraction of the CNCs in contact with water. The critical viscosity—the level at which LC production begins—is pushed to a lower viscosity concentration as the sonication or CNC aspect ratio increases; therefore, at identical volume fractions ratio of crystalline to isotropic will increase.

Although the gradient of the viscosity vs. concentration curves in published reports on cellulose suspensions indicates a rise in biphasic coexistence, no clearly defined maximum exists[179]. This is due to the polydispersity of CNCs, which results in the formation of a broader biphasic region than theoretically predicted, resulting in a decrease in viscosity across the biphasic region, causing the maximum to either disappear or be confounded. [102]. As opposed to these set of observations, Li et al. [180] found that when particles interact and the double layer around them is thin, a local maximum in viscosity versus concentration develops. Therefore, it is possible that emergence of maximum is more easily seen when the double layer is thin.

Connection of a typical flow curves with microstructure of suspension mixed with combination of liquid crystalline and isotropic portion has been shown in **Figure 1a-b.** Because there is no microstructure system to act as a Newtonian fluid in the case of a dilute suspension of CNC, a shear thinning region that can only be explained by a biphasic suspension eventually appears in Region I with the addition of more and more CNC flow curves.

568
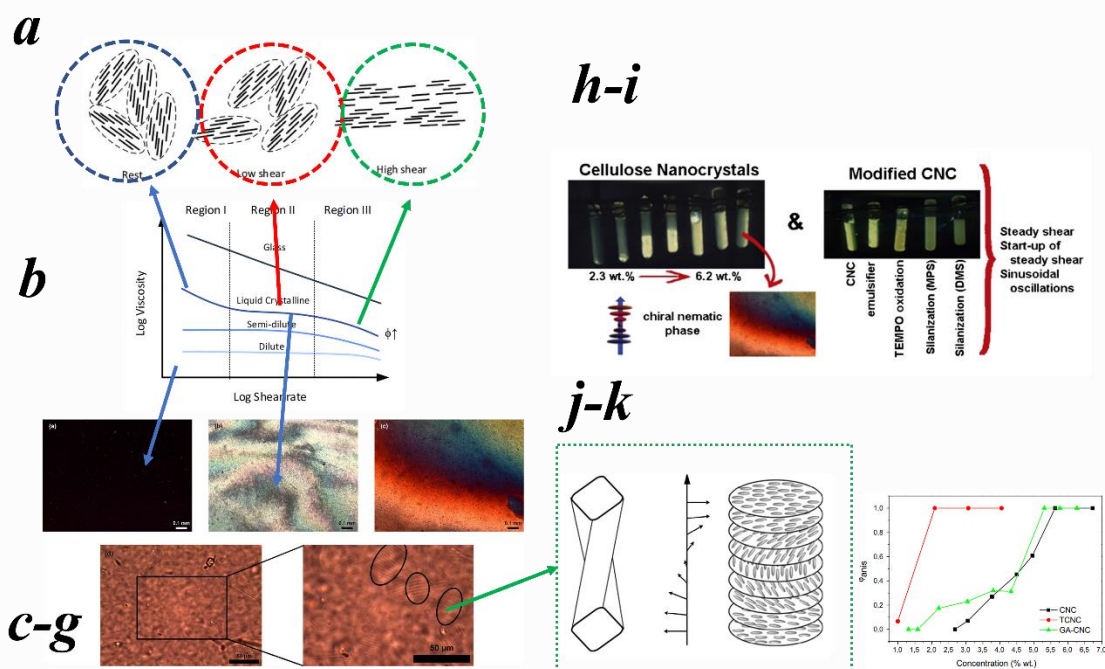
Figure 1. (a) Schematic of domain orientation based on lyotropic liquid crystalline theory. Adapted with permission from ref[102]. **(b)** The shear rate dependence of apparent viscosity for LC, dilute, semi-dilute, liquid crystalline and glassy rod's suspension. Adapted with permission from ref[102]. Visual demonstration of isotropic, biphasic, and liquid crystalline state of CNCs. Micrographs produced with crossed polarizers of CNC suspensions with concentrations in the **(c)** an isotropic, **(d)** coexistence, **(e)** liquid crystalline, and **(f-g)** anisotropic zones, the latter at a greater magnification. Adapted with permission form ref [181]. General liquid crystalline behaviour of CNCs in pristine and modified form **(h)** Photograph of tubes with increasing concentration of CNC (2.5–6.2 wt.%) between crossed polarizers and (right) volumetric fraction of the anisotropic phase as a function of the concentration. Adapted with permission from ref[181]. **(i)** Similar experiment now done on modified CNCs. Adapted with permission from ref[181]. **(j)** chiral nematic structure with directors shown in the middle. **(k)** ratio of anisotropic state in suspension of CNC and modified CNC. Adapted with permission from ref[181].

Figure 1 c-g demonstrates how such an isotropic suspension (a real suspension of CNCs) (1.0 wt%) does not rotate the light, obscuring the image between crossed polarizers; thus it denotes that system is isotropic under cross polarized light. However, when the concentration increases (4.0 wt%), a colourful picture forms, although with some black zones. At large levels (5.5 wt%), when the suspension is completely anisotropic, the colours take centre stage in the image. As seen in **Figure 1 g**, the rods eventually self-assemble into chiral nematic tactoids, displaying the

characteristic "fingerprint" of the chiral nematic LC phases. The fringes seen inside tactoids (enlarged image) are related to the pitch of the helicoidal arrangement. In biphasic materials, raising ionic strength up to 5 mM NaCl reduces the impact of chiral nematic domains, increasing viscosity at low shear speeds. The distinctive rheological properties of LC CNC suspension were investigated in refs. [22, 179], (systems were isotropic up to 3wt%) which also examined the effect of ionic strength on the rheology of the structure of CNC solution as a result of CNC concentration and NaCl concentration (0–15 mM).

For isotropic samples increasing ionic strength till 5mM of NaCl concentration due to compaction of double layer cause a reduction in viscosity however for anisotropic samples chiral domains become more compact and viscosity decreases [165]. In report of ref [91], low-charged CNC suspensions moved to a cholesteric state as the volume fraction rose, but highly charged CNC suspensions did not. To prevent electrostatic attraction from hindering the production of liquid crystalline domains in highly charged CNC, salt is required. Debatable still, however a twist in individual CNCs are required for formation of chiral structures that due to electrostatic repulsion is unable to exert its influence [182].

Beside simple flow curves additional tests such as startup test can provide more information on differences between isotropic and liquid crystalline states. For LC suspensions of rods, contrary to conventional polymers, the onset of continuous shear results in an oscillatory viscosity response that lengthens itself for considerable periods of time with a distinctly consistent period and is primarily dependent on the shear rate and the aspect ratio of the rods[183]. Additionally, the viscosity vs strain (strain = shear rate × time) measurements taken at various shear rates demonstrate that the oscillations have the same strain period[184-185] . Prior research has shown that optical characteristics like dichroism and birefringence exhibit comparable oscillations, demonstrating that the structure is what is causing the stress behaviour in [186]. All length scales in the polydomain structure were determined to vibrate with the same period [187] since the frequency of the oscillations did not rely on the wavelength of the light utilised in the optical test.

Rheological studies may be expanded to include situations in which CNC is combined with previously studied other ingredients such PEG, glycerol, gold nanorods[188], or even gum Arabic. In a thorough rheological analysis of CNCs in water, Buffa et al. [181] concentrated on the key traits of rod-like suspensions that align under flow and can display LC behaviour at rest, at least in a concentration range. Various surface treatment options on the CNC were carried out using TEMPO, chloro(dodecyl)dimethyl silane, and trimethylsilyl propyl methacrylate, also known as TEMPO-CNC, DCNC, and MCNC, respectively. The effect of adding a dispersing agent (gum arabic, GA) to the suspension was investigated. The stable suspensions created by the addition of CNC, TEMPO-CNC, and GA had a concentration range where isotropic and anisotropic (self-organized) phases co-existed in equilibrium (showed in **Figure 1h**). While exhibiting a similar

sort of rheological behaviour to the other nanocrystal solutions, the two silanized CNCs' aqueous suspensions, on the other hand, only displayed flow-induced ordering and had substantial quantitative differences. After a few hours of relaxation, these latter suspensions precipitated since they weren't stable. The observed variations resulted from either modification to the crystals' surfaces or the inclusion of a dispersion agent.

Figures 1h and **1i** show the impact of adding CNC on the isotropic to anisotropic transition in tubes and the liquid crystalline condition within modified CNCs, respectively. **Figure 1j** shows that the chiral nematic ordering of CNC is a macro domain that coexists with both isotropic CNC suspension. Under cross polarizers, isotropic suspension at low concentration appeared dark, middle concentration both stages (isotropic and LC phase) coexisted, and higher concentration specimen emerged anisotropic. Considering the percentage of phases requires optical inspection with a polarizer; these observations clearly show the role of surface treatment of CNCs; the transition (ratio of anisotropic vs. isotropic) shown is not sharp because of CNC polydispersity (see **Figure 1k**). **Table 3** represent connection between volume fraction at isotropic to nematic transition and volume fraction of single-phase liquid crystalline phase with references.

The rheological behaviour of CNCs was discovered to be significantly affected by the isotropic to liquid crystalline transition. **Table 3** was created using information from the literature to provide empirical values relating to the volume % of transition at the beginning of phase separation and the point at which it is complete, which results in the production of a single phase entirely liquid crystalline phase.

Table 3. Derived from the literature resources, a correlation between the volume fraction of the phase transition point and the volume fraction of the completely crystalline point was found with surfaces sulphate groups (0.89-1 wt%) and polydispersity (PDI) (standard deviation(std) around 30–50% of the average value).

Reference	Aspect ratio (l/d)	I-N (%)	LC (%)
21	5	2.5	6.8
189	67	2.1	4.9
190	28	1.2	5.1
190	19	0.5	4.3
27	31	0.5	2.6
191	14.3	2.0	5.1
190	22	3.0	5.8
192	18	3.5	8.9
52	28	3.4	7.8

| 52	30	3.1	7.4
26	16.5	3.1	5.1
52	24	4.7	9.1
52	24	3.5	8.2

648

649 According to Onsager's theory point of transition and point at which fully liquid crystalline state
650 is formed scales with aspect ratio as:

651 $$C_{I-N} = \frac{3.29}{L/d} \qquad\qquad (eq.7)$$

652 $$C_{LC} = \frac{4.19}{L/d} \qquad\qquad (eq.8)$$

653

654 Based on the information gathered here, Onsager's theory has been disproved. Which C (I-N) and
655 C LC are volume fractions at transition sites. The equation's inadequacy for use with aspect ratios
656 higher than 15 may be the cause of the divergence [193]. The variation could also be influenced by
657 the polydispersity of the CNCs used in the testing, which could hide the transitional point, and
658 the resolution constraints of precision optical microscopy. The beginning of the liquid to
659 crystalline transition is therefore seen at higher concentrations.

660
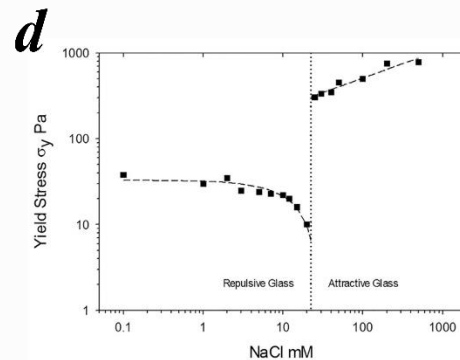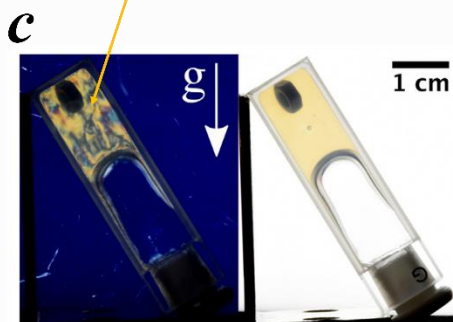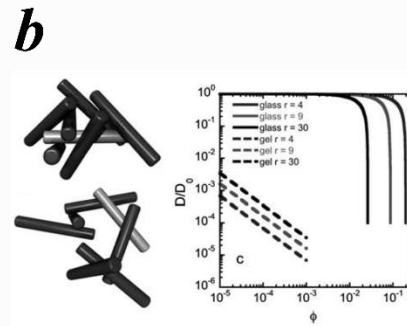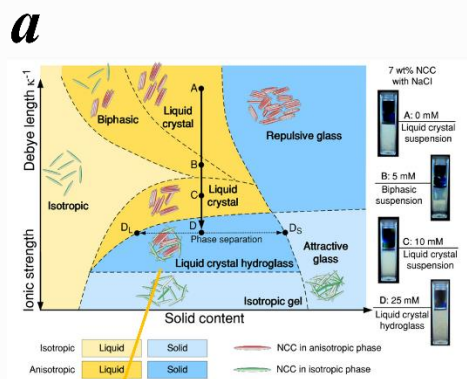
Figure 2. Phase diagram of CNC suspension and its related rheological traits. **(a)** Schematic phase diagram of NCC aqueous suspension as a function of solid content and inter-particle attraction (represented by ionic strength). Adapted with permission from ref [194]. **(b)** Effect of suspension structure on rod dynamics. Adapted with permission from ref. [150]. **(c)** Macroscopic appearance of the CNC-based soft hydro glass (2.0 wt% CNC suspension at 25 mM NaCl) in a 1 cm wide quartz cuvette containing a metallic nut after ca. 2 h ageing upright. Adapted with permission from ref.[195]. **(d)** Yield stress of 11.9 wt% CNC suspension as a function of salinity. Adapted with permission from ref [60].

Figure 2a shows that rising concentration at constant ionic strength, depending on the position on the graph, can transform an isotropic suspension gel into a glassy zone at the greatest concentration of CNCs (both effect of crowding and gelation impede particles movement). An isotropic material can transform instantly into a liquid crystal and subsequently into repulsive glass if the salt concentration (mM) is at the midpoint in the graph. The CNC suspension will initially encounter a biphasic region if the ionic strength is low, followed by liquid crystalline and repulsive glass phases. It is also possible to move perpendicularly to the phase diagram, as seen in the graph. **Figure 2b** is a demonstration of effect of crowding (glassy) and gelation on particle self-diffusive movement; graph sketched based on scaling theories presented in ref[150]. **Figure 2c** displays a hydro glass gel that has both yield stress and is birefringent as well. Hydro glass state has a biphasic structure comprising glassy matrix with liquid crystalline phase thus providing similar viscoelastic property to hydrogels with permitting reversible orientation of rods thus making structural ordering programmable[60]. **Figure 2d** displays yield stress chains as a function of addition of salt first yield stress decrease before it increases. This can be explained as when salt is added, the two conflicting effects on the repellent glass of CNCs:

(1) Compression of the double layer, providing extra wiggle room for the suspension that is already crammed (reduction in yield stress and storage modulus)

(2) Increasing inter-particle attraction by screening charges (thus increase in yield stress and storage modulus)

5.2 Deviation from Cox-Merz rule

The Cox-Merz rule is a phenomenological relationship in academia and industry to determine shear viscosity based on oscillatory shear tests[58]. The non-application of the Cox-Merz rule whenever salt is introduced and the existence of LC domains [181] are two more abnormalities regarding the rheological features of the CNC suspension. When the Cox-Merz rule is used, the shear viscosity vs. shear rate (s^{-1}) and the complex viscosity vs. angular frequency (rad. s^{-1}) agree.

696 The Cox-Merz rule does not apply to biphasic LC phases so because suspensions have a time-
697 dependent structure [21, 181]. The crystalline topology of suspension is the primary cause of
698 deviation for the LC system. The concentration at which the complex viscosity (η^*) and the
699 steady-shear viscosity (η) noticeably diverge from one another affects the growth of an ordered
700 domain. The observed difference between the constant shear viscosity and the complex viscosity
701 may be explained microstructurally by the rising alignment of the domain directors in the
702 polydomain structure of the solution, followed by the crystals. On the other hand, during the
703 sinusoidal oscillation testing, the alignment brought on by flow does not take place. The Cox-
704 Merz rule is not obeyed by such systems[196] because shear flow destroys structure but tiny
705 amplitude oscillations do not disrupt these structure.

5.3 Origin of chirality

708 Origin of chirality in CNC has been debated. Chirality is self-similar as it can be started from spin
709 of electrons, till formation of molecules, molecules into fibrils and later into supramolecules.
710 Chiral LC compounds (molecules or particles) commonly result in chiral mesophases[197]. To
711 prevent the interaction of right- and left-handed entities from cancelling out the chiral effects, the
712 system must not be racemic and the entity trying to build chiral structures must exhibit
713 asymmetry. Due to the cooperative nature of LC ordering, which is often sufficient to create one
714 domain handedness[198], a small quantity of chiral dopant can yield otherwise mesophases.

715 Chiral structure also interacts with light differently as the system may also interact differently
716 with left- and right-handed circularly polarised systems when chiral twist occurs, indicating that
717 these materials serve as polarisation filters [166]. In addition, intriguing optical interference may be
718 seen if the pitch of the twist is on the order of the light's wavelength; this interference with
719 incident light is what gives photonic crystals their colourful look.

720 For CNCs at the particle level, although the twist can be seen clearly in transmission electron
721 microscopy (TEM)[199] and atomic force microscopy (AFM)[200], the right-hand twist of cellulose has
722 already been noted in numerous experiment and simulation studies[199, 201-203]. However, the twist
723 per length of fibrils is still up for debate. In this respect, molecular dynamic simulation is a useful
724 tool for figuring out the twist of a CNC. In general, the twist is influenced by the diameter, or
725 more specifically, by the number of individual chains that make up the CNC[201]. In ref[204], authors
726 showed that twisting angle varies between 9.9 and 1.3 °/nm, for CNC with cross sectional that
727 contains 2 by 2 and 6 by 6 chains. Results of molecular dynamic simulation points to twist around
728 1.4 °/nm[204].

A polysaccharide called cellulose exhibits chirality on a variety of sizes, from the molecular to the supramolecular level as was discussed earlier. This characteristic has been used to produce chiral materials. Due in part to the variability of the cellulose samples obtained via top-down methods, the process of chirality transfer from the molecular level to higher-order assemblies has remained mysterious to this point. To shed light on origin of chirality in CNCs, authors in ref[205], suggested the use of well-defined cellulose oligomers as tools to explain how chirality is transferred from a single oligomer to supramolecular assemblies outside of a single cellulose crystal. This signifies that authors try to make CNC particles from their glucose precursors.

Synthetic cellulose oligomers with certain sequences self-assembled into thin platelets with adjustable thicknesses that were micrometre in size. These platelets then united into bundles with inherent chirality that was connected to the chirality of the monosaccharide. The chirality of the self-assembled bundles was altered by changing the stereochemistry of the oligomer termini, which made it possible to control the cellulose assemblies at the molecular level. Author's ability to regulate and fine-tune cellulose materials will improve this way because of the molecular description of cellulose assemblies and their chirality. Other polysaccharides with less well-understood supramolecular chirality might be included in the bottom-up strategy's use[205].
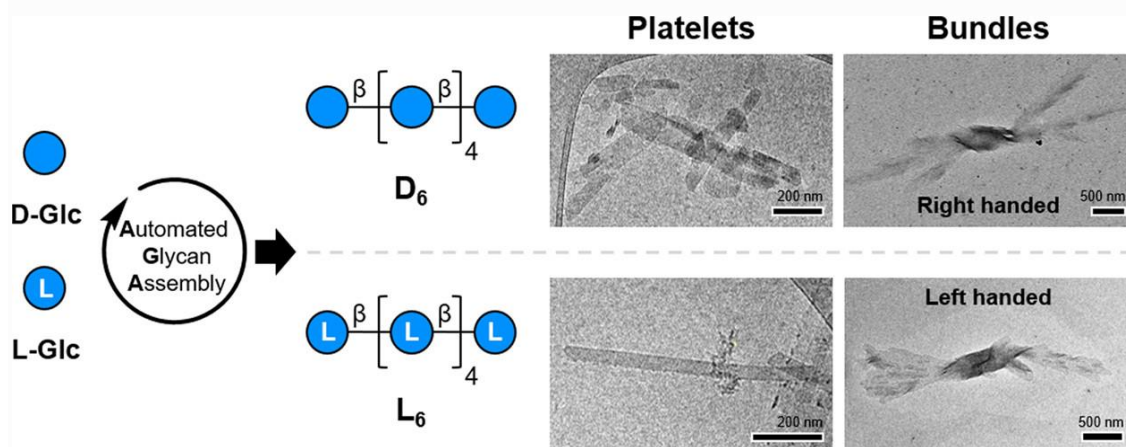
Figure 3. Origin of chirality. TEM image of D6 (1 mg/mL aqueous suspension) shows bundles of platelets with intrinsic chirality (red arrows). TEM images of D6 (1 mg/mL aqueous suspension) bundles showing an intrinsic right-handed chirality (scale bar 500 nm). TEM images of L6 (1 mg/mL aqueous suspension) bundles showing an intrinsic left-handed chirality (scale bar 500 nm). Adapted with permission from ref[205].

Authors[205], synthesized oligomers of natural D-glucose (D-Glc) and its enantiomer L-glucose (L-Glc) with clearly specified sequences were used to control the chirality at the sequence level.

These self-assembling cellulose oligomers had chiral characteristics that were directly related to the monosaccharide content of their bundles, aggregating into platelets with regulated dimensions. The solubility, crystallinity, and chirality of the bundles were significantly affected by the introduction of L-Glc units into the sequence of D-Glc cellulose oligomers. The relevance of the molecular sequence in determining supramolecular assembly and chirality is brought out by the bottom-up method used to analyse polysaccharide materials (see Left-handed and right-handed manufactured bundles in **Figure 3**) [205].

CNC themselves can export chirality to a materially foreign nematic liquid crystalline phase, for instance authors in refs[206-207], utilising a hydrophobic nematic liquid crystalline host as a reporter, recently confirmed that clean and chemically (hydrophobic) altered CNCs may convey chirality over space. To boost their chirality transfer effectiveness in comparison to plain CNCs or even CNCs functionalized with chiral molecules, these modified CNCs had their surfaces functionalized with achiral molecules that were chemically linked to the hydrophobic nematic liquid crystalline host.

6. Application

6.1 Aerogels

Aerogels are made through removal of water or liquid from hydrogels through various methods that has been covered in ref[208]. Aerogels are formed with the aim of producing value-added products such as light weight material for batteries, templating, thermal insulation to just name a few.
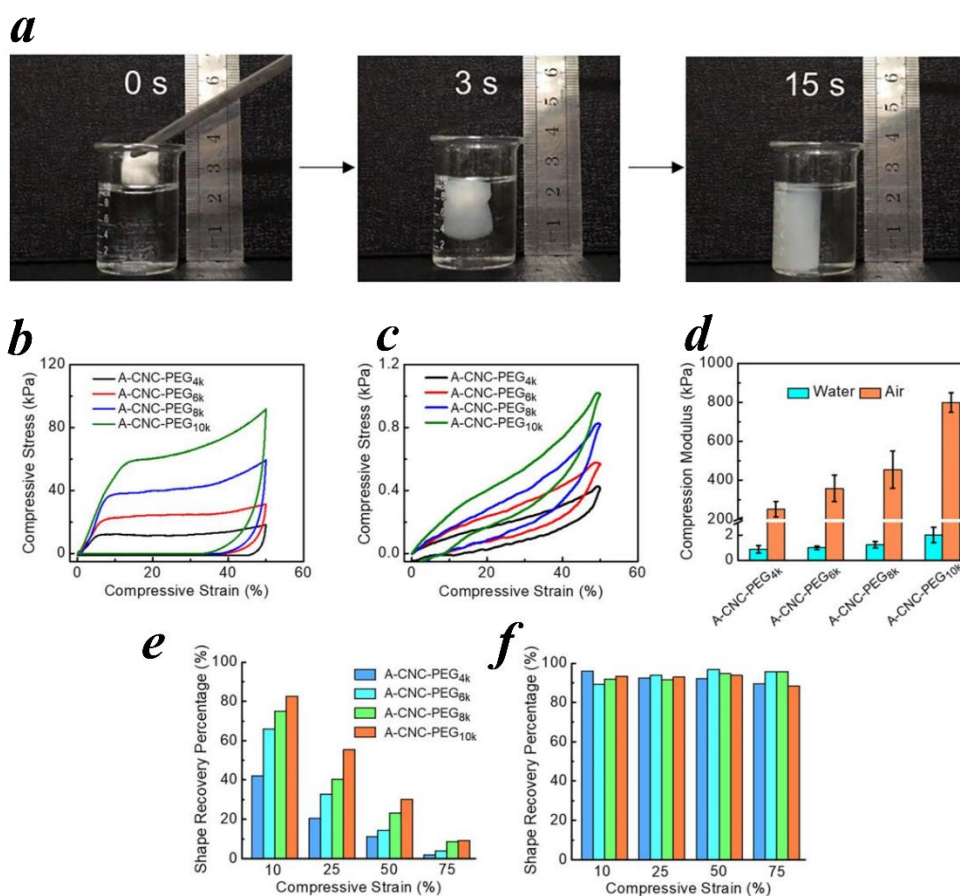
Figure 4. Shape recovery of CNC-PEG. **(a)** Photographs of shape-recovery process of A-CNC-PEG8k in water at different moments. Adapted with permission from ref. [209] **(b-d)** Compression modulus of aerogels of CNC-PEG4k, CNC-PEG6k, CNC-PEG8 and CNC-PEG10k in the dry state and in the water, as well as compressive stress-strain curves for CNC-PEG4k, CNC-PEG6k, CNC-PEG8 and CNC-PEG10k. **(e-f)** Shape recovery % of CNC-PEG4k, CNC-PEG6k, CNC-PEG8k, and CNC-PEG10k aerogels under various compressive stresses, in the dry state, and, in the presence of water. Adapted with permission from ref. [209]

Aerogels made of rod-like CNCs have been employed in anisotropic materials, adsorbent materials, and sensors; but, because of their low elasticity, they are difficult to handle and treat in real-world settings. Authors in ref [209] , cross-linked the CNCs with versatile polyethylene glycol (PEG) to create an aerogel with variable mechanical properties in various environments, taking inspiration from the sea cucumber, which transforms from rigid to flexible when its cross-link network of collagen fibres is weakened by stiparin inhibitor. This aerogel contained a hydrogen bond (H-bond) cross-link network in addition to a chemical-bond cross-link network, which was easily broken down by water. According to the findings, the CNC/PEG aerogel had a developed a highly of 0.80 MPa in its dry state and changed to an elastic condition (modulus of 0.87 kPa) in

794 its wet condition. When the strain exceeded 10% in the dry condition, the CNC/PEG aerogel's
795 shape change was irreversible; however, in the wet state, the shape change was completely
796 reversible. The humid aerogel might then transition back to its stiffer version after freeze drying,
797 which is an interesting transition from the irreversible strain in the dry state to the reversible
798 strain in the wet state; thus, in an event of pore collapse due to mechanical pressing aerogel can
799 be regenerated. The mechanistic research established that the solvation-controlled weakening of
800 the H-bond network between PEG and CNC was the source of these transition. This research
801 provided a straightforward yet effective design for stimulation-response aerogels that can aid in
802 elastification and form recovery.

803 To go into more details, the obtained CNC-PEG was found to be highly elastic, for instance
804 sample with PEG with average molecular weight of 8k could tolerate weight of 200 g without any
805 deformation; in contrast when aerogel became wet aerogel would lose its strength and unable to
806 sustain even 10 g of weight [209]. The compressive modulus of the sample with a 10k molecular
807 weight was almost four times higher, as can be seen in the **Figure 4**, indicating that mechanical
808 reinforcement increased incrementally with higher PEG molecular weight. Whenever the
809 compressed CNC-PEG was moved into the wet state, the unrecovered shape change in the dry
810 state may recover. These wet aerogels could also change from stiff to elastic after being frozen
811 and dried, and this process could be repeated several times. Even while A-CNC-modulus PEGs
812 somewhat dropped throughout the repeating transition, its shape-recovery characteristic barely
813 altered. The result of this study indicates that aerogel developed here might be good a candidate
814 for application such as packaging or thermal insulation however it might not be ideal for tissue
815 engineering or any application that requires the aerogel to get wet. Results also indicate under
816 dynamic condition hydrogel (wet aerogel) is more reusable than dry state aerogel.

817 For aerogel that are developed to be used as thermal insulator it is recommended to have higher
818 thermal resilience than unmodified CNCs. For unaltered CNCs, the findings in report [210]
819 demonstrated that two impressive pyrolysis processes were present during the destruction of
820 CNCs containing acid sulphate groups, which began at a lower temperature. The derivative
821 thermogravimetric curves' profile analysis revealed that each pyrolysis process was made up of
822 many different processes. The deterioration switched to a higher temperature and took place
823 within a constrained temperature range when it was neutralized by NaOH solution. Investigated
824 was the impact of cellulose particle size on degradation. The findings showed that small-sized
825 cellulose degraded at a lower temperature, which aided in the development of char residue.

826 In a similar report[211] focused on deciphering thermal degradation of CNCs, authors examined the
827 heat breakdown of acidic CNCs (CNC-H), which had sulphate half-ester groups on their surface,
828 and neutralized CNCs (CNC-Na), in which the protons have been replaced by sodium ions, and
829 microfibrillar cellulose filaments (CFs). CFs had the highest thermal stability of the three (325 °C)

830 despite having a simple degradation process connected to extensive dehydration,
831 decarboxylation, and decarbonylation as well as an abundance of amorphous regions that make
832 them structurally and morphologically less homogeneous than CNCs with high crystallinity. In
833 contrast, sodium counterions in CNC-Na can improve thermal stability up to 300 °C, in which
834 the pyrolysis leads to partial rehydration and the formation of sodium hydroxide on surfaces.
835 CNC-H decompose in a complex manner below 200 °C, with large char fractions and the
836 evaporation of sulphur compounds at high temperatures. Therefore, it seems that addition of salt
837 in cases that is dually gelify and improves thermal degradation of CNC can be a preferred method
838 of aerogel formation. Research should be continued to decipher impact of other ions such as
839 divalent and multivalent ions on CNC thermal degradation behavior.

840 There are additional mechanisms described in the literature that can lessen the thermal
841 degradation of CNCs. For example, coating CNC with lignin has been suggested because it not
842 only reduces the density of the material by creating a foam when combined with acrylonitrile
843 butadiene styrene, but also increases the product's tensile strength, storage modulus, and thermal
844 stability[212]. Maximum degradation temperature shifting to higher temperatures was
845 demonstrated to significantly increase thermal stability. In another report when mixed with PVA,
846 in comparison to clean PVA, CNC or CNF inclusion in the PVA matrix did not significantly
847 change temperatures at the start of degradation or at the point of maximal degradation during
848 the main stage of pyrolysis. The maximal rate of degradation was, however, reduced by the
849 addition of nanocellulose, with bigger reductions occurring at higher filler levels. After the
850 significant deterioration peak, a larger fraction of the composites' initial mass was still
851 preserved[213].

852 Aerogel can be further mixed with other nanoparticles; this will ensure additional functionalities
853 added into the mix. For instance, specialized components made from biomaterials have become
854 a potential trend to reduce the usage of petroleum derivatives. The usage of electronic systems
855 today has, on the other hand, conditioned the production of electromagnetic waves that interfere
856 with highly accurate equipment and are harmful to human health. To lessen the dispersion of
857 microwaves emitted or received from a device, strong, lightweight, and conductive
858 nanocellulose-based aerogels combined with carbon nanotubes has emerged as an
859 electromagnetic interference (EMI) shielding biomaterial. Increase EMI shielding effectiveness
860 for application in which beside thermal insulation, shielding is also required , the cover also needs
861 to provide shield against penetration for electromagnetic waves. Study in ref[214], suggested an
862 effective aerogel method to block radiation by combining sodium alginate, cationic CNCs, and
863 TEMPO-oxidized cellulose nanofibrils with carbon nanotubes at different concentrations.
864 Aerogels were produced that are low density (density 0.075 g/cm3), highly porous (porosity >
865 95.47%), conductive (up to 26.2 S/m), mechanically robust, and EMI-protective, demonstrating
866 their potential.

867 In some instance, conductive moieties can also be coated onto CNC or CNF for EMI shielding
868 applications. Efforts were concentrated on surface modification of cellulose filter sheets so that
869 they might serve as reliable substrates to reduce EM contamination. Most of the research was on
870 creating conductive cellulose sheets by covering filter papers with conductive inks made of
871 carbon nanofibers, carbon nanotubes, and silver nanowires (AgNWs). These cellulose-based
872 conductive materials showed a high degree of flexibility, an average porosity of 64.7%, and an
873 apparent low density of 0.53 g/cm3. The greatest electrical conductivity they were able to produce
874 with this method was 67.51 S/cm at 0.53 vol% AgNW, and the effective EMI shielding efficiency
875 (EMI SE) value was w48.6 dB at an extremely low thickness of 164.2 mm[215].

876 Aerogels and the topic of photonic crystals can be combined, making aerogels responsive to the
877 absorption of a solvent or liquid because it affects the aerogel's pitch length. The colour of the
878 aerogels produced in ref[216] ranged from white, which results from light scattering to a reflecting
879 photonic crystal that displays vivid iridescent hues depending on the solvent submerged. The
880 pressure-responsive photonic aerogel is used to create a solvent-sensitive ink that reacts quickly
881 to various solvents. This substance exhibits a novel response mechanism for the development of
882 mechanoresponsive and intelligent photonic materials.

883 Research in producing value added products in form of aerogels from nanocellulose is being
884 continued currently.

6.2 Photonic crystals and responsive materials

887 The chiral nematic ordering of CNC can produce a period structure called "photonic crystals"
888 similar to other inclusions such as Tobacco mosaic virus[217], other viruses [218], DNA
889 fragments[219],poly(tetrafluoroethylene)[220], flagella   filaments[221],
890 collagen[222], boehmite[223], cellulose[224], chitin[225], and κ-carageenan[226], synthetic polypeptides (poly—
891 benzyl-L-glutamate PBLG) [227], and polysaccharides (xanthan and schizophyllan) [228]; these
892 materials all show LC formation behavior that is entropy driven. Liquid crystalline phase periodic
893 structure can be maintained both in dried or wet state in 3-D; all these materials are focus of
894 intense investigation to uncover more about their connection between periodic arrangement and
895 their tunable color display; these efforts are easily extendable to CNCs as nature of ordering and
896 coloring are merely physically stemmed. There is still debate on how chiral structure are formed
897 and what are the necessity some argue that inclusion such as CNC have to have chirality within
898 themselves that translate into chiral structure[229] however chiral inclusion such as tobacco mosaic
899 virus cannot form cholesteric or nematic phases.

900 One notable inclusion that share many similarities with CNC is Deoxyribonucleic acid (DNA);
901 the LC phase behaviour of aqueous solution of DNA has been researched extensively by various

optical and scattering techniques since the 1950s[230]. These investigations have showed that duplex DNA, which is a semiflexible polymer with a 500 nm persistence length in aqueous solution [231], is stiff enough to create bulk nematic and columnar LC phases. Since Rosalind Franklin used shear alignment in filaments of hydrated DNA in the columnar phase to produce x-ray diffractograms of oriented single DNA duplex strands that enabled the decipherment of the DNA duplex structure [232], the generation of oriented domains of these phases has been of interest.

According to Onsager's theory[233], a network of long, hard rods interact solely antagonistically, form an orientational pattern, and reach a concentration threshold that is less dense than maximal packing. Initially, rod virus studies were the focus, but after authors discovered the chiral LC property of CNCs in 1959, additional research[40, 234] was carried out to understand the full potential of these self-assembly hierarchical processes. Gray et al. [235] similarly created chiral nematic LCs at low concentrations for another cellulose derivative, hydroxypropyl cellulose. Years later, Revol and coworkers showed that raw materials obtained from cellulose may create a stable lyotropic chiral nematic liquid crystal phase structure.[47, 172].

Cholesteric structures are layered without internal positional ordering; each layer has its own director axis; the axis changes periodically as 3-D structure out of layers are created; director rotates slightly between layers as structure is progress upward. The distance required to complete a full turn of the director also known as pitch length; pitch length can be measured through looking at the peak of the reflected light and can be directly viewed using POM or scanning electron microscopy (SEM). Optical microscopy however has limitation and seldom as accurate as SEM; due to poorer resolution due to usage of higher wavelength of light as electron beam pitch lengths estimation are somewhat an overestimation. The fringe pattern of liquid crystals is muddled with these comparable interreferences because of helicoidal quasi-layers with an angle orientation, different undulations, and interference fringes that may be seen under an optical microscope[236]. At high concentrations, simple aqueous solutions of DNA, a semirigid, strong polyelectrolyte, experience a sequence of transitions between anisotropic phases, including a cholesteric liquid-crystalline phase with a pitch of 2 μm[237]. At a concentration of 250 mg of DNA/mL of solution, sonicated calf thymus DNA with an average length of 100 base pairs was found to form a cholesteric liquid crystal. Small, organised domains of a few micrometres develop immediately after preparation, resulting in an opaque solution. This liquid crystal may easily be directed in an NMR magnet's magnetic field, resulting in a distinct birefringent phase. The DNA molecules aligned with their helix axes perpendicular to the field, resulting in the cholesteric pitch axis being parallel to the field. The optical tests (optical light rotation) and NMR measurements both yielded a pitch length of 2.5 μm for the cholesteric phase (solvent diffusion)[238].

Generation of "tactoid" in the biphasic region was recorded by Gray and colleagues [47]; these tactoids were spherical, ellipsoidal, or spindle-shaped droplets that, when subjected to

938 hydrodynamic forces, tended to join into continuous anisotropic phases [239]. The pitch of the
939 helical organization of CNC in "wet state" is in order of tens of micrometer range; however,
940 after water drying it comes to less than one micrometer in size due to evaporation of water from
941 gaps between the liquid crystalline formations. Moreover these structure were found to have
942 excellent fracture toughness as shown by the cuticles of lobster[240] and other sea
943 microorganism[241], which is connected to fracture energy dissipation via the helix patterning of
944 the fibrillar chitin matrix, an essential rod structure. Chiral organization in colloids is
945 determined by hydrodynamic and thermodynamic; the pitch and its orientation within CNC
946 suspension is impacted by size, charge density, concentration, and ionic strength of the media
947 in which CNCs are floating in. Prior research has shown that augmenting the sulphate
948 concentration increases the pitch value in solid films, in CNCs, the acid hydrolysis process that
949 can be varied by reaction time, acid concentration and temperature of reaction can control the
950 sulphur content[34]. As a reported example; through increasing concentration from 2.5 to 6.5 vol%;
951 the average pitch size saw a reduction from 15 μm to 2 μm with twist angle also undergoing
952 changes from 1° to 4° [189]. Pitch value sizes reported in the literature are 10 to 60 μm [26-27, 172, 242].

954 The literature is also interesting to understand role of surface charge on twist and chirality of
955 CNC ensembles; for instance, Revol and Marchessault claimed, CNC Chiral nematic phase
956 transition is created by the twisted spiral shape of CNCs[47]. Examination through small angle
957 neutron scattering also detect the twisted spiral cylindrical shape of CNCs[24, 243]. Recently, using
958 optically inactive dyes[244], AFM[200, 245], molecular dynamic simulations[201, 204, 246], the right-hand
959 twist in CNCs is proven. Araki and Kuga reported production of CNCs back in 2001 from
960 bacterial sources; suspension of bacterial sourced CNCs initially did not show chirality however
961 after addition of electrolytes the solution phase separated into chiral nematic liquid crystalline
962 structures; authors reasoned that addition of salt make the twist bare that before was hidden by
963 impact of electrostatic repulsion. Thus it is reasonable to assume that twist of CNCs leads to
964 formation of twisted chiral structure as well [49]. The issue of chirality in CNCs is still hotly
965 debated if this issue becomes unlocked it is possible that using for instance chiral dopants
966 chirality[197] can be seen in CNCs at lower concentrations.

968 Changing the structure of the cholesteric helix offers great potential for developing stimuli
969 response (may rely on humidity, temperature, phase transition, etc) materials capable of
970 matching the complexities of biological systems. Because the underlaying nanostructure dictates
971 the reflected colour structural response to an external stimulus, low-cost biodegradable optical
972 sensors are available. Using CNC-based sensors, humidity[247-248], solvent[249], and measuring
973 pressure[249] have all been measured. These sensors can be read with the naked eye by observing
974 how the coloration of chiral liquid crystals changes in response to humidity, solvent, and
975 pressure; however, UV-Vis can read reflected wavelength more precisely.

CNCs-based films, for example, are beneficial due to their inherent sensitivity to water. Because of their low water resistance, they lose their prized iridescent tint even after being slightly swollen by water, limiting their employment in environments with high humidity[250]. Due of its high sensitivity to humidity, the CNC chiral structure is an effective humidity sensor. In contrast to humidity fluctuations, the co-assembly of CNC with oxidised starch and tannic acid was recently examined to improve CNC's solvatochromism. After being immersed in water for 24 hours, the composite film retained its structural integrity and brilliant structural colour; moreover, mechanical properties[251] were enhanced due to tanning acid cross-links.

Sometimes, in addition to coloration, the CNC is required to produce coatings with specific mechanical properties that are edible and mechanically robust, such as by adding proteins or other edibles. For instance, one study shows that treating CNC with tannic acid or starch does not interfere with the self-assembly process. The amount of sensitivity of the chiral structure of CNC towards humidity of solvents in general may be made adjustable because of the knowledge provided here; that is, the chiral molecules reaction to humidity may be enhanced or lowered based on the level of assembly with other agents like as starch or tannic acid.

He et al.[252] were able to make CNC composite films that reacted to humidity and mechanical compression by utilising glycerol as a plasticizer. The films' chiral structure[252] could be made sensitive to change the structural colour. When exposed to 16 to 98 percent relative humidity, the film demonstrated reversible colour change. Furthermore, by altering its iridescent colour, the film could sense compression pressure quantitatively. CNC-based films can also exhibit a dual reactivity to humidity and formaldehyde gas[253], with reversible structural colour change, inducing gas detecting characteristics on CNCs. When compared to a single formaldehyde response[253], when the film is exposed to a humid environment, the colour alteration induced by formaldehyde can be changed from invisible to noticeable.

CNC's chiraloptical characteristics may also be made adjustable with respect to specific solvents. Based on this, the researchers devised a novel method for producing mesoporous CNC sheets. Giese and colleagues[249] used a composite of CNCs and a urea-formaldehyde (UF) resin with an alkaline solution to make highly porous photonic cellulose (MPC) film that could change structural colour in the visible light range fast and reversibly in a polar solvent. They discovered that the maximum reflection wavelength of the composite material in 100 percent ethanol was 430 nm, whereas it was 840 nm in pure water. The tint will "red shift" as the water content increases. The synthetic cellulose films demonstrated remarkable flexibility due to their reduced crystallinity (relative to the crystallinity of the initial CNC films) and the highly porous structure formed by supercritical drying. Furthermore, owing of its rapid and reversible colour shift upon swelling, this MPC film is ideal for pressure sensing. These novel active mesoporous

1012 cellulose materials might be useful in biosensing, functional membranes, chiral separation, and
1013 tissue engineering.

1014

1015 PEG-induced "depletion attraction" has been allowed in a number of systems, including DNA
1016 and lyotropic LC [254-255]. Changing the molecular weight of PEG can change the optical
1017 characteristics of CNCs with chiral nematic structures[256]. Because pure CNC films are brittle,
1018 several water-soluble polymers have been added to increase film flexibility and mechanical
1019 strength, including poly(vinyl alcohol) [127], PEG, and polyurethane[257]. The colour of the film may
1020 be modified by changing the pitch size of these water-soluble polymers. As a result, adding PEG
1021 has two effects: one, it raises the mechanical characteristics of the CNC film, and second, it alters
1022 the pitch size due to depletion forces. Iridescent colours may be changed from red to blue by
1023 depletion by varying the proportion of polymer; however, mechanical qualities can also change
1024 with polymer addition. The concomitant rise in mechanical properties opens up a wide range of
1025 applications, such as humidity sensors, force sensors[258] and anti-counterfeiting papers[166].

1026 To offer some data, the reflectance spectra of pure CNC films exhibit a peak at 242 nm that grows
1027 to 361 nm when the PEG weight fraction increases up to 30 wt percent; moreover, when the PEG
1028 concentration surpasses 25 wt percent, the reflectance band becomes significantly broader.
1029 Tuning reflection spectra may produce items such as inks[259] [256], home décor, and so on. The half-
1030 pitch diameter increases from 103 nm to 143 nm when the PEG weight fraction increases from
1031 10% to 20%. The pitch size can also change by modifying the molecular weight of the non-
1032 adsorbing polymer; similar behaviour was demonstrated in ref[256].

1033 Confinement can also impact LC formation for CNCs. The easiest form of LC under confinement
1034 is the evaporation of a tiny volume of iridescent solution on a Petri plate, which results in thin
1035 sheets; in this case confinement starts when the layer close to the petri dish is very thin. Brilliant
1036 structural colours may be generated even when the thickness of such films is just an order of
1037 magnitude larger than the pitch length [260-261]. A planar orientation of the cholesteric nanostructure
1038 is easily formed in such thin-film confinement[262], even under quick-drying circumstances where
1039 disclinations in the cholesteric order are supposed to be kinetically confined. The discontinuous
1040 pitch shift caused by these disclinations is critical in extremely thin films (approximately 1-2 nm)
1041 and can result in a mosaic of different colours [263]. Some accounts claim that confinement leads the
1042 bulk isotropic-to-nematic transition to become a continuous ordering from a parametric to a
1043 nematic phase; moreover, confinement obscures translational order in smectic crystals[264].

1044 A range of cellulose nanocrystal (CNC)-based nanocomposite materials were developed and
1045 tested to reproduce the cholesteric colourful creatures observed in nature. CNC/Gly films
1046 displayed reversible reflection colours with altering relative humidity due to glycerol's strong
1047 water absorption ability. **Figure 5a** shows a white-light picture; digital photographs of pure CNC

and CNC/glycerol (Gly) composite films were also taken concurrently. The top blue, green, red, and colourless films are pure CNC, CNC/Gly20, CNC/Gly40, and CNC/Gly50 composite films. The CNC/Gly20 film is put on a flower and folded at the bottom to form an iridescent bridge. [259]. These photos show colour variations caused by the addition of glycerol to CNC. **Figure 5b** depicts a schematic of the glycerol assembly. The produced films are also highly robust due to their ability to be folded, twisted, reinforced, and compressed; they may be employed for a wide range of purposes and characteristics (See **Figure 5c**). At changing degrees of relative humidity, produced composite film displays comparable hue variations to how the colour of a beetle varies in a dry and wet environment (See **Figure 5d**). In summary, the researchers created humidity-responsive films, photonic inks, and iridescent coatings using a range of multifunction structure nanocomposites with adjustable and tunable colours. By varying the glycerol content of the CNC composite films, the colours of the reflections can be altered as shown in series of figures displays in **Figure 5a-d**.

Figure 5e shows a sequence of images for the CNC/PEG film with ratio of 80/20 exposed to cyclic humidity conditions. The dry film was subjected to humid air at relative humidity (RH) values ranging from 50% to 100%, and structural colour changes in the visible spectrum were observed. The sample had a comparable green colour at 30 percent and 50 percent RH. As the RH increased from 50% to 100%, the film transformed from green to olive, brown, orange, dark-red, and clear, which is consistent with the UV reflectivity. The expansion of the multilayer structure due by penetration of water leads the structural colour to shift to red at high humidity. When the RH was reduced, the change in periodic multilayer structure was reversed. After the RH was gradually reduced from 100% to 50%, the transparent film returned to dark red, orange, brown, olive, and green. **Figure 5e** depicts the manufacturing of CNCs/PEG composites with chiral nematic structure caused by cellulose nanocrystal self-ordering; additionally, Chiral moieties were characterized by analyzing transmission and reflection spectra of CNC and CNC/PEG films with ultraviolet and visible reflectance at 30% relative humidity. The results clearly reveal that the interaction with light of CNC and PEG is adjustable, i.e., PEG addition modulates the pitch length and chirality of CNC in solid films. Furthermore, the colour shift of composite film was evaluated visually in response to tuning (increasing\decreasing) humidity values ranging from 30 to 100 percent; hue shifts with relative humidity are striking. **Figure 5h** depicts that although the peak location varied slightly, the plot remained consistent, and the shift in peak position was reproducible and reversible, indicating the composite film's excellent stability and reversibility.
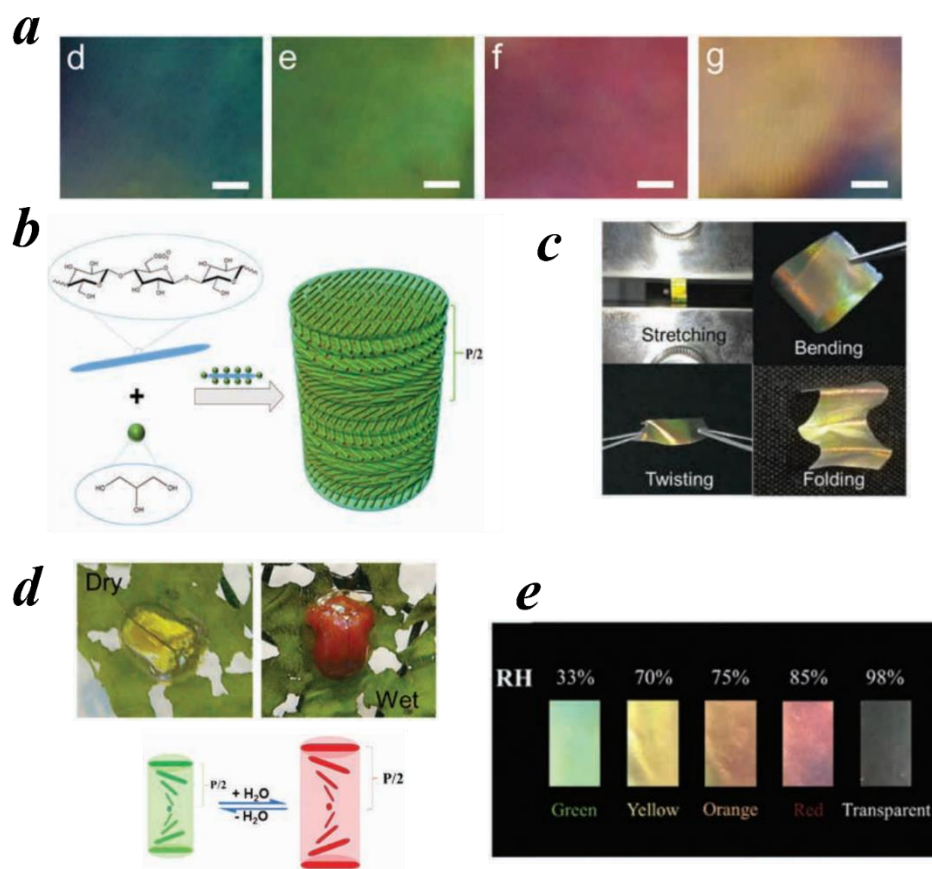
Figure 5. Colorized CNC-PEG nanocomposite. **(a)** POM images of CNC, CNC/Gly20, CNC/Gly40 and CNC/Gly50 films. **(b)** The mechanism for assembling cellulose nanocrystals and glycerol into chiral nematic structures is depicted schematically (P/2 denotes the half-helical pitch). **(c)** CNC/Gly30 composite film under various deformation conditions **(d)** Color changes in the beetle back in a dry and wet environment. Adapted with permission from. [265]. **(e)** Under various RH conditions, the CNC/Gly20 film displays various colors. Adapted with permission from ref[259].

Suspension may also produce a variety of iridescent colours, which are tunable owing to uneven film development on various surfaces. The effect of CNC cholesteric phase growth as a function of the substrate on which the solution dried out was examined in ref[266]. When CNC dispersion was dropped on the substrates, the impact of the substrate on the fading out of CNC suspension and its liquid crystal formation behavior was observed. On stainless steel (SS) and glass, CNCs exhibited initial contact angles of 57.32 and 37.83, respectively. The cholesteric layer self-assembled from the droplet's bottom centre and diffused to the hydrophilic glass substrates' edges[267]. As a result of the edge-centre ordered drying technique 135, the iridescent coating films formed on PS, SS, glass, Cu-Zn alloy, and Cu-Ni alloy display characteristic "coffee rings." The

1098 conclusions of this study apply to spray coating on a variety of substrates; research reports on
1099 whether iridescent colour spontaneously appears on examined surfaces. As a stimulus-response
1100 material, developed iridescence can indicate the nature of the surface.

1101 Thermotropic LCs are interesting guests to be included in chiral systems because they display
1102 large variations in indices of refraction and molecular alignment in induced by temperature
1103 changes, providing a thermal switch to regulate reflection in chiral nematic highly porous organo-
1104 silica films. In 2013, researchers used the thermotropic liquid crystal 4-cyano-4'-octyl phenyl
1105 (8CB) [265] to penetrate octyl-functionalized chiral nematic organo-silica films. The films are very
1106 iridescent at room temperature; when heated, they rapidly change to colorless at the nematic to
1107 isotropic transition point for 8CB at 40 °C.

1108 The absence of the reflection signal in the UV-vis spectra for the LC-loaded films clearly
1109 demonstrates the changes in optical properties. In ref[268], poly(N, N-dimethylamino ethyl
1110 methacrylate) was bonded on CNC, and the resultant lyotropic fingerprint texture varied with
1111 temperature[268]. As a result, future study should focus on this feature of CNC chiral structure as
1112 well. SEM was used to examine CNC film cross-sections, and optical microscopy was used to
1113 examine CNC photonic film pitch; the findings revealed a low-temperature dependence[269]. The
1114 cholesteric stripe's bright and dark margins were not equal, and their difference changed
1115 significantly depending on temperature and nematic phase type. The transition between
1116 (calamitic and discotic cholesteric — ChC and ChD) and one biaxial cholesteric (ChB). Optical
1117 microscopy[270]was used to view the ChC-ChD and ChB-ChC transitions.

1118 The alteration of photonic material optical properties is an important aim in the development of
1119 reflective screens, filters, and detectors. The optical properties of optical substances might be
1120 adjusted by treating both their periodic and refractive index difference. Guests placed within the
1121 channels of a chiral nematic mesoporous host might allow for stimuli-induced changes in
1122 refractive index and hence dynamic modification of the optical properties of the composite.
1123 Therefore, CNC chiral structures may be made temperature change programmable.

1124

1125 Responsive photonic materials are useful in development of sensors, optical filters, inks, among
1126 other [271]; for instance; lyotropic left-handed chiral nematic phases are commonly utilized for
1127 pressure or temperature sensors [249, 272]. It is very simple to understand how a pressure sensor
1128 works because applying pressure to a chiral structure that contains CNC can result in different
1129 pitch sizes, which in turn produce different colours and circularly polarised light angle
1130 dependency behaviour. In a similar way, a temperature sensor works because the polymer or
1131 material used to embed the CNC chiral structure should be temperature-sensitive, such as
1132 PNIPAM or thermos-responsive surfactants. The degree of tuning pitch length can be enhanced
1133 further if the PNIPAM is additionally covalently connected to the photonic crystal components.

In ref[273], as the opal was warmed to 50 ° C in an aqueous solution, a colour change from green to white was noticed, indicating that phase separation had occurred.

Similarly a solvent can change pitch size therefore CNC chiral hydrogel can be used to take advantage of these changes in pitch size; as shown in ref[272]. In terms of solvent, ionic strength, and polymer, the chiral structure is responsive. chiral structure formation in the presence of PAAm monomer; chiral structure locking utilizing polymerization of PAAm; 66wt% CNC implanted in the composite with varying amounts of sodium chloride; increasing ionic strength alters the reflectance Image of an iridescent photopatterned PAAm nanocomposite swelling in water. The masked zone swells quicker, resulting in a latent picture (a photograph of the patterned film before swelling is given in in the inset).

SEM of the dried nanocomposites displays a layered structure and a smooth surface, which is compatible with the chiral nematic texture reported by POM. Hydrogels with a low CNC concentration have a wrinkled structure with a repetition distance of several micrometers over the film's thickness (**Figure 6(b)(i)-(ii)**). In contrast, SEM of an iridescent hydrogel with a high CNC concentration revealed a significantly shorter helical pitch, on the order of hundreds of nanometers, consistent with its iridescence (**Figure 6(b)(iii)**). The left-handed twisting rod shape of the NCC chiral nematic phase is seen at higher magnification, matching micrographs of pure NCC (**Figure 6(b)(iv)**).
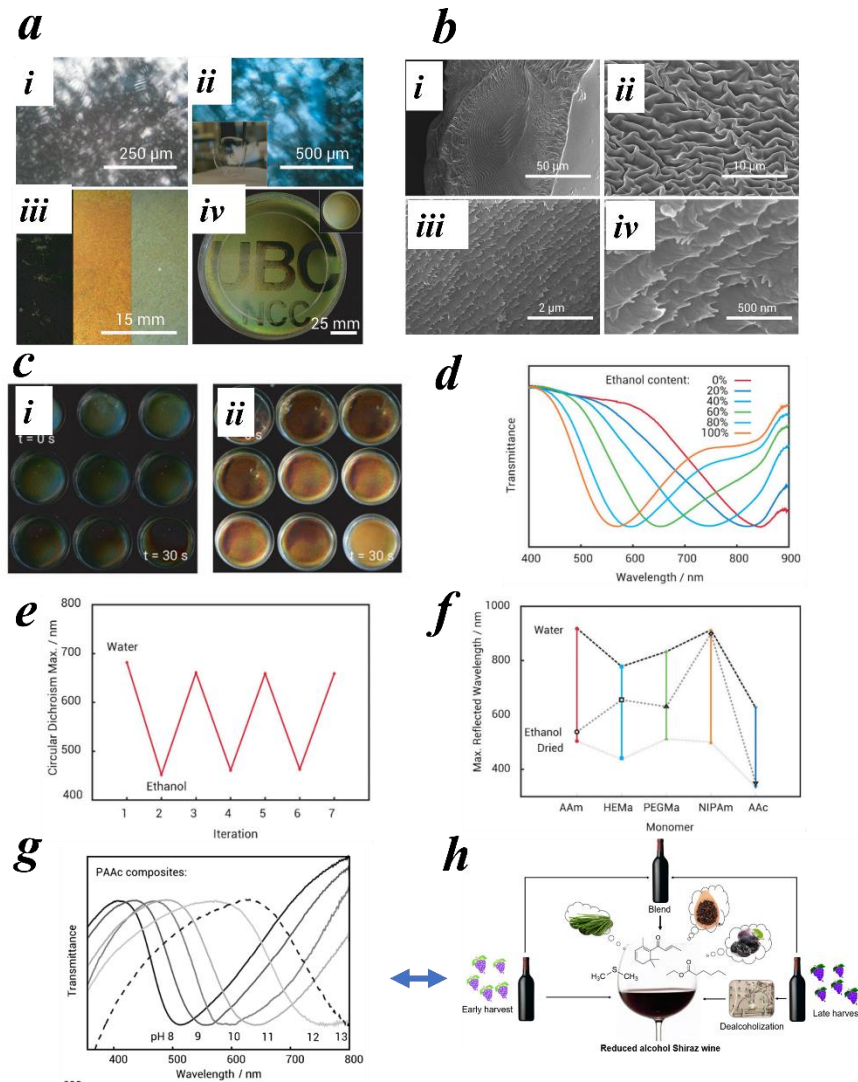
1153

Figure 6. Responsive chiral structure with respect to solvent; ionic strength and polymer. (a) (i) Formation of chiral structure in presence of monomer of PAAm; (ii) locking in chiral structure using polymerization of PAAm; (iii) 66wt% CNC embedded in the composite with various amount of sodium chloride; increasing ionic strength shifts the reflectance (iv) Photograph of an iridescent photopatterned PAAm nanocomposite as the film swells in water. The masked region swells at a faster rate, producing a latent image (a photograph of the patterned film before swelling is given in in the inset). (b) (i) SEM images of composite containing only 10wt% CNC showing fingerprint defect Adapted with permission from [272]. (ii) higher magnification of the same concentration shows wrinkled texture Adapted with permission from [272]. (iii)side view of an iridescent composite containing (66wt%) CNC showing helical pitch Adapted with permission from [272]. (iv) Display of left-handedness of the structure. Adapted with permission from [272]. (e) cyclic response of hydrogel to water and ethanol Adapted with permission from [272]. (f) Tunning hydrogel monomer a way tunning

iridescence Adapted with permission from [272]. (g) response of hydrogel (made with PAA monomer) to pH; maximum wavelength reflected increases from 500 nm to 650 nm as pH increases from 8 to 11. Adapted with permission from [272] (h) A possible application of hydrogel can be in wine industry due to non-toxicity presence of water and ethanol and ease of application of the hydrogel if it's soaked in the wine bottle. Image adapted with permission from ref. [274]

The reflected hue of the nanocomposite hydrogels may be altered reversibly by swelling in different mediums. A hydrated PAAm nanocomposite, for example, exhibits a fast blue-shift following immersion in pure ethanol (see **Figure 6c**). Soaking same composite in mixture of water and ethanol causes a gradual blue shift with increase in alcohol concentration; quantified in **Figure 6d**. The colour shifts are completely reversible; the nanocomposite hydrogels may be submerged in different media or dried and reswollen in water for several cycles with no discernible change in the chiral nematic optical characteristics based on results displayed in **Figure 6e**[272]. Swelling response to solvent can also be tuned by adjusting the hydrogel monomer; for example, both PNIPAM and PAAm composite have similar iridescence after swelling in water, but PNIPAM, unlike PAAm, does not swell as intensely in ethanol, leading to reflection of wavelength (900nm), whereas PAAm composite does swell and thus reflect light at about 550 nm[272]. Tunning hydrogel with PHEMa, a hydrogel famous for swelling in ethanol, shows a blue shift after soaking hydrogel in ethanol; further functionality can be installed into nanocomposite by changing host polymer; for example, polymerizing this time with PAAc nanocomposite shows a red shift in their iridescence when pH increases from semi-basic to very basic state; furthermore, rate of response can be tuned if polymer is chosen appropriately (these developments are shown in Figures 3f,g) [272]. A possible application of hydrogel can be in wine industry due to non-toxicity presence of water and ethanol and ease of application of the hydrogel if its soaked in the wine bottle (See **Figure 6h**)[274].

This study has been tried for other photonic crystals as well[275]. Like what was done with polystyrene particles, scientists created an inverted opal hydrogel in an ethanol and water combination that was responsive to pressure, pH, and L-lysine. Later, PAM and PAMPAA were included into the PS opal template; the amount of PAA might affect the degree of blue shift when compared to samples that solely contained PAM[275].

In the refs[276-278], CNC was first blended with water-soluble phenol-formaldehyde or melamine-urea-formaldehyde, which was followed by curing the composite material before CNC was removed using sodium hyxroxid. An SEM image of the composite material reveals imprints of the CNC chiral structure, which were also tunable with compression. Thus, it was

1205 able to create plastic samples with a photonic outline by first projecting a raised surface onto
1206 the film and then curing.

1207

1208 Finally, a humidity-gated photoactivation artificially nocturnal flower was constructed, which
1209 shuts under daytime conditions when humidity is low and or the light intensity is high and opens
1210 in the dark when humidity is high[279]. This opens the possibility for LCs to be used in applications
1211 like as home decoration and soft robotics.

1212

1213 **6.3 Energy storage applications**

1214

1215 As cutting-edge technology (such portable electronic gadgets, electric cars, and big intermittent
1216 battery systems) are integrated into our everyday lives, the need for sophisticated energy storage
1217 systems with high energy density, high power density, and extended lifespan has continued to
1218 rise[280]. Due to their lengthy lifespan, superior performance, and dependable stability, lithium ion
1219 batteries (LIBs) have been the most extensively used candidate systems in commercial electronic
1220 products [281-282]. Because of their extended cycle life, high specific power, and energy density,
1221 rechargeable LIBs are also seen as viable options for sustainable energy storage devices[283-284]. Since
1222 the introduction of commercial LIBs in 1991, carbonaceous materials have received a great deal
1223 of attention as candidate anode materials due to their respectable theoretical capacity (372 mAh.g^{-1}
1224)[285] , good electrical conductivity, and exceptional mechanical-chemical stability. Examples
1225 include graphite[286-287], CNT[288], and these associated composites[289-290].

1226

1227 At the same time, environmental concerns have sparked a lot of interest in adopting ecologically
1228 benign materials for Li/Na ion batteries that are sourced from sustainable resources such as [291-292],
1229 and [293]. The idea of employing carbon produced from fungi as an anode material for LIBs was put
1230 out by Tang et al. [294]. Several resources have been used as carbon sources and have showed
1231 outstanding electrochemical performances for Li/Na ion batteries. These resources include
1232 banana peels [295], packing peanuts[296], wheat[297], and numerous others [298-299]. The capacity of a battery
1233 is measured in milliamp hours (mAH). For example, if a battery has 250 mAH capacity and
1234 delivers 2 mA average current to a load, it should last 125 hours.

1235 The studies, however, have mostly focused on improving material composition or changing
1236 carbon precursors. These material-oriented techniques have not taken into consideration
1237 additional possible parameters that might affect the overall electrochemical kinetics and cycle
1238 stability of battery electrodes, such as electrode shape, dispersion, and alignment. In other words,
1239 research into the effects of structural orientation (i.e., alignment) of carbon precursors for
1240 rechargeable energy storage devices has received less attention. Even if the fundamental elements

1241 that make up the electrode are the same, it is crucial to note that the architecture (or alignment)
1242 of materials can greatly alter the electrochemical kinetics and stability in energy storage
1243 applications[300-301]. For instance, Liu et al. examined how three inorganic fillers with various
1244 alignments affected the ionic conductivity of composite polymer electrolytes[302]. The ionic
1245 conductivity of aligned inorganic nanowires (NW) was 10 times greater than that of randomly
1246 scattered NWs. In this instance, inorganic nanowires of various orientations were largely used as
1247 fillers to enhance Li ion mobility inside polymer medium and to supplement the inherent flaws
1248 of polymer electrolytes. The overall electrochemical performances of LIBs have not been shown
1249 to be directly influenced by the structural orientation of inorganic (or organic) components. As
1250 carbon precursors for this investigation, CNCs films with various structural orientations were
1251 used to address the fascinating problems raised above.

1252 Due to its exceptional mechanical and optical qualities, distinctive structure, abundance, and
1253 environmental friendliness, nanostructured cellulose has attracted significant interest from a
1254 variety of sectors[303-304] . Intriguing electrochemical phenomena in Li/Na ion batteries have been
1255 observed in a few investigations. As an anode material for Na-ion batteries, CNCs demonstrated
1256 good electrochemical performance, according to Zhu et al. [305]. The structural differences between
1257 CNCs and cellulose nanofibrils (CNFs) were analysed by Kim et al. and their effects on the
1258 electrochemical behaviours of LIBs and Li metal batteries were investigated[306]. However, the
1259 major emphasis of these strategies was on the physical-chemical characteristics of carbonised
1260 cellulose. The direct impact of the structural orientation of carbon precursors, such as cellulose,
1261 on the electrochemical performances of LiBs has received very little attention up to this point.
1262

1263 As anode electrodes for LiBs, two cellulose nanocrystal (CNC) films with two distinct
1264 alignments—aligned CNC (aCNC) and chiral nematic CNC (nCNC) films—were made[307],
1265 carbonised, and tested. The aim of this paper to test out the LC formation on charge transfer.
1266 In comparison to carbonized nCNC (c-nCNC), which only retains 20% of its rate at 200 mA.g^{-}
1267 ^{1}, the design of carbonised aCNC (c-aCNC) offers a favourable channel for ion/electron
1268 transport, resulting in exceptional rate retention (40% at 200 mA.g^{-1}). Additionally, c-aCNC
1269 demonstrated a more consistent cycle performance than c-nCNC (48% capacity across 450
1270 cycles), likely because of the superior electrochemical reactions and heat dispersion of c-
1271 aCNC. There are some issues with regards to batteries; for instance, volume changes and
1272 growth of Li dendrites; results in rapid loss of cell capacities over cycles thereby limiting
1273 practical application of Li-metal anodes[308-309].
1274
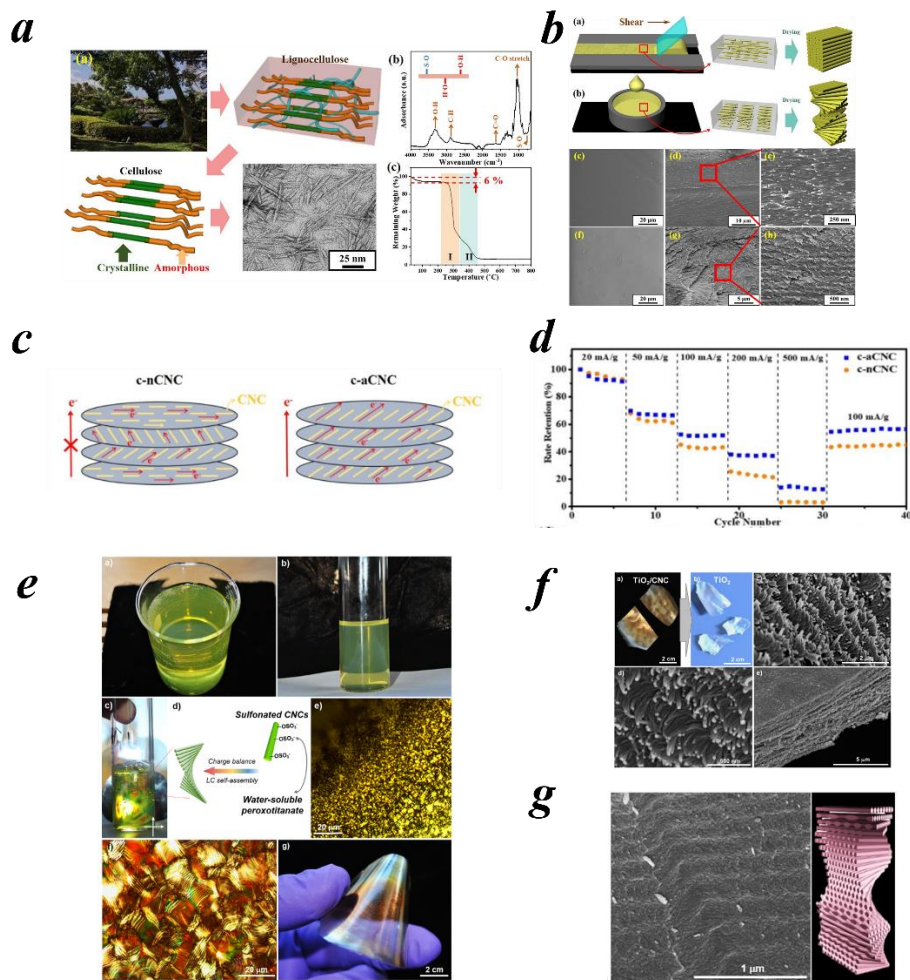
Figure 7. Energy storage applications of LC based CNC meta materials. **(a)** Production of CNC from lignocellulose (nature) to lithium batteries used for various applications (depiction of a process started initially in nature and ended up in meta materials technologically advanced lithium-ion batteries). **(b)** Schematic diagram of preparing aligned CNC films and cholesteric CNC films encompassing a top view, a cross view and SEM images of the films. Adapted with permission from ref [307]. Inefficient mode of electron transfer in chiral and aligned carboned CNCs; schematically theorized. Adapted with permission from ref [307]. (d) Rate retention comparison between aligned and chiral assembly of CNCs. The aligned sample exhibits a much better rate capability from low to high current densities than the chiral nematic sample, indicating a better electrochemical kinetics of aligned sample. Adapted with permission from ref [307]. The use of liquid crystalline self-assembly of CNCs with peroxotitanate to recreate huge freestanding mesoporous TiO_2 films and chiral nematic TiC structures (e) Yellow colour of suspension along with schematic showing chiral nematic structure formation as well as very thin and transparent yet iridescence films of the samples. Adapted with permission from ref[310]. (f) images of iridescent TiO_2/CNC composites and semitransparent TiO_2 films. SEM images of fracture cross-section of

the TiO$_2$/CNC composite film showing TiO$_2$ NPs decorated onto CNCs and SEM images of fracture cross-sections of TiO$_2$ films. Adapted with permission from ref[310]. (g) SEM picture of the TiC film fracture cross-section, model structure of chiral nematic mesoporous TiC crystals; note that the twisted rods indicate the TiC crystallite arrangement, and the areas between them account for the mesoporosity. Adapted with permission from ref[310].

The preparation method of an aligned CNC (aCNC) and a chiral nematically structured CNC is depicted in **Figure 7a-d**. The aCNC was created by applying shear (at a 45-degree angle to the plastic strips) to a highly viscous CNC solution that had been placed between two plastic strips and dried at room temperature. Under order to prepare the nCNC, a CNC suspension was first poured onto a dish, and then it was dried in ambient circumstances for a period that allowed the CNC suspension to self-assemble into chiral structures. Based on the electrochemical data, it was predicted that c-aCNC would have a better structure for transporting electrons/ions in all directions than c-nCNC because each CNC is compactly aligned within the aCNC film. CNC layers close to one another in nCNC, on the other hand, are slightly twisted to produce a chiral nematic structure. In compared to aCNC, the twisted structure of nCNC may be less suitable for transporting electrons across twisted layers.

Very interestingly, Chiral amphiphiles were made with chiral CNT and straight nitrogen doped CNTs that later was similarly followed by pyrolysis; Hydrothermal reaction subsequently anchors MoS2 nanosheets to the mesoporous CNTs matrix [311]. The authors stated that MoS$_2$/S-CNTs have well-aligned morphologies, whereas MoS$_2$/C-CNTs are porous with short tubular shape. MoS$_2$/C-CNTs electrode surpassed its MoS$_2$/S-CNTs counterparts in terms of cycle stability and rate performance, delivering a capacity of 368.8 mA h.g^{-1} after 300 cycles at a high current density of 2 A.g^{-1}. At a scan rate of 2 mV.s^{-1}, the percentage of capacitive charge storage is roughly 93.6%. The quick charge transfer resistance and low Warburg coefficient of MoS$_2$/C-CNTs, which outperform MoS$_2$/S-CNTs, explain the occurrence. It would be interesting if previous paper on CNC could be repeated similar with this ref using MoS2 and result be compared again.

Even though it was shown in previous example that cellulose carbonization by itself is not a good candidate for energy storage materials; it can still be used as a templating material to host other metals. For instance, in ref[310], report describes the use of liquid crystalline self-assembly of CNCs with peroxotitanate to recreate huge freestanding mesoporous TiO$_2$ films and chiral nematic TiC structures. Because cellulose liquid crystals are compatible with water-soluble peroxotitanate, they may self-assemble into flexible chiral nematic TiO$_2$/cellulose composite sheets. The highly compatible peroxotitanate/CNC combination is a novel liquid crystalline system that may be used to study the creation of photonic films with variable optical characteristics and structural replication by adjusting the ingredient ratio. The development for producing these composites is shown in **Figure 7e-g**. Iridescent peroxotitanate/CNC composites were heated hydrothermally

and calcined to produce durable, semitransparent layered mesoporous anatase TiO_2 replicas. Authors converted carbonized peroxotitanate/ CNC assemblies to mesoporous TiC with chiral nematic order via magnesiothermic reduction. Their findings indicated that mesoporous TiC has the potential to act as a long-life cycle rechargeable lithium-ion battery anode material, and this technique might be extended to additional peroxometallate compounds as well. Despite their blackness and high light absorption, these chiral nematic TiC and TiO_2/C structures were also colourful; however, when examined through left- or right-handed circular polarising filters, their hues are similar, implying that the colours are caused by thin-film interference of light rather than circular polarization caused by the chiral structure [310].

In another similar report[312], this time using combined graphene oxide (GO) and SnO_2, using composite of SnO_2/CNC/reduced GO (SnO_2/CNC/rGO) were made; the free-standing films had reversible capacity ~500 mA.h.g^{-1} maintained for 1500 cycles in the film and ~800 mA.h. g^{-1} maintained for 150 cycles in the textile at a current density of 500 mA.g^{-1}. Similarly, without disrupting the chiral nematic CNC aerogel, GeO_2 nanoparticles with specific surface areas of up to 705 m^2.g^{-1} were randomly dispersed over the aerogel[313]; here again chiral structure acted as a templating material. The combination of the carbonaceous skeleton's electrochemical double layer capacitance and the pseudocapacitive contribution from the GeO_2 nanoparticles resulted in materials with a maximum capacitance (Cp) of 113 F.g^{-1} and high capacitance retention.

The introduction of hierarchy and chirality into structures is of great interest because it has the potential to provide novel optical and electrical characteristics owing to the synergistic impact of helical and anisotropic structures. To employ CNCs for energy storage applications, conductivity must be added to them; this may be accomplished by mixing CNCs with a conductive filler or coating CNCs with a conductive polymer. For example, for potential energy storage applications, CNC can be coupled with such a 2-D graphene oxide nanostructure and loaded with active $SnO2$. The resultant SnO_2/CNC/reduced GO (SnO_2/CNC/rGO) composite has a tensile strength of 100 MPa and may be manufactured as a film, fibre, or fabric. The free-standing (SnO_2/CNC/rGO) electrodes demonstrate much improved energy storage capability at a current density of 500 mA/g [312], with a reversible capacity of 500 mAh/g maintained for 1500 cycles in the film and 800 mAh/g maintained for 150 cycles in the textile.

Likewise, the author of ref[314] polymerizes pyrrole in situ onto modified chiral nematic cellulose nanocrystal sheets by covering them with a conductive polymer. TEMPO-oxidation, acetylation, desulfation, and cationization had no effect on the chiral structures. Because they were simple to make, these new materials offer tempting alternatives for environmentally friendly sensors and energy storage devices. It should be noted that the chiral structure was unaffected by TEMPO oxidation, acetylation, desulfation, or cationization.

1363 The findings of this section suggest that carbonization of CNC or using CNC that has been
1364 made conductive or mixed with conductive fillers can be an appealing tool to produce anode
1365 for batteries. This is because carbonised CNC or CNC that has been made conductive or mixed
1366 with conductive fillers tend to self-assemble.
1367
1368
1369 **6.5 Optical and Optoelectronic applications**
1370

1371 Other materials can be used to further refine LC formation and create products with unique
1372 optical or optoelectronic applications. Using CNCs that are responsive to electric or magnetic
1373 fields to rearrange their position in space and provide different optical properties under applied
1374 fields is one strategy that can help achieve this goal. A potential material option for cutting-edge
1375 optoelectronic devices may be liquid crystalline CNCs, which may alter their structure and
1376 optical characteristics under an electric field. There hasn't been much research done on how it
1377 performs in an electric field. As a result, authors in ref[315], demonstrated some intriguing CNC
1378 liquid crystal dielectric coupling behaviours in an electric field as the CNC tactoid's helix axis was
1379 shown to become aligned normal to the direction of the electric field. The tactoid may then be
1380 stretched along with a rise in pitch, using a deformation process that differs dramatically at
1381 different frequencies, and lastly, upon increasing the electric field strength, the helix axis untwists
1382 to create a nematic structure. Therefore, in this case, the electric field's frequency would also have
1383 an impact on the optical properties. Additionally, by fusing polarised optical microscopy with
1384 CNC uniform laying helix textures, a simple approach to view the electric field is provided. These
1385 insights could make it easier to construct liquid crystalline CNC for the creation of electro-optical
1386 devices.

1387 It is critical to understand where the colour in chiral structures derives from. Reflected light
1388 produces the colour of films, which is affected by the wavelength and angle of incoming light
1389 (these structurally coloured materials are angle-dependent). When the incoming light
1390 wavelength is in the visible range, the material looks colourful to the human eye. The left
1391 circularly polarised light is totally reflected by the helical structure's lefthanded axis, while the
1392 right circularly polarised light travels through the crystals[316]. Thus, the polarization of reflected
1393 light gives accurate data concerning the chiral order of colorful CNC films [317]. The colour of films
1394 is iridescent in typical lighting conditions, depending on pitch length produced; iridescent nature
1395 of films comes from angle dependency and inhomogeneity of average pitch size across the
1396 produced film[318]. The immaculate films are fragile and have a non-uniform structure, limiting
1397 their use[242]; as previously stated and suggested in other publications, it is advised to mix them
1398 with flexible particles and polymer.

The chiral structure of CNCs, which is stated in the energy storage application, may also be used to template optical characteristics. A notable example of using CNC embedded systems for optoelectronic applications is the production of crack-free, chiral nematic GeO_2/CNC composite films with tunable photonic properties from the controlled assembly of germanium (IV) alkoxides with lyotropic liquid-crystalline CNCs in a water/DMF mixed solvent [313].

Photonic GeO_2/CNC composites may be transformed into semiconducting mesoporous GeO_2/C and Ge/C copies, freestanding chiral nematic films of amorphous GeO_2, and photonic GeO_2/CNC composites using different pyrolysis conditions. These novel materials have applications in chiral separation, enantioselective adsorption, catalysis, sensing, optoelectronics, and lithium-ion batteries, among others. Furthermore, the unique, repeatable synthesis procedures outlined might be used to create a wide range of chiral nematically organised composites and porous materials.

Only left circularly polarised (LCP) light is reflected by CNC sheets, whereas right circularly polarised (RCP) light is not reflected. The unusual way chiral cellulose nanorods self-assemble causes this phenomenon. Fernandes et al. [319] developed a novel photonic structure based on the cuticle of the beetle Plusiotis resplendens, in which chiral CNCs can reflect both LCP and RCP light. To construct this photonic structure, an anisotropic nematic liquid layer of -cyano-4'-pentylbiphenyl is sandwiched into a micro gap between two left-handed cholesteric nanocellulose domains with comparable pitches. The nematic layer is a half-wave retardation plate that converts RCP light to LCP light and vice versa. As a result, the RCP light may be efficiently reflected [320].The transition from right to left-handed can be regulated by adjusting the temperature or applying an electric field.

The researchers further demonstrate that the RCP light reflection can be adjusted by changing the temperature or applying an electric field due to the reversible transformation of the anisotropic liquid crystal layer from nematic to isotropic. At temperatures above the nematic-to-isotropic transition temperature, for example, all RCP light is transmitted (colourless reflection), whereas LCP light is still reflected, but at a longer wavelength, due to a decrease in the material refractive index and an increase in the pitch of the cholesteric chiral phases. Despite the fact that certain cellulose derivatives can produce chiral nematic LCs with both left- and right-handed structures[321], CNC dispersions appear to invariably produce left-handed chiral nematic phases.

CNCs can also incorporate photoluminescence. CNC's [322]chiral structure was created using a low molecular weight nematic liquid crystal (NLC), 4'-(hexyloxy)-4-biphenylcarbonitrile (HOBC). The resultant composite material combines the rich structural coloration of photonic cellulose with the thermal and conductive properties of NLC. Pitch length was constant after

1436 treatment with HOBC[322]. The twisted spindle feature in the edge view of the damaged film
1437 under SEM spun counterclockwise, demonstrating that the nanocrystals formed left-handed
1438 helicoids. Photoluminescence was seen in nematic HOBC-LCs films[323].

1439

1440 For Broadband optical properties, variations in helical pitch length and helical axis orientations
1441 within film domains contributed to a subtly broader chiral reflection band, resulting in a broad
1442 band circular polarizer, i.e., the ability to reflect certain circularly polarised light while
1443 transmitting others. The work not only proposes a simple approach for producing a film with
1444 broadband reflection, but it also provides a model for examining the interactions between
1445 nanosized supramolecular aggregates and CNC assemblies (broadband reflection). This method
1446 might be used to modify the optical characteristics of various chiral liquid crystal systems, which
1447 could be employed in optical filters, polarizers, and coatings. It is noteworthy that studies like
1448 this one make an effort to widen the wavelength at which light is reflected in a circular pattern.

1449 Natural-derived CNC-based materials' flexibility, along with their biocompatibility, enables for
1450 a wide range of uses, from low-cost decoration to more sophisticated objectives. Crushing CNC
1451 films into flakes of varied sizes produces edible structurally coloured glitter or powder ideal for
1452 spray application in food colouring paints or cosmetics[324]. Aside from aesthetics, the ability to
1453 reflect just one polarisation of light at a certain wavelength band is advantageous for
1454 anticounterfeiting[166, 325]. Temperature, compression, swelling, magnetic field orientation, or other
1455 CNC-based depolarizing coatings, as well as optically active dopants such upconverting brilliant
1456 dyes or nanoparticles, might be used to further diversify this property.

1457 Zhang and colleagues demonstrated that adding a fluorescent whitening chemical to a CNC-
1458 based LC linear structure may enhance the spacing while keeping the iridescence features of the
1459 films at low concentrations[166]. Compared to the usual whole-film application, the effective
1460 techniques of proper grinding and different post-treatments produced films with a tiny platelet
1461 form and an average thickness of 25 micrometer[324]. These structural colours were maintained in
1462 fragment films, giving them an iridescent appearance, and making them counterfeitable. Gan et
1463 al. [326] recently examined how a vertically built CNC and the associated film with an anti-
1464 counterfeiting pattern could hide information under natural light when the CNC was shorter
1465 than 144nm and disclose hidden information under UV radiation when the CNC was shorter than
1466 144nm.

1467 Optical diffusers provide soft light with a uniform spatial and directional intensity distribution.
1468 Because of their excellent scattering properties, optical diffusers have been widely used for
1469 uniform backlighting, scanning bar codes, computer screens and other monitors, luminance
1470 augmentation, efficiency, and higher susceptibility in liquid crystal displays (LCDs) [327-328], light-

1471 emitting diodes (LEDs) [329], solar cells [330], and photodetectors[331]. There is currently no
1472 documentation of research on the use of CNC chiral structures for optical diffusing.

1473 **6.6 Templating**

1474

1475 Artificial chiral material produced employing nano-micro sized matrixes has benefitted
1476 chemical synthesis, chiral sensing, chiral catalysis, and meta-material-based enhanced optical
1477 devices. Hard templates techniques and soft templates methods are the two most used
1478 methodologies for manufacturing chiral substances. This method may be utilised to develop
1479 novel nanostructured materials with chiral characteristics. (i) When producing chiral materials,
1480 hard template techniques are widely used as a mesoporous host to transfer their nanostructure
1481 to other materials. (ii) Soft template method: material is generated by selectively removing the
1482 host template. To prepare the template, molecular evaporation, rapid self-assembly, or super
1483 molecular aggregation are used. Soft template preparation is more flexible than hard template
1484 preparation for nano-mesoporous materials. As chiral research progresses from the molecular
1485 to the nanoscale, cellulose-based chiral materials have gained in popularity.

1486

1487 Pattern generation from nano colloidal LCs in constrained geometry, also known as templates,
1488 can be utilized as a template for nanoparticle organization. Three-dimensional confinement of
1489 cholesteric liquid crystal was explored in ref. [80] under two-dimensional confinement. Material
1490 organization in certain pattern through natural self-assembly process is time consuming. The
1491 phase-separated cholesteric shell was constructed using concentric CNC pseudo layers with a
1492 helicoidal axis perpendicular to the inner surface of the capillary walls and an isotropic core
1493 thread running parallel to the capillary's long axis. As the degree of confinement rose, the shape
1494 of the LCs altered, indicating that the generated core-shell LCs might be employed in optical
1495 wave guides. According to the scientists, POM images were used to examine the structure over
1496 time, and after 6 hours, a well-defined isotropic core was produced, which did not relax until 168
1497 hours had passed. This suggests that isotropic and cholesteric CNC rearrangement takes time [80].

1498

1499 In ref[332], mesoporous titanium dioxide (TiO$_2$x) with the chiral nematic structure of core-shell
1500 nanorod was characterized via templating once again. Carbonized TiO$_2$/CNC helical materials
1501 are created by chiral transferring TiO$_2$ nanoparticles onto gelatin functionalized CNCs and then
1502 calcining to recover TiO$_2$ copies after the carbon is removed. The black TiO$_2$x is a semiconducting
1503 mesoporous structure composed of chiral nematic crystalline-amorphous TiO$_2$ core-shell
1504 nanorods. The anode electrodes of lithium-ion batteries are made up of chiral black TiO$_2$x
1505 nanoparticles supported by mesoporous nanocarbon networks. Beyond the current efforts, these
1506 black TiO$_2$x materials and composites may be useful in the fields of energy storage and catalysis.

1507 Evaporation-induced self-assembly of CNC with silica precursors, according to MacLachlan et al
1508 [333]., can result in composite films containing chiral nematic structures.

1509 After pyrolyzing and etching the silica, freestanding sheets of chiral nematic mesoporous carbon
1510 are formed. In a symmetrical capacitor with H2SO4 as the electrolyte, mesoporous carbon sheets
1511 display near-ideal capacitor behaviour, with a specific capacitance of 170 F g-1 at 230 mA.g-1..

1512

1513 Templating can also be utilised for diverse interactions with light. The templating process allows
1514 for more than merely transferring the helical structure to different materials. The inorganic
1515 duplicate's optical sensitivity might differ greatly from that of a dried CNC film. The refractive
1516 index of air and the single refractive index of the optically isotropic amorphous inorganic material
1517 are repeated discrete contrasts in a templated amorphous inorganic film, whereas the latter has a
1518 continuously varying refractive index due to the rotation of the birefringent CNC rods. As a
1519 consequence, the reflection may be switched on and off by filling the voids with an index matched
1520 fluid and drying the liquid. The switching may be very quick and reversible if the voids were
1521 filled with a thermotropic nematic, whose refractive index in the absence of a field matched that
1522 of the inorganic material. When an electric field is applied to a thermotropic nematic, the index
1523 matching is lost, and the film looks coloured.

1524 Even though the initial dried CNC film is porous, such ON/OFF switching of photonic crystal
1525 characteristics is not achievable because a birefringent matrix material lacks an index matching
1526 fluid. It is also probable that, in comparison to visible light wavelengths, the thicknesses of the
1527 inorganic and air layers, as well as their sum (which forms the local optical period), are especially
1528 important for the colours produced. Prospective uses of transparent CNC-templated inorganic
1529 materials that have yet to be investigated include cholesteric-based mirrorless lasing.

1530 Finally, it should be highlighted that novel materials and technologies for energy storage should
1531 be researched employing different types of nanocellulose and their combinations as building
1532 blocks, depending on the sizes, structures, and surface chemical performance of nanocellulose.
1533 This is since nanocellulose may be manufactured from several sources utilizing a range of
1534 processes. By combining TEMPO-oxidized CNCs with transparent conductive materials, for
1535 example, optically transparent and flexible electrodes may be created. Chiral nematic
1536 mesoporous carbon electrodes may be made using sulfuric-acid hydrolyzed CNC as a template.
1537 The investigation of novel materials and manufacturing techniques may lead to opportunities in
1538 a range of applications.

1539 Nanocellulose and its derivatives substances have been widely employed in supercapacitors and
1540 lithium-ion batteries (LIBs); however, only a few investigations on their application in Li-S
1541 batteries and sodium-ion batteries have been published[307]. Furthermore, several novel energy

1542 storage devices, such as Mg (Al, Mn)-ion batteries, have received little attention. Nanocellulose
1543 and its derivatives may be easily tailored as a green material alternative for fast-growing energy
1544 storage devices since they are physically robust and have changeable structure and
1545 surface/interface chemistry.

1546 In the ref [334], chiral structures were created via evaporation-induced self-assembly with the
1547 addition of glutaraldehyde, a famous CNC crosslinker. The self-standing form was then coated
1548 with the conducting polymer polypyrrole and used as a template for metal oxide iron oxide.

1549 Bottom up self-assembly is preferable over top down self-assembly[335-336] because it allows for
1550 more arbitrary and customizable geometries, which is important for advanced applications such
1551 metal materials with negative refractive index[337], ultrasensitive biosensing, and sophisticated
1552 optical filters using plasmonic nanomaterials[338-339].

1553 In ref[340], authors compiled a basic structure of silica with PMMA shells; then titania was
1554 developed in the void spaces and later PMMA was eliminated through calcination procedure;
1555 the porous structure could now be made tunable in colour if the pores have been packed that
1556 matched silica such a way as to produce a shift in colour if the hydrogel surrounding the
1557 photonic crystals was also changeable.
1558

1559 **6.7 Advanced application**
1560

1561 Since the invention of photonic crystals, numerous ways for producing these materials have
1562 been investigated; among these, self-assembly of particles has been intensively examined; one
1563 of the benefits of colloidal photonic crystals is the tunability of reflection peaks (the stop
1564 bands). The optical reflection peaks are equivalent to the diffraction peaks in an X-ray power
1565 pattern, but instead of being in angstrom scale, they are at submicrometric sizes in photonic
1566 crystals. The idea behind making photonic crystals adjustable is to vary the position or
1567 technique of interaction of particles within the crystals.
1568

1569 A key for preparation of hydrogel with well-defined response to environmental alteration is
1570 to surround CNC chiral structures with a network that contain molecular recognition
1571 element; for instance in ref[341]; a hydrogel was made to make the system able to detect glucose
1572 through network interaction with boronic acid groups that were connected to the network;
1573 these upon glucose infiltration could convert to boronate groups that increase degree of
1574 ionization of hydrogel thus created a change in pitch (red shift). A similar approach as been
1575 used for opal sensors [342]. It should be mentioned that for glucose detection being used for
1576 diabetic screening, if a person's blood sugar (glucose concentration on an empty belly is

1577 greater than 11 m M, the individual is identified as diabetic, and between 7.8 m M and 11 m
1578 M, the person is borderline diabetic.
1579

1580 Through a combined reaction between 2-nitrophenol groups and the enzyme creatinine
1581 deiminase, hydrogels may also detect creatine[343]. High levels of creatine in bodily fluids are a
1582 sign of renal disease; in this case, creatine was digested by an enzyme, which released
1583 hydroxide ions and deprotonated 2-nitrophenol. Because this product was more soluble in
1584 the hydrogel, it swelled and produced a red shift.
1585

1586 These structures can profit from organic compounds shifting their configuration when
1587 exposed to UV or visible light. In ref[344], authors created polystyrene (PS) opals with
1588 azobenzene groups covalently adhered that can be tuned to the cis form through Ultraviolet
1589 (UV) light and recover to the trans state through white light irradiation. The cis form is more
1590 readily blended with hydrogel, causing to red shift by 60 nm depending on concentration.
1591

1592 Additionally, opals and inverse opals cancoexist with liquid crystals. The great advantage of
1593 these systems is a way to tune the photonic band gap by applying an electric field or changing
1594 the temperature, which changes the molecular orientation of liquid crystals. For example, in
1595 ref, the author investigated using an electric field to change the orientation of a silica opal
1596 with a nematic liquid crystal called 4-pentyl-4 '-cyanobiphenyl (5CB) [345-346].
1597

1598 In ref [347], elastomeric films were created that could be compressed in one direction while only
1599 having little effects in the other two. This caused a blue shift in the stop position, and the
1600 material could be evaluated for biometric recognition systems that could take fingerprints.
1601 Additionally, PbS quantum dots were used to modify the photoluminescence of the films. In
1602 ref[348], opal structure were infiltrated with poly(dimethylsiloxane); exposure to 2-propanol
1603 could swell the matrix and change color of elastomer; this was reversible with cycles that
1604 could be repeated 10 times; photonic elastomeric paper was suggested as an application of
1605 this study[349-350]. In ref[351], authors developed an inverse opal in which PS spheres were arranged
1606 periodically in a cell with a ferrofluid containing particles with a diameter less than 15 nm;
1607 after solvent removal and elimination of the template, a porous made with magnetic structure
1608 was obtained; small sheets of this material could be rotated with a magnetic field when
1609 soaked, making the colour tunable. These advanced applications can be easily extended to
1610 CNC chiral nematic structures and their interesting colorations.
1611

1612 **Conclusions and Future works**
1613

A new horizon for the enhanced use of CNC-based materials is now available thanks to the researcher's present toolkit for characterization and subsequent development of unique sustainable product.

Consequently, the easiness of CNC 3-D printing process is made possible by the configurable rheological properties of CNC suspension (from fluid dominant to solid dominant behaviour), coupled with high shear thinning and flexible yield stress, while yield stress and viscoelasticity of the structure can create the extrudate retain its shape fidelity. For instance, Ma et al. [2] studied the printability of CNC suspensions by adjusting the concentration of CNC particles (0.5–25 wt%) while maximising the rheological characteristics. It was found that 20 weight % CNC hydrogels showed the best print quality and resolution. The printing abilities of CNC hydrogels in the presence of high/low methoxy pectin were also examined by the scientists. Another innovative use of CNC suspensions for rheology was put out by Wang et al. [352], who demonstrated the capability of CNC particles to stabilise magnetorheological fluids. According to studies in ref, CNC hydrogel was made to be excellent for water purifications[353] by stabilising it with zirconia [354] and graphene.

Two key points about the generic characteristics of liquid crystalline suspension rheology arose from the material of this manuscript:

> I) Viscosity drops when a substance transitions from an isotropic to a liquid crystalline condition

> II) Three areas of a flow curve emerging (different from isotropic state)

But as far as we can tell, there are problems that need to be fixed right away. Examples include using Doi theory to evaluate how the orientation of the cholesteric helix affects the intensity of the viscoelastic response and analysing the time-dependent behaviour of the apparent pitch of CNC liquid crystals during shearing deformation [355]. Additionally, there hasn't been much significant research done in the areas where linear and non-linear rheology may be utilised to analyse optical properties in combination with CNC liquid crystal orientation using magnetic or electric fields. These concentrated efforts might create new opportunities for the more precise and microstructurally informed rheological characterization of these suspensions.

A variety of designs for producing special properties out of CNC were introduced; these designs included them becoming conductive, being mixed with other ingredients, etc. In part related to applications of CNC, LC optical, aerogel, energy storage application, and templating variety of designs were introduced. So far, for instance, we have shown how to make a CNC-made aerogel that is responsive to light, pressure, the type of solvent used, humidity, glucose, or temperature. It is also conductive and effective at shielding EMI. Additionally, it can be packaged and be structurally colored, edible, and thermally insulating.

1649 To fully utilise their capacity to transform daily used materials, more research needs to be done
1650 on CNC LC formation and its properties. With the aid of a variety of characterization tools that
1651 can precisely establish the relationship between microstructure and property, these complexities
1652 need to be addressed in the literature.
1653
References
1655
1656
1657 1.   George, J.; Sabapathi, S., Cellulose nanocrystals: synthesis, functional properties, and
1658 applications. *Nanotechnology, science and applications* **2015,** *8*, 45.
1659 2.   Gahrooee, T. R.; Moud, A. A.; Danesh, M.; Hatzikiriakos, S. G., Rheological Characterization of
1660 CNC-CTAB Network below and above Critical Micelle Concentration (CMC). *Carbohydr. Polym.* **2021,**
1661 117552.
1662 3.   Moud, A. A.; Arjmand, M.; Yan, N.; Nezhad, A. S.; Hejazi, S. H., Colloidal behavior of cellulose
1663 nanocrystals in presence of sodium chloride. *ChemistrySelect* **2018,** *3* (17), 4969-4978.
1664 4.   Moud, A. A.; Arjmand, M.; Liu, J.; Yang, Y.; Sanati-Nezhad, A.; Hejazi, S. H., Cellulose nanocrystal
1665 structure in the presence of salts. *Cellulose* **2019,** *26* (18), 9387-9401.
1666 5.   Moud, A. A.; Kamkar, M.; Sanati-Nezhad, A.; Hejazi, S. H., Suspensions and hydrogels of cellulose
1667 nanocrystals (CNCs): characterization using microscopy and rheology. *Cellulose* **2022,** 1-33.
1668 6.   Shang, Z.; An, X.; Seta, F. T.; Ma, M.; Shen, M.; Dai, L.; Liu, H.; Ni, Y., Improving dispersion
1669 stability of hydrochloric acid hydrolyzed cellulose nano-crystals. *carbohydrate Polym.* **2019,** *222*, 115037.
1670 7.   Yu, H.; Qin, Z.; Liang, B.; Liu, N.; Zhou, Z.; Chen, L., Facile extraction of thermally stable cellulose
1671 nanocrystals with a high yield of 93% through hydrochloric acid hydrolysis under hydrothermal
1672 conditions. *journal Mater. Chem. A* **2013,** *1* (12), 3938-3944.
1673 8.   Russel, W. B.; Russel, W.; Saville, D. A.; Schowalter, W. R., *Colloidal dispersions*. Cambridge
1674 university press: 1991.
1675 9.   Larson, R. G., *The structure and rheology of complex fluids*. Oxford university press New York:
1676 1999; Vol. 150.
1677 10.   Eisenlauer, J.; Killmann, E., Stability of colloidal silica (aerosil) hydrosols. I. Preparation and
1678 characterization of silica (aerosil) hydrosols. *journal Colloid Interface Sci.* **1980,** *74* (1), 108-119.
1679 11.   Dickinson, E., *Introduction to food colloids*. Oxford university press: 1992.
1680 12.   Lewis, J. A., Colloidal processing of ceramics. *journal Am. Ceram. Soc.* **2000,** *83* (10), 2341-2359.
1681 13.   Smay, J. E.; Cesarano, J.; Lewis, J. A., Colloidal inks for directed assembly of 3-D periodic
1682 structures. *Langmuir* **2002,** *18* (14), 5429-5437.
1683 14.   Sonntag, R.; Russel, W., Elastic properties of flocculated networks. *journal Colloid Interface Sci.*
1684 **1987,** *116* (2), 485-489.
1685 15.   Buscall, R.; Mills, P.; Stewart, R.; Sutton, D.; White, L.; Yates, G., The rheology of strongly-
1686 flocculated suspensions. *Journal of Non-Newtonian Fluid Mechanics* **1987,** *24* (2), 183-202.
1687 16.   Chen, M.; Russel, W., Characteristics of flocculated silica dispersions. *journal Colloid Interface*
1688 *Sci.* **1991,** *141* (2), 564-577.
1689 17.   Rueb, C.; Zukoski, C., Viscoelastic properties of colloidal gels. *journal Rheol.* **1997,** *41* (2), 197-
1690 218.
1691 18.   Fagan, M.; Zukoski, C., The rheology of charge stabilized silica suspensions. *journal Rheol.* **1997,**
1692 *41* (2), 373-397.
1693 19.   Onogi, S.; Asada, T., Rheology and rheo-optics of polymer liquid crystals. In *Rheology*, Springer:
1694 1980; pp 127-147.

1695   20.   Bercea, M.; Navard, P., Shear dynamics of aqueous suspensions of cellulose whiskers.
1696   *Macromolecules* **2000,** *33* (16), 6011-6016.
1697   21.   Ureña-Benavides, E. E.; Ao, G.; Davis, V. A.; Kitchens, C. L., Rheology and phase behavior of
1698   lyotropic cellulose nanocrystal suspensions. *Macromolecules* **2011,** *44* (22), 8990-8998.
1699   22.   Shafiei-Sabet, S.; Hamad, W. Y.; Hatzikiriakos, S. G., Rheology of nanocrystalline cellulose
1700   aqueous suspensions. *Langmuir* **2012,** *28* (49), 17124-17133.
1701   23.   González-Labrada, E.; Gray, D. G., Viscosity measurements of dilute aqueous suspensions of
1702   cellulose nanocrystals using a rolling ball viscometer. *Cellulose* **2012,** *19* (5), 1557-1565.
1703   24.   Orts, W. J.; Godbout, L.; Marchessault, R. H.; Revol, J.-F., Enhanced ordering of liquid crystalline
1704   suspensions of cellulose microfibrils: a small angle neutron scattering study. *Macromolecules* **1998,** *31*
1705   (17), 5717-5725.
1706   25.   Solomon, E. B.; Niemira, B. A.; Sapers, G. M.; Annous, B. A., Biofilm formation, cellulose
1707   production, and curli biosynthesis by Salmonella originating from produce, animal, and clinical sources.
1708   *journal Food Prot.* **2005,** *68* (5), 906-912.
1709   26.   Dong, X. M.; Kimura, T.; Revol, J.-F.; Gray, D. G., Effects of ionic strength on the isotropic– chiral
1710   nematic phase transition of suspensions of cellulose crystallites. *Langmuir* **1996,** *12* (8), 2076-2082.
1711   27.   Hirai, A.; Inui, O.; Horii, F.; Tsuji, M., Phase separation behavior in aqueous suspensions of
1712   bacterial cellulose nanocrystals prepared by sulfuric acid treatment. *Langmuir* **2009,** *25* (1), 497-502.
1713   28.   Gong, J.; Kuang, Y.; Zhang, X.; Luan, P.; Xiang, P.; Liu, K.; Mo, L.; Xu, J.; Li, J.; Wan, J., Efficient
1714   Shaping of Cellulose Nanocrystals Based on Allomorphic Modification: Understanding the Correlation
1715   between Morphology and Allomorphs. *Biomacromolecules* **2022,** *23* (3), 687-698.
1716   29.   Jin, E.; Guo, J.; Yang, F.; Zhu, Y.; Song, J.; Jin, Y.; Rojas, O. J., On the polymorphic and
1717   morphological changes of cellulose nanocrystals (CNC-I) upon mercerization and conversion to CNC-II.
1718   *carbohydrate Polym.* **2016,** *143*, 327-335.
1719   30.   Wegst, U. G.; Bai, H.; Saiz, E.; Tomsia, A. P.; Ritchie, R. O., Bioinspired structural materials. *nature*
1720   *mater.* **2015,** *14* (1), 23-36.
1721   31.   Kim, S.; Laschi, C.; Trimmer, B., Soft robotics: a new perspective in robot evolution. *Trends*
1722   *Biotechnol* **2013,** *31*, 287-294.
1723   32.   Maeda, S.; Hara, Y.; Sakai, T.; Yoshida, R.; Hashimoto, S., Self-walking gel. *advanced Mater.* **2007,**
1724   *19* (21), 3480-3484.
1725   33.   Liu, K.; Yao, X.; Jiang, L., Recent developments in bio-inspired special wettability. *chemical Soc.*
1726   *Rev.* **2010,** *39* (8), 3240-3255.
1727   34.   Casado, U.; Mucci, V. L.; Aranguren, M. I., Cellulose nanocrystals suspensions: Liquid crystal
1728   anisotropy, rheology and films iridescence. *carbohydrate Polym.* **2021,** *261*, 117848.
1729   35.   Nechyporchuk, O.; Belgacem, M. N.; Pignon, F., Current progress in rheology of cellulose
1730   nanofibril suspensions. *Biomacromolecules* **2016,** *17* (7), 2311-2320.
1731   36.   Abbasi Moud, A.; Piette, J.; Danesh, M.; Georgiou, G. C.; Hatzikiriakos, S. G., Apparent slip in
1732   colloidal suspensions. *journal Rheol.* **2022,** *66* (1), 79-90.
1733   37.   Scaramuzza, N.; Carbone, V.; Barberi, R., Dynamical response of cholesteric liquid crystals to
1734   mechanical shearing deformations. *Molecular Crystals and Liquid Crystals* **1991,** *195* (1), 31-37.
1735   38.   Moud, A. A., Chiral Liquid Crystalline Properties of Cellulose Nanocrystals: Fundamentals and
1736   Applications. *ACS omega* **2022,** *7* (35), 30673.
1737   39.   Abbasi Moud, A.; Abbasi Moud, A., Cellulose Nanocrystals (CNC) Liquid Crystalline State in
1738   Suspension: An Overview. *applied Biosci.* **2022,** *1* (3), 244-278.
1739   40.   Marchessault, R.; Morehead, F.; Koch, M. J., Some hydrodynamic properties of neutral
1740   suspensions of cellulose crystallites as related to size and shape. *Journal of Colloid Science* **1961,** *16* (4),
1741   327-344.

1742   41.   Asada, T.; Muramatsu, H.; Watanabe, R.; Onogi, S., Rheooptical studies of racemic poly (γ-benzyl
1743   glutamate) liquid crystals. *Macromolecules* **1980,** *13* (4), 867-871.
1744   42.   Burghardt, W. R., Molecular orientation and rheology in sheared lyotropic liquid crystalline
1745   polymers. *macromolecular Chem. Phys.* **1998,** *199* (4), 471-488.
1746   43.   Walker, L.; Wagner, N., Rheology of region I flow in a lyotropic liquid-crystal polymer: The
1747   effects of defect texture. *journal Rheol.* **1994,** *38* (5), 1525-1547.
1748   44.   Montesi, A.; Pena, A. A.; Pasquali, M., Vorticity alignment and negative normal stresses in
1749   sheared attractive emulsions. *physical Rev. Lett.* **2004,** *92* (5), 058303.
1750   45.   Davis, V. A.; Ericson, L. M.; Parra-Vasquez, A. N. G.; Fan, H.; Wang, Y.; Prieto, V.; Longoria, J. A.;
1751   Ramesh, S.; Saini, R. K.; Kittrell, C., Phase behavior and rheology of SWNTs in superacids.
1752   *Macromolecules* **2004,** *37* (1), 154-160.
1753   46.   Giasson, J.; Revol, J. F.; Ritcey, A. M.; Gray, D. G., Electron microscopic evidence for cholesteric
1754   structure in films of cellulose and cellulose acetate. *Biopolymers* **1988,** *27* (12), 1999-2004.
1755   47.   Revol, J.-F.; Bradford, H.; Giasson, J.; Marchessault, R.; Gray, D., Helicoidal self-ordering of
1756   cellulose microfibrils in aqueous suspension. *international J. Biological Macromol.* **1992,** *14* (3), 170-172.
1757   48.   Araki, J.; Wada, M.; Kuga, S.; Okano, T., Influence of surface charge on viscosity behavior of
1758   cellulose microcrystal suspension. *Journal of wood science* **1999,** *45* (3), 258-261.
1759   49.   Araki, J.; Wada, M.; Kuga, S.; Okano, T., Flow properties of microcrystalline cellulose suspension
1760   prepared by acid treatment of native cellulose. *colloids Surf. Physicochem. Eng. Asp.* **1998,** *142* (1), 75-
1761   82.
1762   50.   Araki, J.; Wada, M.; Kuga, S.; Okano, T., Birefringent glassy phase of a cellulose microcrystal
1763   suspension. *Langmuir* **2000,** *16* (6), 2413-2415.
1764   51.   Araki, J.; Wada, M.; Kuga, S., Steric stabilization of a cellulose microcrystal suspension by poly
1765   (ethylene glycol) grafting. *Langmuir* **2001,** *17* (1), 21-27.
1766   52.   Beck-Candanedo, S.; Roman, M.; Gray, D. G., Effect of reaction conditions on the properties and
1767   behavior of wood cellulose nanocrystal suspensions. *Biomacromolecules* **2005,** *6* (2), 1048-1054.
1768   53.   Hasani, M.; Cranston, E. D.; Westman, G.; Gray, D. G., Cationic surface functionalization of
1769   cellulose nanocrystals. *soft Matter* **2008,** *4* (11), 2238-2244.
1770   54.   Xu, Q.; Yi, J.; Zhang, X.; Zhang, H., A novel amphotropic polymer based on cellulose nanocrystals
1771   grafted with azo polymers. *european Polym. J.* **2008,** *44* (9), 2830-2837.
1772   55.   Yi, J.; Xu, Q.; Zhang, X.; Zhang, H., Chiral-nematic self-ordering of rodlike cellulose nanocrystals
1773   grafted with poly (styrene) in both thermotropic and lyotropic states. *Polymer* **2008,** *49* (20), 4406-4412.
1774   56.   Edwards, S.; Doi, M., Thetheory of polymer dynamics. Oxford Science Publications, Oxford, UK:
1775   1986.
1776   57.   Mu, X.; Gray, D. G., Formation of chiral nematic films from cellulose nanocrystal suspensions is a
1777   two-stage process. *Langmuir* **2014,** *30* (31), 9256-9260.
1778   58.   Wu, Q.; Meng, Y.; Wang, S.; Li, Y.; Fu, S.; Ma, L.; Harper, D., Rheological behavior of cellulose
1779   nanocrystal suspension: Influence of concentration and aspect ratio. *journal Appl. Polym. Sci.* **2014,** *131*
1780   (15).
1781   59.   Xu, H.-N.; Tang, Y.-Y.; Ouyang, X.-K., Shear-induced breakup of cellulose nanocrystal aggregates.
1782   *Langmuir* **2017,** *33* (1), 235-242.
1783   60.   Xu, Y.; Atrens, A. D.; Stokes, J. R., "Liquid, gel and soft glass" phase transitions and rheology of
1784   nanocrystalline cellulose suspensions as a function of concentration and salinity. *soft Matter* **2018,** *14*
1785   (10), 1953-1963.
1786   61.   Liao, J.; Pham, K. A.; Breedveld, V., TEMPO-CNF suspensions in the viscoelastic regime: capturing
1787   the effect of morphology and surface charge with a rheological parameter. *Cellulose* **2021,** *28* (2), 813-
1788   827.

1789 62.   Isogai, A.; Zhou, Y., Diverse nanocelluloses prepared from TEMPO-oxidized wood cellulose
1790 fibers: Nanonetworks, nanofibers, and nanocrystals. *Current Opinion in Solid State and Materials Science*
1791 **2019,** *23* (2), 101-106.
1792 63.   Saito, T.; Nishiyama, Y.; Putaux, J.-L.; Vignon, M.; Isogai, A., Homogeneous suspensions of
1793 individualized microfibrils from TEMPO-catalyzed oxidation of native cellulose. *Biomacromolecules* **2006,**
1794 *7* (6), 1687-1691.
1795 64.   Pääkkö, M.; Ankerfors, M.; Kosonen, H.; Nykänen, A.; Ahola, S.; Österberg, M.; Ruokolainen, J.;
1796 Laine, J.; Larsson, P. T.; Ikkala, O., Enzymatic hydrolysis combined with mechanical shearing and high-
1797 pressure homogenization for nanoscale cellulose fibrils and strong gels. *Biomacromolecules* **2007,** *8* (6),
1798 1934-1941.
1799 65.   Wågberg, L.; Decher, G.; Norgren, M.; Lindström, T.; Ankerfors, M.; Axnäs, K., The build-up of
1800 polyelectrolyte multilayers of microfibrillated cellulose and cationic polyelectrolytes. *Langmuir* **2008,** *24*
1801 (3), 784-795.
1802 66.   Mendoza, L.; Batchelor, W.; Tabor, R. F.; Garnier, G., Gelation mechanism of cellulose nanofibre
1803 gels: A colloids and interfacial perspective. *journal colloid interface sci.* **2018,** *509*, 39-46.
1804 67.   Shogren, R. L.; Peterson, S. C.; Evans, K. O.; Kenar, J. A., Preparation and characterization of
1805 cellulose gels from corn cobs. *carbohydrate Polym.* **2011,** *86* (3), 1351-1357.
1806 68.   Benhamou, K.; Dufresne, A.; Magnin, A.; Mortha, G.; Kaddami, H., Control of size and
1807 viscoelastic properties of nanofibrillated cellulose from palm tree by varying the TEMPO-mediated
1808 oxidation time. *carbohydrate Polym.* **2014,** *99*, 74-83.
1809 69.   Bettaieb, F.; Nechyporchuk, O.; Khiari, R.; Mhenni, M. F.; Dufresne, A.; Belgacem, M. N., Effect of
1810 the oxidation treatment on the production of cellulose nanofiber suspensions from Posidonia oceanica:
1811 the rheological aspect. *carbohydrate Polym.* **2015,** *134*, 664-672.
1812 70.   Jowkarderis, L.; van de Ven, T. G., Intrinsic viscosity of aqueous suspensions of cellulose
1813 nanofibrils. *Cellulose* **2014,** *21* (4), 2511-2517.
1814 71.   Tanaka, R.; Saito, T.; Hondo, H.; Isogai, A., Influence of flexibility and dimensions of
1815 nanocelluloses on the flow properties of their aqueous dispersions. *Biomacromolecules* **2015,** *16* (7),
1816 2127-2131.
1817 72.   Zakani, B.; Grecov, D., Yield stress analysis of cellulose nanocrystalline gels. *Cellulose* **2020,** *27*
1818 (16), 9337-9353.
1819 73.   Hyun, K.; Wilhelm, M.; Klein, C. O.; Cho, K. S.; Nam, J. G.; Ahn, K. H.; Lee, S. J.; Ewoldt, R. H.;
1820 McKinley, G. H., A review of nonlinear oscillatory shear tests: Analysis and application of large amplitude
1821 oscillatory shear (LAOS). *progress Polym. Sci.* **2011,** *36* (12), 1697-1753.
1822 74.   Saengow, C.; Giacomin, A. J., Review of nonlinear oscillatory shear flow notations and
1823 presentations: polymeric liquids. *current Opin. Colloid Interface Sci.* **2019,** *43*, 26-38.
1824 75.   Stolz, J.; Oguzlu, H.; Khalili, Z.; Boluk, Y., Exploring the gelation of aqueous cellulose nanocrystals
1825 (CNCs)-hydroxyethyl cellulose (HEC) mixtures. *rheologica Acta* **2021,** *60* (9), 483-495.
1826 76.   Calabrese, V.; Haward, S. J.; Shen, A. Q., Effects of shearing and extensional flows on the
1827 alignment of colloidal rods. *Macromolecules* **2021,** *54* (9), 4176-4185.
1828 77.   Cai, R.; Xiao, H.; Christov, I. C.; Zhao, Y., Diffusion of ellipsoidal granular particles in shear flow.
1829 *aiche J.* **2021,** *67* (2), e17109.
1830 78.   Babaei-Ghazvini, A.; Acharya, B., Influence of cellulose nanocrystal aspect ratio on shear force
1831 aligned films: Physical and mechanical properties. *Carbohydrate Polymer Technologies and Applications*
1832 **2022,** *3*, 100217.
1833 79.   Momeni, A.; Walters, C. M.; Xu, Y.-T.; Hamad, W. Y.; MacLachlan, M. J., Concentric chiral
1834 nematic polymeric fibers from cellulose nanocrystals. *Nanoscale Advances* **2021,** *3* (17), 5111-5121.
1835 80.   Prince, E.; Wang, Y.; Smalyukh, I. I.; Kumacheva, E., Cylindrical confinement of nanocolloidal
1836 cholesteric liquid crystal. *the J. Phys. Chem. B* **2021,** *125* (29), 8243-8250.

1837   81.   Browne, C.; Raghuwanshi, V. S.; Lin, M.; Garnier, G.; Batchelor, W., Characterisation of Cellulose
1838   Nanocrystals by Rheology and Small Angle X-Ray Scattering (SAXS). *colloids Surf. Physicochem. Eng. Asp.*
1839   **2022**, 129532.
1840   82.   Zakani, B.; Grecov, D., Effect of ultrasonic treatment on yield stress of highly concentrated
1841   cellulose nano-crystalline (CNC) aqueous suspensions. *carbohydrate Polym.* **2022**, 119651.
1842   83.   Qin, J.; Wang, Z.; Hu, J.; Yuan, Y.; Liu, P.; Cheng, L.; Kong, Z.; Liu, K.; Yan, S.; Zhang, J., Distinct
1843   liquid crystal self-assembly behavior of cellulose nanocrystals functionalized with ionic liquids. *colloids*
1844   *Surf. Physicochem. Eng. Asp.* **2022,** *632*, 127790.
1845   84.   Rajeev, A.; Natale, G., Anisotropy and Nanomechanics of Cellulose Nanocrystals/Polyethylene
1846   Glycol Composite Films. *Biomacromolecules* **2022,** *23* (4), 1592-1600.
1847   85.   Beuguel, Q.; Tavares, J. R.; Carreau, P. J.; Heuzey, M.-C., Rheological behavior of cellulose
1848   nanocrystal suspensions in polyethylene glycol. *journal Rheol.* **2018,** *62* (2), 607-618.
1849   86.   Del Gado, E.; Fiocco, D.; Foffi, G.; Manley, S.; Trappe, V.; Zaccone, A., Colloidal gelation. *Fluids,*
1850   *Colloids and Soft Materials: An Introduction to Soft Matter Physics* **2016**, 279-292.
1851   87.   Elazzouzi-Hafraoui, S.; Putaux, J.-L.; Heux, L., Self-assembling and chiral nematic properties of
1852   organophilic cellulose nanocrystals. *the J. Phys. Chem. B* **2009,** *113* (32), 11069-11075.
1853   88.   Hu, Z.; Cranston, E. D.; Ng, R.; Pelton, R., Tuning cellulose nanocrystal gelation with
1854   polysaccharides and surfactants. *Langmuir* **2014,** *30* (10), 2684-2692.
1855   89.   Oguzlu, H.; Boluk, Y., Interactions between cellulose nanocrystals and anionic and neutral
1856   polymers in aqueous solutions. *Cellulose* **2017,** *24* (1), 131-146.
1857   90.   Zhong, L.; Fu, S.; Peng, X.; Zhan, H.; Sun, R., Colloidal stability of negatively charged cellulose
1858   nanocrystalline in aqueous systems. *carbohydrate Polym.* **2012,** *90* (1), 644-649.
1859   91.   Lenfant, G.; Heuzey, M.-C.; van de Ven, T. G.; Carreau, P. J., A comparative study of ECNC and
1860   CNC suspensions: effect of salt on rheological properties. *rheologica Acta* **2017,** *56* (1), 51-62.
1861   92.   Prathapan, R.; Thapa, R.; Garnier, G.; Tabor, R. F., Modulating the zeta potential of cellulose
1862   nanocrystals using salts and surfactants. *colloids Surf. Physicochem. Eng. Asp.* **2016,** *509*, 11-18.
1863   93.   Peddireddy, K. R.; Capron, I.; Nicolai, T.; Benyahia, L., Gelation kinetics and network structure of
1864   cellulose nanocrystals in aqueous solution. *Biomacromolecules* **2016,** *17* (10), 3298-3304.
1865   94.   Ranjbar, D.; Hatzikiriakos, S. G., Effect of ionic surfactants on the viscoelastic properties of chiral
1866   nematic cellulose nanocrystal suspensions. *Langmuir* **2019,** *36* (1), 293-301.
1867   95.   Lewis, L.; Derakhshandeh, M.; Hatzikiriakos, S. G.; Hamad, W. Y.; MacLachlan, M. J.,
1868   Hydrothermal gelation of aqueous cellulose nanocrystal suspensions. *Biomacromolecules* **2016,** *17* (8),
1869   2747-2754.
1870   96.   Lewis, L.; Hatzikiriakos, S. G.; Hamad, W. Y.; MacLachlan, M. J., Freeze–thaw gelation of cellulose
1871   nanocrystals. *ACS Macro Letters* **2019,** *8* (5), 486-491.
1872   97.   Lai, P.-C.; Ren, Z.-F.; Yu, S.-S., Thermally Induced Gelation of Cellulose Nanocrystals in Deep
1873   Eutectic Solvents for 3D Printable and Self-Healable Ionogels. *ACS Appl. Polym. Mater.* **2022**.
1874   98.   Moberg, T.; Sahlin, K.; Yao, K.; Geng, S.; Westman, G.; Zhou, Q.; Oksman, K.; Rigdahl, M.,
1875   Rheological properties of nanocellulose suspensions: effects of fibril/particle dimensions and surface
1876   characteristics. *Cellulose* **2017,** *24* (6), 2499-2510.
1877   99.   Li, M.-C.; Wu, Q.; Song, K.; Lee, S.; Qing, Y.; Wu, Y., Cellulose nanoparticles: structure–
1878   morphology–rheology relationships. *ACS SUSTAIN CHEM ENG* **2015,** *3* (5), 821-832.
1879   100.   Cabane, B.; Wong, K.; Lindner, P.; Lafuma, F., Shear induced gelation of colloidal dispersions.
1880   *journal Rheol.* **1997,** *41* (3), 531-547.
1881   101.   Sarangapani, P. S.; Yu, Y.; Zhao, J.; Zhu, Y., Direct visualization of colloidal gelation under
1882   confinement. *physical Rev. E* **2008,** *77* (6), 061406.
1883   102.   Xu, Y.; Atrens, A.; Stokes, J. R., A review of nanocrystalline cellulose suspensions: Rheology,
1884   liquid crystal ordering and colloidal phase behaviour. *advances Colloid Interface Sci.* **2020,** *275*, 102076.

1885   103.   Abbasi Moud, A.; Sanati-Nezhad, A.; Hejazi, S. H., Confocal analysis of cellulose nanocrystal
1886   (CNC) based hydrogels and suspensions. *Cellulose* **2021,** *28* (16), 10259-10276.
1887   104.   Way, A. E.; Hsu, L.; Shanmuganathan, K.; Weder, C.; Rowan, S. J., pH-responsive cellulose
1888   nanocrystal gels and nanocomposites. *ACS MACRO LETT* **2012,** *1* (8), 1001-1006.
1889   105.   Chau, M.; Sriskandha, S. E.; Pichugin, D.; Thérien-Aubin, H. l.; Nykypanchuk, D.; Chauve, G. g.;
1890   Méthot, M.; Bouchard, J.; Gang, O.; Kumacheva, E., Ion-mediated gelation of aqueous suspensions of
1891   cellulose nanocrystals. *Biomacromolecules* **2015,** *16* (8), 2455-2462.
1892   106.   Han, J.; Lei, T.; Wu, Q., Facile preparation of mouldable polyvinyl alcohol-borax hydrogels
1893   reinforced by well-dispersed cellulose nanoparticles: physical, viscoelastic and mechanical properties.
1894   *Cellulose* **2013,** *20* (6), 2947-2958.
1895   107.   Chen, Y.; Xu, W.; Liu, W.; Zeng, G., Responsiveness, swelling, and mechanical properties of PNIPA
1896   nanocomposite hydrogels reinforced by nanocellulose. *J. Mater. Res.* **2015,** *30* (11), 1797-1807.
1897   108.   Karaaslan, M. A.; Tshabalala, M. A.; Yelle, D. J.; Buschle-Diller, G., Nanoreinforced biocompatible
1898   hydrogels from wood hemicelluloses and cellulose whiskers. *Carbohydr. Polym.* **2011,** *86* (1), 192-201.
1899   109.   De France, K. J.; Chan, K. J.; Cranston, E. D.; Hoare, T., Enhanced mechanical properties in
1900   cellulose nanocrystal–poly (oligoethylene glycol methacrylate) injectable nanocomposite hydrogels
1901   through control of physical and chemical cross-linking. *Biomacromolecules* **2016,** *17* (2), 649-660.
1902   110.   Yang, J.; Han, C.-R.; Duan, J.-F.; Xu, F.; Sun, R.-C., Mechanical and viscoelastic properties of
1903   cellulose nanocrystals reinforced poly (ethylene glycol) nanocomposite hydrogels. *ACS APPL. MATER.*
1904   *INTER.* **2013,** *5* (8), 3199-3207.
1905   111.   Le Goff, K. J.; Gaillard, C.; Helbert, W.; Garnier, C.; Aubry, T., Rheological study of reinforcement
1906   of agarose hydrogels by cellulose nanowhiskers. *Carbohydr. Polym.* **2015,** *116*, 117-123.
1907   112.   McKee, J. R.; Appel, E. A.; Seitsonen, J.; Kontturi, E.; Scherman, O. A.; Ikkala, O., Healable, stable
1908   and stiff hydrogels: combining conflicting properties using dynamic and selective three-component
1909   recognition with reinforcing cellulose nanorods. *advanced Funct. Mater.* **2014,** *24* (18), 2706-2713.
1910   113.   Wang, Y.; Chen, L., Impacts of nanowhisker on formation kinetics and properties of all-cellulose
1911   composite gels. *Carbohydr. Polym.* **2011,** *83* (4), 1937-1946.
1912   114.   Yang, J.; Han, C., Mechanically viscoelastic properties of cellulose nanocrystals skeleton
1913   reinforced hierarchical composite hydrogels. *ACS APPL. MATER. INTER.* **2016,** *8* (38), 25621-25630.
1914   115.   You, J.; Cao, J.; Zhao, Y.; Zhang, L.; Zhou, J.; Chen, Y., Improved mechanical properties and
1915   sustained release behavior of cationic cellulose nanocrystals reinforeced cationic cellulose injectable
1916   hydrogels. *Biomacromolecules* **2016,** *17* (9), 2839-2848.
1917   116.   Yuk, H.; Lu, B.; Lin, S.; Qu, K.; Xu, J.; Luo, J.; Zhao, X., 3D printing of conducting polymers. *Nat.*
1918   *Commun* **2020,** *11* (1), 1-8.
1919   117.   Mewis, J.; Wagner, N. J., *Colloidal suspension rheology*. Cambridge university press: 2012.
1920   118.   Vermant, J.; Solomon, M. J., Flow-induced structure in colloidal suspensions. *journal Phys.*
1921   *Condens. Matter* **2005,** *17* (4), R187.
1922   119.   Sonntag, R. C.; Russel, W. B., Structure and breakup of flocs subjected to fluid stresses: I. Shear
1923   experiments. *journal Colloid Interface Sci.* **1986,** *113* (2), 399-413.
1924   120.   Serra, T.; Casamitjana, X., Effect of the shear and volume fraction on the aggregation and
1925   breakup of particles. *aiche J.* **1998,** *44* (8), 1724-1730.
1926   121.   Tolpekin, V.; Duits, M. H.; Van den Ende, D.; Mellema, J., Aggregation and breakup of colloidal
1927   particle aggregates in shear flow, studied with video microscopy. *Langmuir* **2004,** *20* (7), 2614-2627.
1928   122.   Sommer, M. M., *Mechanical production of nanoparticles in stirred media mills*. Cuvillier Verlag:
1929   2007.
1930   123.   Eberle, A. P.; Martys, N.; Porcar, L.; Kline, S. R.; George, W. L.; Kim, J. M.; Butler, P. D.; Wagner,
1931   N. J., Shear viscosity and structural scalings in model adhesive hard-sphere gels. *physical Rev. E* **2014,** *89*
1932   (5), 050302.

1933   124.   Grenard, V.; Taberlet, N.; Manneville, S., Shear-induced structuration of confined carbon black
1934   gels: Steady-state features of vorticity-aligned flocs. *soft Matter* **2011,** *7* (8), 3920-3928.
1935   125.   Mewis, J.; Wagner, N. J., Thixotropy. *advances Colloid Interface Sci.* **2009,** *147*, 214-227.
1936   126.   Larson, R. G.; Wei, Y., A review of thixotropy and its rheological modeling. *journal Rheol.* **2019,**
1937   *63* (3), 477-501.
1938   127.   Moud, A. A.; Kamkar, M.; Sanati-Nezhad, A.; Hejazi, S. H.; Sundararaj, U., Viscoelastic properties
1939   of poly (vinyl alcohol) hydrogels with cellulose nanocrystals fabricated through sodium chloride addition:
1940   Rheological evidence of double network formation. *colloids Surf. Physicochem. Eng. Asp.* **2021,** *609*,
1941   125577.
1942   128.   Oguzlu, H.; Danumah, C.; Boluk, Y., Colloidal behavior of aqueous cellulose nanocrystal
1943   suspensions. *Curr Opin Colloid In* **2017,** *29*, 46-56.
1944   129.   Gicquel, E.; Martin, C.; Gauthier, Q.; Engström, J.; Abbattista, C.; Carlmark, A.; Cranston, E. D.;
1945   Jean, B.; Bras, J., Tailoring rheological properties of thermoresponsive hydrogels through block
1946   copolymer adsorption to cellulose nanocrystals. *Biomacromolecules* **2019,** *20* (7), 2545-2556.
1947   130.   Qiao, C.; Chen, G.; Zhang, J.; Yao, J., Structure and rheological properties of cellulose
1948   nanocrystals suspension. *FOOD HYDROCOLLOID* **2016,** *55*, 19-25.
1949   131.   Moud, A. A.; Kamkar, M.; Sanati-Nezhad, A.; Hejazi, S. H.; Sundararaj, U., Nonlinear viscoelastic
1950   characterization of charged cellulose nanocrystal network structure in the presence of salt in aqueous
1951   media. *Cellulose* **2020,** *27* (10), 5729-5743.
1952   132.   Liao, J.; Pham, K. A.; Breedveld, V., Rheological characterization and modeling of cellulose
1953   nanocrystal and TEMPO-oxidized cellulose nanofibril suspensions. *Cellulose* **2020,** *27* (7), 3741-3757.
1954   133.   Danesh, M.; Mauran, D.; Hojabr, S.; Berry, R.; Pawlik, M.; Hatzikiriakos, S. G., Yielding of cellulose
1955   nanocrystal suspensions in the presence of electrolytes. *physics Fluid* **2020,** *32* (9), 093103.
1956   134.   Sahlin, K.; Forsgren, L.; Moberg, T.; Bernin, D.; Rigdahl, M.; Westman, G., Surface treatment of
1957   cellulose nanocrystals (CNC): effects on dispersion rheology. *Cellulose* **2018,** *25* (1), 331-345.
1958   135.   Honorato-Rios, C.; Lehr, C.; Schütz, C.; Sanctuary, R.; Osipov, M. A.; Baller, J.; Lagerwall, J. P.,
1959   Fractionation of cellulose nanocrystals: enhancing liquid crystal ordering without promoting gelation.
1960   *NPG Asia Mater.* **2018,** *10* (5), 455-465.
1961   136.   Bagheriasl, D.; Carreau, P. J.; Riedl, B.; Dubois, C.; Hamad, W. Y., Shear rheology of polylactide
1962   (PLA)–cellulose nanocrystal (CNC) nanocomposites. *Cellulose* **2016,** *23* (3), 1885-1897.
1963   137.   Yoon, H. S.; Yang, K.; Kim, Y. M.; Nam, K.; Roh, Y. H., Cellulose nanocrystals as support
1964   nanomaterials for dual droplet-based freeform 3D printing. *carbohydrate Polym.* **2021,** *272*, 118469.
1965   138.   Freundlich, H., *The colloidal state. 1. Thixotropy*. Hermann: 1935.
1966   139.   Abbasi Moud, A.; Poisson, J.; Hudson, Z. M.; Hatzikiriakos, S. G., Yield stress and wall slip of
1967   kaolinite networks. *physics Fluid* **2021,** *33* (5), 053105.
1968   140.   Heggset, E. B.; Strand, B. L.; Sundby, K. W.; Simon, S.; Chinga-Carrasco, G.; Syverud, K.,
1969   Viscoelastic properties of nanocellulose based inks for 3D printing and mechanical properties of
1970   CNF/alginate biocomposite gels. *Cellulose* **2019,** *26* (1), 581-595.
1971   141.   Fazilati, M.; Ingelsten, S.; Wojno, S.; Nypelö, T.; Kádár, R., Thixotropy of cellulose nanocrystal
1972   suspensions. *journal Rheol.* **2021,** *65* (5), 1035-1052.
1973   142.   Cheng, D.; Wen, Y.; Wang, L.; An, X.; Zhu, X.; Ni, Y., Adsorption of polyethylene glycol (PEG) onto
1974   cellulose nano-crystals to improve its dispersity. *carbohydrate Polym.* **2015,** *123*, 157-163.
1975   143.   Padalkar, S.; Capadona, J. R.; Rowan, S. J.; Weder, C.; Won, Y.-H.; Stanciu, L. A.; Moon, R. J.,
1976   Natural biopolymers: novel templates for the synthesis of nanostructures. *Langmuir* **2010,** *26* (11), 8497-
1977   8502.
1978   144.   An, X.; Long, Y.; Ni, Y., Cellulose nanocrystal/hexadecyltrimethylammonium bromide/silver
1979   nanoparticle composite as a catalyst for reduction of 4-nitrophenol. *carbohydrate Polym.* **2017,** *156*,
1980   253-258.

1981	145.	Tavera, R.; Calderón, E., Use of CTAB as a cost-effective solution to an old problem: the
1982	interference of the mucilage of desmids for scanning electron microscopy. *Phycologia* **2013,** *52* (5), 422-
1983	425.
1984	146.	Gahrooee, T. R.; Moud, A. A.; Danesh, M.; Hatzikiriakos, S. G., Rheological characterization of
1985	CNC-CTAB network below and above critical micelle concentration (CMC). *carbohydrate Polym.* **2021,**
1986	*257*, 117552.
1987	147.	Wang, D.; Yang, T.; Li, J.; Zhang, J.; Yu, J.; Zhang, X.; Zhang, J., Thermostable and redispersible
1988	cellulose nanocrystals with thixotropic gelation behavior by a facile desulfation process. *ACS Sustain.*
1989	*Chem. Eng.* **2020,** *8* (31), 11737-11746.
1990	148.	da Fonsêca, J. H. L.; d'Ávila, M. A., Rheological behavior of carboxymethylcellulose and cellulose
1991	nanocrystal aqueous dispersions. *rheologica acta* **2021,** *60* (9), 497-509.
1992	149.	Boonlai, W.; Tantishaiyakul, V.; Hirun, N., Characterization of κ-
1993	carrageenan/methylcellulose/cellulose nanocrystal hydrogels for 3D bioprinting. *polymer Int.* **2022,** *71*
1994	(2), 181-191.
1995	150.	Solomon, M. J.; Spicer, P. T., Microstructural regimes of colloidal rod suspensions, gels, and
1996	glasses. *soft matter* **2010,** *6* (7), 1391-1400.
1997	151.	Schilling, T.; Jungblut, S.; Miller, M. A., Depletion-induced percolation in networks of nanorods.
1998	*physical Rev. Lett.* **2007,** *98* (10), 108303.
1999	152.	Bauer, T.; Höfling, F.; Munk, T.; Frey, E.; Franosch, T., The localization transition of the two-
2000	dimensional Lorentz model. *The European Physical Journal Special Topics* **2010,** *189* (1), 103-118.
2001	153.	Rogers, S. A.; Erwin, B. M.; Vlassopoulos, D.; Cloitre, M., A sequence of physical processes
2002	determined and quantified in LAOS: Application to a yield stress fluid. *journal Rheol.* **2011,** *55* (2), 435-
2003	458.
2004	154.	Bonn, D.; Denn, M. M.; Berthier, L.; Divoux, T.; Manneville, S., Yield stress materials in soft
2005	condensed matter. *Reviews of Modern Physics* **2017,** *89* (3), 035005.
2006	155.	Dimitriou, C. J.; Ewoldt, R. H.; McKinley, G. H., Describing and prescribing the constitutive
2007	response of yield stress fluids using large amplitude oscillatory shear stress (LAOStress). *journal Rheol.*
2008	**2013,** *57* (1), 27-70.
2009	156.	Rogers, S. A.; Lettinga, M. P., A sequence of physical processes determined and quantified in
2010	large-amplitude oscillatory shear (LAOS): Application to theoretical nonlinear models. *journal Rheol.*
2011	**2012,** *56* (1), 1-25.
2012	157.	Donley, G. J.; Singh, P. K.; Shetty, A.; Rogers, S. A., Elucidating the G "overshoot in soft materials
2013	with a yield transition via a time-resolved experimental strain decomposition. *proceedings National*
2014	*Acad. Sci.* **2020,** *117* (36), 21945-21952.
2015	158.	Shao, Z.; Negi, A. S.; Osuji, C. O., Role of interparticle attraction in the yielding response of
2016	microgel suspensions. *soft Matter* **2013,** *9* (22), 5492-5500.
2017	159.	Ewoldt, R. H., Defining nonlinear rheological material functions for oscillatory shear. *journal*
2018	*Rheol.* **2013,** *57* (1), 177-195.
2019	160.	Wang, Y.; Xu, C.; Wu, D.; Xie, W.; Wang, K.; Xia, Q.; Yang, H., Rheology of the cellulose
2020	nanocrystals filled poly (ε-caprolactone) biocomposites. *Polymer* **2018,** *140*, 167-178.
2021	161.	Wojno, S.; Fazilati, M.; Nypelö, T.; Westman, G.; Kádár, R., Phase transitions of cellulose
2022	nanocrystal suspensions from nonlinear oscillatory shear. *Cellulose* **2022,** *29* (7), 3655-3673.
2023	162.	Kamkar, M.; Janmaleki, M.; Erfanian, E.; Sanati-Nezhad, A.; Sundararaj, U., Covalently cross-
2024	linked hydrogels: Mechanisms of nonlinear viscoelasticity. *the Can. J. Chem. Eng.*
2025	163.	Lagerwall, J. P.; Scalia, G., A new era for liquid crystal research: Applications of liquid crystals in
2026	soft matter nano-, bio-and microtechnology. *current Appl. Phys.* **2012,** *12* (6), 1387-1412.
2027	164.	De Gennes, P.-G.; Prost, J., *The physics of liquid crystals*. Oxford university press: 1993.

165.   Parker, R. M.; Guidetti, G.; Williams, C. A.; Zhao, T.; Narkevicius, A.; Vignolini, S.; Frka-Petesic, B., The self-assembly of cellulose nanocrystals: Hierarchical design of visual appearance. *advanced Mater.* **2018,** *30* (19), 1704477.

166.   Zhang, Y. P.; Chodavarapu, V. P.; Kirk, A. G.; Andrews, M. P., Nanocrystalline cellulose for covert optical encryption. *Journal of Nanophotonics* **2012,** *6* (1), 063516.

167.   Shopsowitz, K. E.; Qi, H.; Hamad, W. Y.; MacLachlan, M. J., Free-standing mesoporous silica films with tunable chiral nematic structures. *Nature* **2010,** *468* (7322), 422-425.

168.   Lehmann, O., Die Struktur krystallinischer Flüssigkeiten. *zeitschrift fur Phys. Chem.* **1890,** *5* (1), 427-435.

169.   Porter, R. S.; Johnson, J. F., Orientation of nematic mesophases. *The Journal of Physical Chemistry* **1962,** *66* (10), 1826-1829.

170.   Porter, R. S.; Johnson, J. F., The rheology of liquid crystals. In *Rheology*, Elsevier: 1967; pp 317-345.

171.   Gong, X.; Wang, Y.; Zeng, H.; Betti, M.; Chen, L., Highly porous, hydrophobic, and compressible cellulose nanocrystals/poly (vinyl alcohol) aerogels as recyclable absorbents for oil–water separation. *ACS Sustain. Chem. Eng.* **2019,** *7* (13), 11118-11128.

172.   Revol, J.-F.; Godbout, L.; Dong, X.-M.; Gray, D. G.; Chanzy, H.; Maret, G., Chiral nematic suspensions of cellulose crystallites; phase separation and magnetic field orientation. *Liquid Crystals* **1994,** *16* (1), 127-134.

173.   Sun, B.; Hou, Q.; Liu, Z.; Ni, Y., Sodium periodate oxidation of cellulose nanocrystal and its application as a paper wet strength additive. *Cellulose* **2015,** *22* (2), 1135-1146.

174.   Davies, G.; Stokes, J., Thin film and high shear rheology of multiphase complex fluids. *Journal of Non-newtonian fluid mechanics* **2008,** *148* (1-3), 73-87.

175.   Johnston, M. T.; Ewoldt, R. H., Precision rheometry: Surface tension effects on low-torque measurements in rotational rheometers. *journal Rheol.* **2013,** *57* (6), 1515-1532.

176.   Zhang, S.; Kumar, S., Carbon nanotubes as liquid crystals. *Small* **2008,** *4* (9), 1270-1283.

177.   Abbasi Moud, A.; Hatzikiriakos, S. G., Kaolinite colloidal suspensions under the influence of sodium dodecyl sulfate. *physics Fluid* **2022,** *34* (1), 013107.

178.   Larson, R. G.; Doi, M., Mesoscopic domain theory for textured liquid crystalline polymers. *journal Rheol.* **1991,** *35* (4), 539-563.

179.   Shafiei-Sabet, S.; Hamad, W.; Hatzikiriakos, S., Ionic strength effects on the microstructure and shear rheology of cellulose nanocrystal suspensions. *Cellulose* **2014,** *21* (5), 3347-3359.

180.   Li, J.; Revol, J.; Marchessault, R., Rheological properties of aqueous suspensions of chitin crystallites. *journal Colloid Interface Sci.* **1996,** *183* (2), 365-373.

181.   Buffa, J. M.; Casado, U.; Mucci, V.; Aranguren, M. I., Cellulose nanocrystals in aqueous suspensions: rheology of lyotropic chiral liquid crystals. *Cellulose* **2019,** *26* (4), 2317-2332.

182.   Delepierre, G.; Eyley, S.; Thielemans, W.; Weder, C.; Cranston, E. D.; Zoppe, J. O., Patience is a virtue: Self-assembly and physico-chemical properties of cellulose nanocrystal allomorphs. *Nanoscale* **2020,** *12* (33), 17480-17493.

183.   Vermant, J.; Moldenaers, P.; Picken, S.; Mewis, J., A comparison between texture and rheological behaviour of lyotropic liquid crystalline polymers during flow. *Journal of non-newtonian fluid mechanics* **1994,** *53*, 1-23.

184.   Moldenaers, P.; Mewis, J., Relaxational phenomena and anisotrophy in lyotropic polymeric liquid crystals. *Journal of non-newtonian fluid mechanics* **1990,** *34* (3), 359-374.

185.   Picken, S.; Aerts, J.; Doppert, H.; Reuvers, A.; Northolt, M., Structure and rheology of aramid solutions: transient rheological and rheooptical measurements. *Macromolecules* **1991,** *24* (6), 1366-1375.

2075   186.   Beekmans, F., Rheology and changes in structure of thermotropic liquid crystalline polymers.
2076   **1998**.
2077   187.   Burghardt, W. R.; Fuller, G. G., Role of director tumbling in the rheology of polymer liquid crystal
2078   solutions. *Macromolecules* **1991,** *24* (9), 2546-2555.
2079   188.   Cheng, Z.; Ma, Y.; Yang, L.; Cheng, F.; Huang, Z.; Natan, A.; Li, H.; Chen, Y.; Cao, D.; Huang, Z.,
2080   Plasmonic-Enhanced Cholesteric Films: Coassembling Anisotropic Gold Nanorods with Cellulose
2081   Nanocrystals. *advanced Opt. Mater.* **2019,** *7* (9), 1801816.
2082   189.   Schutz, C.; Agthe, M.; Fall, A. B.; Gordeyeva, K.; Guccini, V.; Salajková, M.; Plivelic, T. S.;
2083   Lagerwall, J. P.; Salazar-Alvarez, G.; Bergstrom, L., Rod packing in chiral nematic cellulose nanocrystal
2084   dispersions studied by small-angle X-ray scattering and laser diffraction. *Langmuir* **2015,** *31* (23), 6507-
2085   6513.
2086   190.   Zhang, Y.; Cheng, Q.; Chang, C.; Zhang, L., Phase transition identification of cellulose nanocrystal
2087   suspensions derived from various raw materials. *journal Appl. Polym. Sci.* **2018,** *135* (24), 45702.
2088   191.   Xu, Y.; Atrens, A. D.; Stokes, J. R., Liquid crystal hydroglass formed via phase separation of
2089   nanocellulose colloidal rods. *soft Matter* **2019,** *15* (8), 1716-1720.
2090   192.   Abitbol, T.; Kam, D.; Levi-Kalisman, Y.; Gray, D. G.; Shoseyov, O., Surface charge influence on the
2091   phase separation and viscosity of cellulose nanocrystals. *Langmuir* **2018,** *34* (13), 3925-3933.
2092   193.   Gray, D. G., Order and gelation of cellulose nanocrystal suspensions: an overview of some issues.
2093   *philosophical Trans. R. Soc. Math. Phys. Eng. Sci.* **2018,** *376* (2112), 20170038.
2094   194.   Xu, Y.; Atrens, A.; Stokes, J. R., Structure and rheology of liquid crystal hydroglass formed in
2095   aqueous nanocrystalline cellulose suspensions. *journal Colloid Interface Sci.* **2019,** *555*, 702-713.
2096   195.   Calabrese, V.; Varchanis, S.; Haward, S. J.; Tsamopoulos, J.; Shen, A. Q., Structure-property
2097   relationship of a soft colloidal glass in simple and mixed flows. *journal Colloid Interface Sci.* **2021,** *601*,
2098   454-466.
2099   196.   Shafeiei-Sabet, S.; Hamad, W. Y.; Hatzikiriakos, S. G., Influence of degree of sulfation on the
2100   rheology of cellulose nanocrystal suspensions. *rheologica acta* **2013,** *52* (8), 741-751.
2101   197.   Parton, T. G.; Parker, R. M.; van de Kerkhof, G. T.; Narkevicius, A.; Haataja, J. S.; Frka-Petesic, B.;
2102   Vignolini, S., Chiral self-assembly of cellulose nanocrystals is driven by crystallite bundles. *nature
2103   commun.* **2022,** *13* (1), 1-9.
2104   198.   Friedel, G. In *Les états mésomorphes de la matière*, Annales de physique, 1922; pp 273-474.
2105   199.   Conley, K.; Godbout, L.; Whitehead, M. T.; van de Ven, T. G., Origin of the twist of cellulosic
2106   materials. *Carbohydrate polymers* **2016,** *135*, 285-299.
2107   200.   Usov, I.; Nyström, G.; Adamcik, J.; Handschin, S.; Schütz, C.; Fall, A.; Bergström, L.; Mezzenga, R.,
2108   Understanding nanocellulose chirality and structure–properties relationship at the single fibril level.
2109   *nature commun.* **2015,** *6* (1), 1-11.
2110   201.   Matthews, J. F.; Skopec, C. E.; Mason, P. E.; Zuccato, P.; Torget, R. W.; Sugiyama, J.; Himmel, M.
2111   E.; Brady, J. W., Computer simulation studies of microcrystalline cellulose Iβ. *carbohydrate res.* **2006,**
2112   *341* (1), 138-152.
2113   202.   Hadden, J. A.; French, A. D.; Woods, R. J., Unraveling cellulose microfibrils: a twisted tale.
2114   *Biopolymers* **2013,** *99* (10), 746-756.
2115   203.   Paajanen, A.; Ceccherini, S.; Maloney, T.; Ketoja, J. A., Chirality and bound water in the
2116   hierarchical cellulose structure. *Cellulose* **2019,** *26* (10), 5877-5892.
2117   204.   Zhao, Z.; Shklyaev, O. E.; Nili, A.; Mohamed, M. N. A.; Kubicki, J. D.; Crespi, V. H.; Zhong, L.,
2118   Cellulose microfibril twist, mechanics, and implication for cellulose biosynthesis. *The Journal of Physical
2119   Chemistry A* **2013,** *117* (12), 2580-2589.
2120   205.   Fittolani, G.; Vargová, D.; Seeberger, P. H.; Ogawa, Y.; Delbianco, M., Bottom-Up Approach to
2121   Understand Chirality Transfer across Scales in Cellulose Assemblies. *journal Am. Chem. Soc.* **2022,** *144*
2122   (27), 12469-12475.

2123   206.   Gonçalves, D. P.; Ogolla, T.; Hegmann, T., Chirality Transfer from an Innately Chiral Nanocrystal
2124   Core to a Nematic Liquid Crystal 2: Lyotropic Chromonic Liquid Crystals. *ChemPhysChem* **2022**.
2125   207.   Gonçalves, D. P.; Hegmann, T., Chirality Transfer from an Innately Chiral Nanocrystal Core to a
2126   Nematic Liquid Crystal: Surface-Modified Cellulose Nanocrystals. *angewandte Chem. Int. Ed.* **2021,** *60*
2127   (32), 17344-17349.
2128   208.   Moud, A. A., Advanced cellulose nanocrystals (CNC) and cellulose nanofibrils (CNF) aerogels:
2129   Bottom-up assembly perspective for production of adsorbents. *international J. Biological Macromol.*
2130   **2022**.
2131   209.   Li, D.; Wang, Y.; Long, F.; Gan, L.; Huang, J., Solvation-controlled elastification and shape-
2132   recovery of cellulose nanocrystal-based aerogels. *ACS Appl. Mater. Interface* **2019,** *12* (1), 1549-1557.
2133   210.   Wang, N.; Ding, E.; Cheng, R., Thermal degradation behaviors of spherical cellulose nanocrystals
2134   with sulfate groups. *Polymer* **2007,** *48* (12), 3486-3493.
2135   211.   D'Acierno, F.; Hamad, W. Y.; Michal, C. A.; MacLachlan, M. J., Thermal degradation of cellulose
2136   filaments and nanocrystals. *Biomacromolecules* **2020,** *21* (8), 3374-3386.
2137   212.   Feng, X.; Yang, Z.; Rostom, S. S.; Dadmun, M.; Xie, Y.; Wang, S., Structural, mechanical, and
2138   thermal properties of 3D printed L-CNC/acrylonitrile butadiene styrene nanocomposites. *journal appl.*
2139   *polym. sci.* **2017,** *134* (31), 45082.
2140   213.   Rowe, A. A.; Tajvidi, M.; Gardner, D. J., Thermal stability of cellulose nanomaterials and their
2141   composites with polyvinyl alcohol (PVA). *Journal of Thermal Analysis and Calorimetry* **2016,** *126* (3),
2142   1371-1386.
2143   214.   Zhu, G.; Giraldo Isaza, L.; Huang, B.; Dufresne, A., Multifunctional Nanocellulose/Carbon
2144   Nanotube Composite Aerogels for High-Efficiency Electromagnetic Interference Shielding. *ACS Sustain.*
2145   *Chem. Eng.* **2022,** *10* (7), 2397-2408.
2146   215.   Lee, T.-W.; Lee, S.-E.; Jeong, Y. G., Highly effective electromagnetic interference shielding
2147   materials based on silver nanowire/cellulose papers. *ACS Appl. Mater. Interface* **2016,** *8* (20), 13123-
2148   13132.
2149   216.   Cao, Y.; Lewis, L.; Hamad, W. Y.; MacLachlan, M. J., Pressure-responsive hierarchical chiral
2150   photonic aerogels. *advanced Mater.* **2019,** *31* (21), 1808186.
2151   217.   Oster, G., Two-phase formation in solutions of tobacco mosaic virus and the problem of long-
2152   range forces. *The Journal of general physiology* **1950,** *33* (5), 445-473.
2153   218.   Dogic, Z.; Fraden, S., Cholesteric phase in virus suspensions. *Langmuir* **2000,** *16* (20), 7820-7824.
2154   219.   Leforestier, A.; Bertin, A.; Dubochet, J.; Richter, K.; Blanc, N. S.; Livolant, F., Expression of
2155   chirality in columnar hexagonal phases or DNA and nucleosomes. *Comptes Rendus Chimie* **2008,** *11* (3),
2156   229-244.
2157   220.   Folda, T.; Hoffmann, H.; Chanzy, H.; Smith, P., Nature1988, 333, 55. *Google Scholar There is no*
2158   *corresponding record for this reference*.
2159   221.   Barry, E.; Hensel, Z.; Dogic, Z.; Shribak, M.; Oldenbourg, R., Entropy-driven formation of a chiral
2160   liquid-crystalline phase of helical filaments. *physical rev. lett.* **2006,** *96* (1), 018305.
2161   222.   Giraud-Guille, M.-M., Twisted plywood architecture of collagen fibrils in human compact bone
2162   osteons. *Calcified tissue international* **1988,** *42* (3), 167-180.
2163   223.   Buining, P.; Lekkerkerker, H., Isotropic-nematic phase separation of a dispersion of organophilic
2164   boehmite rods. *The Journal of Physical Chemistry* **1993,** *97* (44), 11510-11516.
2165   224.   Chan, C. L. C.; Bay, M. M.; Jacucci, G.; Vadrucci, R.; Williams, C. A.; van de Kerkhof, G. T.; Parker,
2166   R. M.; Vynck, K.; Frka-Petesic, B.; Vignolini, S., Visual Appearance of Chiral Nematic Cellulose-Based
2167   Photonic Films: Angular and Polarization Independent Color Response with a Twist. *advanced Mater.*
2168   **2019,** *31* (52), 1905151.
2169   225.   Revol, J.-F.; Marchessault, R., In vitro chiral nematic ordering of chitin crystallites. *international J.*
2170   *Biological Macromol.* **1993,** *15* (6), 329-335.

226.   Borgström, J.; Quist, P.; Piculell, L., Macromolecules1996, 29, 5926– 5933. *Google Scholar There is no corresponding record for this reference.*

227.   DuPré, D. B.; Duke, R. W., Temperature, concentration, and molecular weight dependence of the twist elastic constant of cholesteric poly-γ-benzyl-L-glutamate. *the J. Chem. Phys.* **1975,** *63* (1), 143-148.

228.   Livolant, F.; Bouligand, Y., Liquid crystalline phases given by helical biological polymers (DNA, PBLG and xanthan). Columnar textures. *Journal de physique* **1986,** *47* (10), 1813-1827.

229.   Grelet, E.; Fraden, S., What is the origin of chirality in the cholesteric phase of virus suspensions? *physical rev. lett.* **2003,** *90* (19), 198302.

230.   Franklin, R. E.; Gosling, R. G., Molecular configuration in sodium thymonucleate. *Nature* **1953,** *171* (4356), 740-741.

231.   Hagerman, P. J., Flexibility of DNA. *Annual review of biophysics and biophysical chemistry* **1988,** *17* (1), 265-286.

232.   Watson, J. D.; Crick, F. H., Molecular structure of nucleic acids: a structure for deoxyribose nucleic acid. *Nature* **1953,** *171* (4356), 737-738.

233.   Onsager, L., The effects of shape on the interaction of colloidal particles. *Annals of the New York Academy of Sciences* **1949,** *51* (4), 627-659.

234.   Marchessault, R.; Morehead, F.; Walter, N., Liquid crystal systems from fibrillar polysaccharides. *Nature* **1959,** *184* (4686), 632-633.

235.   Werbowyi, R.; Gray, D., Liquid crystalline state of concentrated solution cyanoethyl derivatives. *Mol. Cryst. Liq. Crys. Lett* **1976,** *34*, 97.

236.   Wilts, B.; Dumanli, A. G.; Middleton, R.; Vukusic, P.; Vignolini, S., Invited Article: Chiral optics of helicoidal cellulose nanocrystal films. *APL Photonics* **2017,** *2* (4), 040801.

237.   Strzelecka, T. E.; Davidson, M. W.; Rill, R. L., Multiple liquid crystal phases of DNA at high concentrations. *Nature* **1988,** *331* (6155), 457-460.

238.   Brandes, R.; Kearns, D. R., Magnetic ordering of DNA liquid crystals. *Biochemistry* **1986,** *25* (20), 5890-5895.

239.   Wang, P.-X.; Hamad, W. Y.; MacLachlan, M. J., Structure and transformation of tactoids in cellulose nanocrystal suspensions. *nature commun.* **2016,** *7* (1), 1-8.

240.   Nikolov, S.; Petrov, M.; Lymperakis, L.; Friák, M.; Sachs, C.; Fabritius, H. O.; Raabe, D.; Neugebauer, J., Revealing the design principles of high-performance biological composites using ab initio and multiscale simulations: the example of lobster cuticle. *advanced Mater.* **2010,** *22* (4), 519-526.

241.   Weaver, J. C.; Milliron, G. W.; Miserez, A.; Evans-Lutterodt, K.; Herrera, S.; Gallana, I.; Mershon, W. J.; Swanson, B.; Zavattieri, P.; DiMasi, E., The stomatopod dactyl club: a formidable damage-tolerant biological hammer. *Science* **2012,** *336* (6086), 1275-1280.

242.   Gray, D., Chiral nematic ordering of polysaccharides. *carbohydrate Polym.* **1994,** *25* (4), 277-284.

243.   Orts, W.; Revol, J.-F.; Godbout, L.; Marchessault, R., SANS study of chirality and order in liquid crystalline cellulose suspensions. *MRS Online Proceedings Library (OPL)* **1994,** *376*.

244.   Conley, K.; Whitehead, M.; van de Ven, T. G., Probing the structural chirality of crystalline cellulose with induced circular dichroism. *Cellulose* **2017,** *24* (2), 479-486.

245.   Nystrom, G.; Arcari, M.; Adamcik, J.; Usov, I.; Mezzenga, R., Nanocellulose fragmentation mechanisms and inversion of chirality from the single particle to the cholesteric phase. *ACS nano* **2018,** *12* (6), 5141-5148.

246.   Paavilainen, S.; Róg, T.; Vattulainen, I., Analysis of twisting of cellulose nanofibrils in atomistic molecular dynamics simulations. *the J. Phys. Chem. B* **2011,** *115* (14), 3747-3755.

247.   Wu, T.; Li, J.; Li, J.; Ye, S.; Wei, J.; Guo, J., A bio-inspired cellulose nanocrystal-based nanocomposite photonic film with hyper-reflection and humidity-responsive actuator properties. *journal Mater. Chem. C* **2016,** *4* (41), 9687-9696.

2219   248.   Lu, T.; Pan, H.; Ma, J.; Li, Y.; Bokhari, S. W.; Jiang, X.; Zhu, S.; Zhang, D., Cellulose
2220   nanocrystals/polyacrylamide composites of high sensitivity and cycling performance to gauge humidity.
2221   *ACS Appl. Mater. Interface* **2017,** *9* (21), 18231-18237.
2222   249.   Giese, M.; Blusch, L. K.; Khan, M. K.; Hamad, W. Y.; MacLachlan, M. J., Responsive mesoporous
2223   photonic cellulose films by supramolecular cotemplating. *angewandte Chem.* **2014,** *126* (34), 9026-9030.
2224   250.   Hou, Y.; Guan, Q.-F.; Xia, J.; Ling, Z.-C.; He, Z.; Han, Z.-M.; Yang, H.-B.; Gu, P.; Zhu, Y.; Yu, S.-H.,
2225   Strengthening and toughening hierarchical nanocellulose via humidity-mediated interface. *ACS nano*
2226   **2020,** *15* (1), 1310-1320.
2227   251.   Feng, K.; Dong, C.; Gao, Y.; Jin, Z., A green and iridescent composite of cellulose nanocrystals
2228   with wide solvent resistance and strong mechanical properties. *ACS Sustain. Chem. Eng.* **2021,** *9* (19),
2229   6764-6775.
2230   252.   He, Y.-D.; Zhang, Z.-L.; Xue, J.; Wang, X.-H.; Song, F.; Wang, X.-L.; Zhu, L.-L.; Wang, Y.-Z.,
2231   Biomimetic optical cellulose nanocrystal films with controllable iridescent color and environmental
2232   stimuli-responsive chromism. *ACS Appl. Mater. Interface* **2018,** *10* (6), 5805-5811.
2233   253.   Zhao, G.; Zhang, Y.; Zhai, S.; Sugiyama, J.; Pan, M.; Shi, J.; Lu, H., Dual response of photonic films
2234   with chiral nematic cellulose nanocrystals: Humidity and formaldehyde. *ACS Appl. Mater. Interface*
2235   **2020,** *12* (15), 17833-17844.
2236   254.   Park, H.-S.; Kang, S.-W.; Tortora, L.; Kumar, S.; Lavrentovich, O. D., Condensation of self-
2237   assembled lyotropic chromonic liquid crystal sunset yellow in aqueous solutions crowded with
2238   polyethylene glycol and doped with salt. *Langmuir* **2011,** *27* (7), 4164-4175.
2239   255.   Vasilevskaya, V.; Khokhlov, A.; Matsuzawa, Y.; Yoshikawa, K., Collapse of single DNA molecule in
2240   poly (ethylene glycol) solutions. *the J. Chem. Phys.* **1995,** *102* (16), 6595-6602.
2241   256.   Lin, M.; Raghuwanshi, V. S.; Browne, C.; Simon, G. P.; Garnier, G., Modulating transparency and
2242   colour of cellulose nanocrystal composite films by varying polymer molecular weight. *journal colloid
2243   interface sci.* **2021,** *584*, 216-224.
2244   257.   Wan, H.; Li, X.; Zhang, L.; Li, X.; Liu, P.; Jiang, Z.; Yu, Z.-Z., Rapidly responsive and flexible chiral
2245   nematic cellulose nanocrystal composites as multifunctional rewritable photonic papers with eco-
2246   friendly inks. *ACS Appl. Mater. Interface* **2018,** *10* (6), 5918-5925.
2247   258.   Kose, O.; Tran, A.; Lewis, L.; Hamad, W. Y.; MacLachlan, M. J., Unwinding a spiral of cellulose
2248   nanocrystals for stimuli-responsive stretchable optics. *nature commun.* **2019,** *10* (1), 1-7.
2249   259.   Xu, M.; Li, W.; Ma, C.; Yu, H.; Wu, Y.; Wang, Y.; Chen, Z.; Li, J.; Liu, S., Multifunctional chiral
2250   nematic cellulose nanocrystals/glycerol structural colored nanocomposites for intelligent responsive
2251   films, photonic inks and iridescent coatings. *journal Mater. Chem. C* **2018,** *6* (20), 5391-5400.
2252   260.   Sheikhi, A.; Hayashi, J.; Eichenbaum, J.; Gutin, M.; Kuntjoro, N.; Khorsandi, D.; Khademhosseini,
2253   A., Recent advances in nanoengineering cellulose for cargo delivery. *journal Control. Release* **2019,** *294*,
2254   53-76.
2255   261.   John, W. S.; Fritz, W.; Lu, Z.; Yang, D.-K., Bragg reflection from cholesteric liquid crystals. *Physical
2256   Review E* **1995,** *51* (2), 1191.
2257   262.   Urbanski, M.; Reyes, C. G.; Noh, J.; Sharma, A.; Geng, Y.; Jampani, V. S. R.; Lagerwall, J. P., Liquid
2258   crystals in micron-scale droplets, shells and fibers. *Journal of Physics: Condensed Matter* **2017,** *29* (13),
2259   133003.
2260   263.   Dumanli, A. G. m.; Van Der Kooij, H. M.; Kamita, G.; Reisner, E.; Baumberg, J. J.; Steiner, U.;
2261   Vignolini, S., Digital color in cellulose nanocrystal films. *ACS Appl. Mater. Interface* **2014,** *6* (15), 12302-
2262   12306.
2263   264.   Ji, Q.; Lefort, R.; Busselez, R.; Morineau, D., Structure and dynamics of a Gay–Berne liquid crystal
2264   confined in cylindrical nanopores. *the J. Chem. Phys.* **2009,** *130* (23), 234501.

2265   265.   Giese, M.; De Witt, J. C.; Shopsowitz, K. E.; Manning, A. P.; Dong, R. Y.; Michal, C. A.; Hamad, W.
2266   Y.; MacLachlan, M. J., Thermal switching of the reflection in chiral nematic mesoporous organosilica
2267   films infiltrated with liquid crystals. *ACS Appl. Mater. Interface* **2013,** *5* (15), 6854-6859.
2268   266.   Guo, M.; Li, Y.; Yan, X.; Song, J.; Liu, D.; Li, Q.; Su, F.; Shi, X., Sustainable iridescence of cast and
2269   shear coatings of cellulose nanocrystals. *carbohydrate Polym.* **2021,** *273*, 118628.
2270   267.   Feng, K.; Gao, X.; Gu, Z.; Jin, Z., Improving homogeneity of iridescent cellulose nanocrystal films
2271   by surfactant-assisted spreading self-assembly. *ACS Sustain. Chem. Eng.* **2019,** *7* (23), 19062-19071.
2272   268.   Yi, J.; Xu, Q.; Zhang, X.; Zhang, H., Temperature-induced chiral nematic phase changes of
2273   suspensions of poly (N, N-dimethylaminoethyl methacrylate)-grafted cellulose nanocrystals. *Cellulose*
2274   **2009,** *16* (6), 989-997.
2275   269.   Parton, T. G.; van de Kerkhof, G. T.; Narkevicius, A.; Haataja, J. S.; Parker, R. M.; Frka-Petesic, B.;
2276   Vignolini, S., Chiral self-assembly of cellulose nanocrystals is driven by crystallite bundles. *arXiv preprint
2277   arXiv:2107.04772* **2021**.
2278   270.   Arcolezi, G.; Luders, D.; Sampaio, A.; Simões, M.; Braga, W.; Santos, O.; Palangana, A.; Kimura,
2279   N., Computational method to determine the pitch length in cholesteric liquid crystals. *journal Mol. Liq.*
2280   **2020,** *298*, 111752.
2281   271.   Aguirre, C. I.; Reguera, E.; Stein, A., Tunable colors in opals and inverse opal photonic crystals.
2282   *advanced Funct. Mater.* **2010,** *20* (16), 2565-2578.
2283   272.   Kelly, J. A.; Shukaliak, A. M.; Cheung, C. C.; Shopsowitz, K. E.; Hamad, W. Y.; MacLachlan, M. J.,
2284   Responsive photonic hydrogels based on nanocrystalline cellulose. *angewandte Chem. Int. Ed.* **2013,** *52*
2285   (34), 8912-8916.
2286   273.   Hu, Z., Lu, x., Gao, J. *Hydrogel Opals. Adv. Mater* **2001,** *13* (22), 1708-1712.
2287   274.   Longo, R.; Blackman, J. W.; Antalick, G.; Torley, P. J.; Rogiers, S. Y.; Schmidtke, L. M., Volatile and
2288   sensory profiling of Shiraz wine in response to alcohol management: Comparison of harvest timing
2289   versus technological approaches. *Food Research International* **2018,** *109*, 561-571.
2290   275.   Wang, J.; Cao, Y.; Feng, Y.; Yin, F.; Gao, J., Multiresponsive Inverse-Opal Hydrogels. *advanced
2291   Mater.* **2007,** *19* (22), 3865-3871.
2292   276.   Khan, M. K.; Giese, M.; Yu, M.; Kelly, J. A.; Hamad, W. Y.; MacLachlan, M. J., Flexible mesoporous
2293   photonic resins with tunable chiral nematic structures. *angewandte Chem.* **2013,** *125* (34), 9089-9092.
2294   277.   Giese, M.; Blusch, L. K.; Khan, M. K.; MacLachlan, M. J., Functional materials from cellulose-
2295   derived liquid-crystal templates. *angewandte Chem. Int. Ed.* **2015,** *54* (10), 2888-2910.
2296   278.   Giese, M.; Khan, M. K.; Hamad, W. Y.; MacLachlan, M. J., Imprinting of photonic patterns with
2297   thermosetting amino-formaldehyde-cellulose composites. *ACS Macro Lett.* **2013,** *2* (9), 818-821.
2298   279.   Wani, O. M.; Verpaalen, R.; Zeng, H.; Priimagi, A.; Schenning, A. P., An Artificial Nocturnal Flower
2299   via Humidity-Gated Photoactuation in Liquid Crystal Networks. *advanced Mater.* **2019,** *31* (2), 1805985.
2300   280.   Nitta, N.; Wu, F.; Lee, J. T.; Yushin, G., Li-ion battery materials: present and future. *materials
2301   Today* **2015,** *18* (5), 252-264.
2302   281.   Aurbach, D.; Markovsky, B.; Weissman, I.; Levi, E.; Ein-Eli, Y., On the correlation between surface
2303   chemistry and performance of graphite negative electrodes for Li ion batteries. *Electrochimica acta*
2304   **1999,** *45* (1-2), 67-86.
2305   282.   Liang, Y.; Zhao, C. Z.; Yuan, H.; Chen, Y.; Zhang, W.; Huang, J. Q.; Yu, D.; Liu, Y.; Titirici, M. M.;
2306   Chueh, Y. L., A review of rechargeable batteries for portable electronic devices. *InfoMat* **2019,** *1* (1), 6-
2307   32.
2308   283.   Dunn, B.; Kamath, H.; Tarascon, J.-M., Electrical energy storage for the grid: a battery of choices.
2309   *Science* **2011,** *334* (6058), 928-935.
2310   284.   Posada, J. O. G.; Rennie, A. J.; Villar, S. P.; Martins, V. L.; Marinaccio, J.; Barnes, A.; Glover, C. F.;
2311   Worsley, D. A.; Hall, P. J., Aqueous batteries as grid scale energy storage solutions. *Renewable and
2312   Sustainable Energy Reviews* **2017,** *68*, 1174-1182.

2313 285.   Hu, B. L.-H.; Wu, F.; Lin, C.; Khlobystov, A.; Li, L., Graphenemodified LiFePO4 cathode for lithium
2314 ion battery beyond theoretical capacity, Nat. Commun. 4 (2013) 1687.
2315 286.   Yoshio, M.; Wang, H.; Fukuda, K.; Hara, Y.; Adachi, Y., Effect of carbon coating on
2316 electrochemical performance of treated natural graphite as lithium-ion battery anode material. *Journal*
2317 *of the Electrochemical Society* **2000,** *147* (4), 1245.
2318 287.   Peled, E.; Menachem, C.; Bar-Tow, D.; Melman, A., Improved graphite anode for lithium-ion
2319 batteries chemically: Bonded solid electrolyte interface and nanochannel formation. *Journal of The*
2320 *Electrochemical Society* **1996,** *143* (1), L4.
2321 288.   Ko, S.; Lee, J. I.; Yang, H. S.; Park, S.; Jeong, U., Mesoporous CuO particles threaded with CNTs for
2322 high-performance lithium-ion battery anodes. *advanced Mater.* **2012,** *24* (32), 4451-4456.
2323 289.   Xu, Y.; Zhu, Y.; Liu, Y.; Wang, C., Electrochemical performance of porous carbon/tin composite
2324 anodes for sodium-ion and lithium-ion batteries. *Advanced Energy Materials* **2013,** *3* (1), 128-133.
2325 290.   Zhou, J.; Qin, J.; Zhang, X.; Shi, C.; Liu, E.; Li, J.; Zhao, N.; He, C., 2D space-confined synthesis of
2326 few-layer MoS2 anchored on carbon nanosheet for lithium-ion battery anode. *ACS nano* **2015,** *9* (4),
2327 3837-3848.
2328 291.   Ou, J.; Zhang, Y.; Chen, L.; Zhao, Q.; Meng, Y.; Guo, Y.; Xiao, D., Nitrogen-rich porous carbon
2329 derived from biomass as a high performance anode material for lithium ion batteries. *journal Mater.*
2330 *Chem. A* **2015,** *3* (12), 6534-6541.
2331 292.   Wang, L.; Schnepp, Z.; Titirici, M. M., Rice husk-derived carbon anodes for lithium ion batteries.
2332 *journal Mater. Chem. A* **2013,** *1* (17), 5269-5273.
2333 293.   Kim, P. J.; Fontecha, H. D.; Kim, K.; Pol, V. G., Toward high-performance lithium–sulfur batteries:
2334 upcycling of LDPE plastic into sulfonated carbon scaffold via microwave-promoted sulfonation. *ACS Appl.*
2335 *Mater. Interface* **2018,** *10* (17), 14827-14834.
2336 294.   Tang, J.; Etacheri, V.; Pol, V. G., Wild fungus derived carbon fibers and hybrids as anodes for
2337 lithium-ion batteries. *ACS Sustain. Chem. Eng.* **2016,** *4* (5), 2624-2631.
2338 295.   Lotfabad, E. M.; Ding, J.; Cui, K.; Kohandehghan, A.; Kalisvaart, W. P.; Hazelton, M.; Mitlin, D.,
2339 High-density sodium and lithium ion battery anodes from banana peels. *ACS nano* **2014,** *8* (7), 7115-
2340 7129.
2341 296.   Etacheri, V.; Hong, C. N.; Pol, V. G., Upcycling of packing-peanuts into carbon microsheet anodes
2342 for lithium-ion batteries. *Environmental Science & Technology* **2015,** *49* (18), 11191-11198.
2343 297.   Lim, D. G.; Kim, K.; Razdan, M.; Diaz, R.; Osswald, S.; Pol, V. G., Lithium storage in structurally
2344 tunable carbon anode derived from sustainable source. *Carbon* **2017,** *121*, 134-142.
2345 298.   Kim, K.; Lim, D. G.; Han, C. W.; Osswald, S.; Ortalan, V.; Youngblood, J. P.; Pol, V. G., Tailored
2346 carbon anodes derived from biomass for sodium-ion storage. *ACS Sustain. Chem. Eng.* **2017,** *5* (10),
2347 8720-8728.
2348 299.   Kim, K.; Kim, P. J.; Youngblood, J. P.; Pol, V. G., Surface Functionalization of Carbon Architecture
2349 with Nano-MnO2 for Effective Polysulfide Confinement in Lithium–Sulfur Batteries. *ChemSusChem* **2018,**
2350 *11* (14), 2375-2381.
2351 300.   Kim, J. H.; Lee, S.; Lee, J. W.; Song, T.; Paik, U., 3D-interconnected nanoporous RGO-CNT
2352 structure for supercapacitors application. *Electrochimica Acta* **2014,** *125*, 536-542.
2353 301.   Shokhen, V.; Zitoun, D., Platinum-group metal grown on vertically aligned MoS2 as
2354 electrocatalysts for hydrogen evolution reaction. *Electrochimica Acta* **2017,** *257*, 49-55.
2355 302.   Liu, W.; Lee, S. W.; Lin, D.; Shi, F.; Wang, S.; Sendek, A. D.; Cui, Y., Enhancing ionic conductivity in
2356 composite polymer electrolytes with well-aligned ceramic nanowires. *Nature energy* **2017,** *2* (5), 1-7.
2357 303.   Moon, R. J.; Martini, A.; Nairn, J.; Simonsen, J.; Youngblood, J., Cellulose nanomaterials review:
2358 structure, properties and nanocomposites. *chemical Soc. Rev.* **2011,** *40* (7), 3941-3994.

2359   304.   Chowdhury, R. A.; Clarkson, C.; Apalangya, V. A.; Islam, S.; Youngblood, J. P., Roll-to-roll
2360   fabrication of cellulose nanocrystal-poly (vinyl alcohol) composite coatings with controlled anisotropy.
2361   *Cellulose* **2018,** *25* (11), 6547-6560.
2362   305.   Zhu, H.; Shen, F.; Luo, W.; Zhu, S.; Zhao, M.; Natarajan, B.; Dai, J.; Zhou, L.; Ji, X.; Yassar, R. S.,
2363   Low temperature carbonization of cellulose nanocrystals for high performance carbon anode of sodium-
2364   ion batteries. *Nano Energy* **2017,** *33*, 37-44.
2365   306.   Kim, P. J.; Kim, K.; Pol, V. G., A comparative study of cellulose derived structured carbons on the
2366   electrochemical behavior of lithium metal-based batteries. *Energy Storage Materials* **2019,** *19*, 179-185.
2367   307.   Kim, K.; Kim, P. J.; Chowdhury, R. A.; Kantharaj, R.; Candadai, A.; Marconnet, A.; Pol, V. G.;
2368   Youngblood, J. P., Structural orientation effect of cellulose nanocrystals (CNC) films on electrochemical
2369   kinetics and stability in lithium-ion batteries. *chemical Eng. J.* **2021,** *417*, 128128.
2370   308.   Lin, D.; Liu, Y.; Cui, Y., Reviving the lithium metal anode for high-energy batteries. *nature
2371   nanotechnol.* **2017,** *12* (3), 194-206.
2372   309.   Alvarado, J.; Schroeder, M. A.; Pollard, T. P.; Wang, X.; Lee, J. Z.; Zhang, M.; Wynn, T.; Ding, M.;
2373   Borodin, O.; Meng, Y. S., Bisalt ether electrolytes: a pathway towards lithium metal batteries with Ni-rich
2374   cathodes. *Energy & Environmental Science* **2019,** *12* (2), 780-794.
2375   310.   Nguyen, T.-D.; Lizundia, E.; Niederberger, M.; Hamad, W. Y.; MacLachlan, M. J., Self-assembly
2376   route to TiO2 and TiC with a liquid crystalline order. *chemistry Mater.* **2019,** *31* (6), 2174-2181.
2377   311.   Liu, X.; Ji, H.; Fan, H.; Tan, Z.; Liu, Q.; Wang, Y.; Yang, L.; Li, M.; Chen, Y.; Wang, D., Chiral carbon
2378   nanotubes decorated MoS2 nanosheets as stable anode materials for sodium-ion batteries. *Journal of
2379   Alloys and Compounds* **2021,** *887*, 161354.
2380   312.   Pan, H.; Ma, J.; Tao, J.; Zhu, S., Hierarchical architecture for flexible energy storage. *Nanoscale
2381   **2017,** *9* (20), 6686-6694.
2382   313.   Walters, C. M.; Matharu, G. K.; Hamad, W. Y.; Lizundia, E.; MacLachlan, M. J., Chiral nematic
2383   cellulose nanocrystal/germania and carbon/germania composite aerogels as supercapacitor materials.
2384   *chemistry Mater.* **2021,** *33* (13), 5197-5209.
2385   314.   Lizundia, E.; Nguyen, T.-D.; Vilas, J. L.; Hamad, W. Y.; MacLachlan, M. J., Chiroptical,
2386   morphological and conducting properties of chiral nematic mesoporous cellulose/polypyrrole composite
2387   films. *journal Mater. Chem. A* **2017,** *5* (36), 19184-19194.
2388   315.   Qu, D.; Zussman, E., Electro-responsive liquid crystalline nanocelluloses with reversible
2389   switching. *the J. Phys. Chem. Lett.* **2020,** *11* (16), 6697-6703.
2390   316.   Nishio, Y.; Sato, J.; Sugimura, K., Liquid crystals of cellulosics: fascinating ordered structures for
2391   the design of functional material systems. *Cellulose Chemistry and Properties: Fibers, Nanocelluloses and
2392   Advanced Materials* **2015**, 241-286.
2393   317.   Kelly, J. A.; Giese, M.; Shopsowitz, K. E.; Hamad, W. Y.; MacLachlan, M. J., The development of
2394   chiral nematic mesoporous materials. *K* **2014,** *47* (4), 1088-1096.
2395   318.   Guidetti, G.; Frka-Petesic, B.; Dumanli, A. G.; Hamad, W. Y.; Vignolini, S., Effect of thermal
2396   treatments on chiral nematic cellulose nanocrystal films. *carbohydrate Polym.* **2021,** *272*, 118404.
2397   319.   Fernandes, S. N.; Almeida, P. L.; Monge, N.; Aguirre, L. E.; Reis, D.; de Oliveira, C. L.; Neto, A. M.;
2398   Pieranski, P.; Godinho, M. H., Mind the microgap in iridescent cellulose nanocrystal films. *advanced
2399   Mater.* **2017,** *29* (2), 1603560.
2400   320.   Sun, W., Cellulose reflects left and right. *nature nanotechnol.* **2017**, 1-1.
2401   321.   Harkness, B. R.; Gray, D. G., Left-and right-handed chiral nematic mesophase of (trityl)(alkyl)
2402   cellulose derivatives. *Canadian journal of chemistry* **1990,** *68* (7), 1135-1139.
2403   322.   Santos, M. V.; Tercjak, A.; Gutierrez, J.; Barud, H. S.; Napoli, M.; Nalin, M.; Ribeiro, S. J., Optical
2404   sensor platform based on cellulose nanocrystals (CNC)–4'-(hexyloxy)-4-biphenylcarbonitrile (HOBC) bi-
2405   phase nematic liquid crystal composite films. *carbohydrate Polym.* **2017,** *168*, 346-355.

2406 323.   Tercjak, A.; Gutierrez, J.; Ocando, C.; Peponi, L.; Mondragon, I., Thermoresponsive
2407 inorganic/organic hybrids based on conductive TiO2 nanoparticles embedded in poly (styrene-b-
2408 ethylene oxide) block copolymer dispersed liquid crystals. *Acta materialia* **2009,** *57* (15), 4624-4631.
2409 324.   Bardet, R.; Roussel, F.; Coindeau, S.; Belgacem, N.; Bras, J., Engineered pigments based on
2410 iridescent cellulose nanocrystal films. *carbohydrate Polym.* **2015,** *122*, 367-375.
2411 325.   Hong, W.; Yuan, Z.; Chen, X., Structural color materials for optical anticounterfeiting. *Small* **2020,**
2412 *16* (16), 1907626.
2413 326.   Gan, L.; Feng, N.; Liu, S.; Zheng, S.; Li, Z.; Huang, J., Assembly-induced emission of cellulose
2414 nanocrystals for hiding information. *Particle & Particle Systems Characterization* **2019,** *36* (3), 1800412.
2415 327.   Kuo, H.; Chuang, M.; Lin, C., Design correlations for the optical performance of the particle-
2416 diffusing bottom diffusers in the LCD backlight unit. *Powder Technology* **2009,** *192* (1), 116-121.
2417 328.   Mingyan, L.; Daming, W.; Yajun, Z.; Jian, Z., Optimization and design of LCD diffuser plate with
2418 micro-semisphere structure. *Procedia Engineering* **2011,** *16*, 306-311.
2419 329.   Chen, C. Y.; Lee, W. K.; Chen, Y. J.; Lu, C. Y.; Lin, H. Y.; Wu, C. C., Enhancing optical out-coupling
2420 of organic light-emitting devices with nanostructured composite electrodes consisting of indium tin
2421 oxide nanomesh and conducting polymer. *advanced Mater.* **2015,** *27* (33), 4883-4888.
2422 330.   Fang, Z.; Zhu, H.; Yuan, Y.; Ha, D.; Zhu, S.; Preston, C.; Chen, Q.; Li, Y.; Han, X.; Lee, S., Novel
2423 nanostructured paper with ultrahigh transparency and ultrahigh haze for solar cells. *nano lett.* **2014,** *14*
2424 (2), 765-773.
2425 331.   Bin, W.; Qing-Kang, W., High sensitivity transmission-type SPR sensor by using Metallic–
2426 Dielectric mixed gratings. *Chinese Physics Letters* **2008,** *25* (5), 1668.
2427 332.   Nguyen, T. D.; Li, J.; Lizundia, E.; Niederberger, M.; Hamad, W. Y.; MacLachlan, M. J., Black
2428 titania with nanoscale helicity. *advanced Funct. Mater.* **2019,** *29* (40), 1904639.
2429 333.   Shopsowitz, K. E.; Hamad, W. Y.; MacLachlan, M. J., Chiral nematic mesoporous carbon derived
2430 from nanocrystalline cellulose. *angewandte Chem. Int. Ed.* **2011,** *50* (46), 10991-10995.
2431 334.   Hanif, Z.; Choi, D.; Tariq, M. Z.; La, M.; Park, S. J., Water-stable flexible nanocellulose chiral
2432 nematic films through acid vapor cross-linked glutaraldehyde for chiral nematic templating. *ACS Macro*
2433 *Lett.* **2020,** *9* (2), 146-151.
2434 335.   Gansel, J. K.; Thiel, M.; Rill, M. S.; Decker, M.; Bade, K.; Saile, V.; von Freymann, G.; Linden, S.;
2435 Wegener, M., Gold helix photonic metamaterial as broadband circular polarizer. *Science* **2009,** *325*
2436 (5947), 1513-1515.
2437 336.   Esposito, M.; Tasco, V.; Todisco, F.; Cuscunà, M.; Benedetti, A.; Sanvitto, D.; Passaseo, A., Triple-
2438 helical nanowires by tomographic rotatory growth for chiral photonics. *nature commun.* **2015,** *6* (1), 1-7.
2439 337.   Jakšić, Z.; Vuković, S.; Matovic, J.; Tanasković, D., Negative refractive index metasurfaces for
2440 enhanced biosensing. *Materials* **2010,** *4* (1), 1-36.
2441 338.   Mejía-Salazar, J.; Oliveira Jr, O. N., Plasmonic biosensing: Focus review. *chemical rev.* **2018,** *118*
2442 (20), 10617-10625.
2443 339.   Wang, M.; Huang, Z.; Salut, R.; Suarez, M. A.; Lu, H.; Martin, N.; Grosjean, T., Plasmonic helical
2444 nanoantenna as a converter between longitudinal fields and circularly polarized waves. *nano lett.* **2021,**
2445 *21* (8), 3410-3417.
2446 340.   Ruhl, T.; Spahn, P.; Hermann, C.; Jamois, C.; Hess, O., Double-Inverse-Opal Photonic Crystals: The
2447 Route to Photonic Bandgap Switching. *advanced Funct. Mater.* **2006,** *16* (7), 885-890.
2448 341.   Asher, S. A.; Alexeev, V. L.; Goponenko, A. V.; Sharma, A. C.; Lednev, I. K.; Wilcox, C. S.; Finegold,
2449 D. N., Photonic crystal carbohydrate sensors: low ionic strength sugar sensing. *journal Am. Chem. Soc.*
2450 **2003,** *125* (11), 3322-3329.
2451 342.   Lee, Y.-J.; Pruzinsky, S. A.; Braun, P. V., Glucose-sensitive inverse opal hydrogels: analysis of
2452 optical diffraction response. *Langmuir* **2004,** *20* (8), 3096-3106.

2453   343.   Sharma, A. C.; Jana, T.; Kesavamoorthy, R.; Shi, L.; Virji, M. A.; Finegold, D. N.; Asher, S. A., A
2454   general photonic crystal sensing motif: creatinine in bodily fluids. *journal Am. Chem. Soc.* **2004,** *126* (9),
2455   2971-2977.
2456   344.   Kamenjicki, M.; Lednev, I. K.; Mikhonin, A.; Kesavamoorthy, R.; Asher, S. A., Photochemically
2457   controlled photonic crystals. *advanced Funct. Mater.* **2003,** *13* (10), 774-780.
2458   345.   Shimoda, Y.; Ozaki, M.; Yoshino, K., Electric field tuning of a stop band in a reflection spectrum
2459   of synthetic opal infiltrated with nematic liquid crystal. *Applied Physics Letters* **2001,** *79* (22), 3627-3629.
2460   346.   Ozaki, M.; Shimoda, Y.; Kasano, M.; Yoshino, K., Electric field tuning of the stop band in a liquid-
2461   crystal-infiltrated polymer inverse opal. *advanced Mater.* **2002,** *14* (7), 514-518.
2462   347.   Arsenault, A.; Clark, T.; von Freymann, G.; Cademartiri, L.; Sapienza, R.; Bertolotti, J.; Vekris, E.;
2463   Wong, S.; Kitaev, V., Manners, 1.; Wang, RZ; John, S.; Wiersma, D.; Ozin, GA. *nat Mater* **2006,** *5*, 179.
2464   348.   Fudouzi, H.; Xia, Y., Photonic papers and inks: color writing with colorless materials. *advanced*
2465   *Mater.* **2003,** *15* (11), 892-896.
2466   349.   Fudouzi, H.; Xia, Y., Colloidal crystals with tunable colors and their use as photonic papers.
2467   *Langmuir* **2003,** *19* (23), 9653-9660.
2468   350.   Fudouzi, H.; Sawada, T., Photonic rubber sheets with tunable color by elastic deformation.
2469   *Langmuir* **2006,** *22* (3), 1365-1368.
2470   351.   Gates, B.; Xia, Y., Photonic crystals that can be addressed with an external magnetic field.
2471   *advanced Mater.* **2001,** *13* (21), 1605-1608.
2472   352.   Wang, Y.; Huang, W.; Wang, Y.; Mu, X.; Ling, S.; Yu, H.; Chen, W.; Guo, C.; Watson, M. C.; Yu, Y.,
2473   Stimuli-responsive composite biopolymer actuators with selective spatial deformation behavior. *P NATL*
2474   *A SCI* **2020,** *117* (25), 14602-14608.
2475   353.   Khabibullin, A.; Alizadehgiashi, M.; Khuu, N.; Prince, E.; Tebbe, M.; Kumacheva, E., Injectable
2476   shear-thinning fluorescent hydrogel formed by cellulose nanocrystals and graphene quantum dots.
2477   *Langmuir* **2017,** *33* (43), 12344-12350.
2478   354.   Danesh, M.; Mauran, D.; Berry, R.; Pawlik, M.; Hatzikiriakos, S. G., High-concentrated zirconia
2479   suspensions stabilized by cellulose nanocrystals. *ceramics Int.* **2022**.
2480   355.   Rey, A. D., Theory of linear viscoelasticity of cholesteric liquid crystals. *journal Rheol.* **2000,** *44*
2481   (4), 855-869.

2482